ANALYSIS OF BRITTLE FRACTURE CHARACTERISTICS OF AN INFINITE PLATE WITH AN FGM COATING AROUND A CIRCULAR HOLE

by

Shahereen Chowdhury

Department of Mechanical Engineering

BANGLADESH UNIVERSITY OF ENGINEERING AND TECHNOLOGY

A thesis submitted for the degree of
Master of Science

June 2015

Certificate of Approval

The thesis titled, "**ANALYSIS OF BRITTLE FRACTURE CHARACTERISTICS OF AN INFINITE PLATE WITH AN FGM COATING AROUND A CIRCULAR HOLE**", submitted by Shahereen Chowdhury, Roll No: 0409102075 P, Session: April, 2009, has been accepted as satisfactory in partial fulfillment of the requirements for the degree of **MASTER OF SCIENCE IN MECHANICAL ENGINEERING** on **June 8, 2015**.

Dr. Md. Afsar Ali
Professor
Department of Mechanical Engineering
BUET, Dhaka, Bangladesh

Chairman

Dr. Md. Zahurul Haq
Professor & Head
Department of Mechanical Engineering
BUET, Dhaka, Bangladesh

Member
(Ex-Officio)

Dr. Monon Mahbub
Assistant Professor
Department of Mechanical Engineering
BUET, Dhaka, Bangladesh

Member
(Internal)

Dr. Md. Abdul Matin
Assistant Professor
Department of Glass and Ceramic Engineering
BUET, Dhaka, Bangladesh

Member
(External)

Candidate's Declaration

It is hereby declared that this thesis or any part of it has not been submitted elsewhere for the award of any degree or diploma.

_____

Shahereen Chowdhury

Acknowledgements

The author wishes to express her deepest gratitude and indebtedness to Dr. Md. Afsar Ali, Professor, Department of Mechanical Engineering, Bangladesh university of Engineering and Technology, for his kind supervision, guidance, inspiration, and invaluable suggestions throughout the research work.

The author is also grateful to Dr. Md. Zahurul Haq, Professor and Head, Department of Mechanical Engineering, Bangladesh University of Engineering and Technology, for his valuable co-operation from time to time.

The author also sincerely expresses her thankfulness to all the beautiful souls around her for their help and moral support during the work.

ABSTRACT

This study is concerned with the brittle fracture characteristics of an infinite plate with a functionally graded material (FGM) coating around a circular hole. The incompatible eigenstrain induced in the FGM coating after cooling from the sintering temperature, due to mismatch in the coefficients of thermal expansion (CTE), is taken into consideration. Two diametrically opposed radial edge cracks emanating from the circular hole are considered for the analysis of brittle fracture characteristic. A uniform internal pressure is assumed to be applied to the surfaces of the hole and cracks. The FGM coating is homogenized simulating the material nonhomogeneity by distribution of equivalent eigenstrain. Consequently, an approximation method of determining stress intensity factors (SIFs) is introduced representing the cracks by a continuous distribution of edge dislocations. This approximation method is used in analyzing the effects of material distribution in the coating, crack length, temperature, coating thickness and strength factor on fracture characteristics of the plate. Furthermore, apparent fracture toughness corresponding to prescribed material distributions is also analyzed as a function of the above mentioned parameters except for strength factor. To present numerical results, an infinite plate with TiC/Al_2O_3 FGM coating around a circular hole is considered. It is found that material distribution in the FGM coating around a circular hole has significant effects on the SIF and apparent fracture toughness which can be controlled by choosing the material distribution appropriately.

List of Symbols

A	Dispersed Material
B	Parent/Base material
E	Young's modulus of *A/B* FGM
E_0	Young's modulus of base material *B*
F	Geometric Factor
T_s	Traction along crack surface
l	Crack length
K_{IC}^{a}	Apparent fracture toughness of FGM
K_C	Intrinsic fracture toughness of FGM
K_C^B	Intrinsic fracture toughness of material *B*
V_A	Volume fraction of material *A*
V_B	Volume fraction of material *B*
ΔT	Difference between processing and room temperatures
γ	Bulk modulus
S_f	Strength factor
R_f	Radius of coating thickness
R	Radius of hole
r	Any radius
p	Internal pressure
p_c	Critical pressure
μ	Shear modulus of elasticity
ν	Poisson's ratio
ε	Strain
ε^*	Incompatible thermal eigenstrain

ε_e	Equivalent eigenstrain
α	Coefficient of thermal expansion(CTE)
U	Displacement components
σ_s^h	Stress component in uncracked homogenized plate
σ_s^d	Stress component of the disturbed field for crack
T_s	Traction along crack surface
$\Phi(z), \Psi(z)$	Complex potential functions
κ_0	Kolosov's constant
b_1, b_2	Components of Burger vector
σ_θ, σ_r	Circumferential and radial stress component

Table of Contents

List of Figures

List of Tables

Chapter 1 : INTRODUCTION

1.1 Background

Functionally graded materials (FGMs) are new generation materials consisting of two or more material phases, such as different ceramics or ceramics and metals. It is characterized by the variation in microstructure details with space variables through the non uniform distribution of these reinforcement phases. This continuously varying material distribution induces chemical, material, and microstructural gradients, and makes functionally graded materials different in behavior from homogeneous materials and traditional composite materials [1,2]. Traditional composite materials are homogeneous mixtures of two or more ingredients with distinct physical and chemical properties. Composite material offers an excellent combination of properties which are different from the individual parent materials but fail under extreme working conditions through a process called delamination (separation of fibers from the matrix). The solution to this problem leads to the use of FGM, as it eliminates the sharp interfaces existing in traditional composite material which is where failure is initiated.

The concept of a typical FGM body consisting of two different materials A and B is illustrated in Fig. 1.1. The left surface of the FGM plate shown in Fig. 1.1(a) has 100% material A while the right surface of the plate has 100% material B. In between these two surfaces, the material distribution composition denoted by the volume fractions V_A and V_B of the constituents A and B, respectively, continuously changes as shown in Fig. 1.1(b). The material distribution shown in Fig. 1.1(b) may vary linearly, exponentially, or following any power function depending on the desired properties and application of FGMs.

One unique characteristic of FGMs is the ability to tailor a material for specific application via the design of the gradients in chemistry and microstructure, which, in turn, depend on the material distribution. A specific property of FGMs can be optimized by properly selecting their material distribution profiles. From a mechanics viewpoint, the main advantages of material property grading appear to be improved bonding strength, toughness, wear and corrosion resistance, and reduced residual and thermal stresses.

Initially, the purpose of these materials was to develop superheat resistant material for propulsion systems and airframes of spacecraft. Now they are also used as high temperature, wear- and corrosion-resistant materials. Some typical applications include thermal barrier coatings of high temperature components in gas turbines, surface hardening for tribological protection and graded interlayers used in multilayered microelectronic and optoelectronic components, artificial bones, joints and teeth. [3]

On the basis of wide applications in many branches of engineering, one of the important analyses regarding FGMs is to identify their probable failure modes and design them against those failures. In designing with FGMs, a crucial aspect of the problem is the mechanical failure, specifically the fracture failure. Although the absence of discontinuous interfaces in FGMs does largely reduce material property mismatch, crack may occur when they are subjected to external loadings [1, 2]. In most of the cases, the failure process starts with the formation of microcracks at locations of corrosion pits, surface flaws, or stress concentration. These microcracks are coalesced into a local dominant crack, which would then propagate under cyclic or sustained loading. Even very small mechanical imperfection such as uncertainties arising from voids and defects has adverse effect on the fracture strength. Therefore, fracture analysis of these materials is important in order to understand, quantify, and improve their toughness.

The study of fracture of solids is carried out from one of the three points of view, namely microscopic or atomic, microstructural, and macroscopic or continuum mechanics [4]. From the standpoint of engineering applications, it has been the macroscopic theories based on the notion of continuum solid mechanics and classical thermodynamics that have provided the quantitative working tools in dealing with the fracture of structural materials. From the macroscopic point of view, the fracture may roughly be classified as brittle and ductile. Brittle fracture is associated with low energy, and for unstable loading conditions, it usually takes place under high fracture velocities. Ductile fracture is associated with large deformations, high energy dissipation rates, and slow fracture velocities. Again loading of cracked body is usually accompanied by inelastic deformation and other nonlinear effect in the neighborhood of the crack tip, except for the case of ideally brittle materials. But in the situations where inelastic deformation and nonlinear effects are very small compared to the crack size and any other characteristic length of the body, the linear theory is adequately justified to address the problem of stress distribution in the cracked body.

The microstructure is another factor that affects the fracture characteristics of solids. The techniques often used to fabricate FGMs are thermal spray, powder processing and chemical vapor deposition (CVD). The microstructure of FGMs depends on these manufacturing processes [5].However, in the idealized case of FGMs, the effect of microstructure is neglected and materials are assumed to be simple nonhomogeneous with continuous variation of material properties. It has been found that the stress intensity factor approach holds as long as the elastic properties remain piecewise continuous and differentiable [6].

Another important factor in the fracture study of FGMs is the eigenstrain, which is a generic name of such nonelastic strains as thermal expansion, phase transformation, initial strains, plastic strains and misfit strains [7]. The incompatibility of this eigenstrain produces eigenstress, which affect the fracture strength of FGMs. In FGMs, eigenstrain is induced due to nonuniform coefficient of thermal expansion (CTE) when FGMs are cooled from sintering temperature.

1.2 Motivation of the Present Work

The thermo-mechanical deformation of FGM structures have attracted the attention of many researchers in the past few years in different engineering applications which include design of aerospace structures, heat engine components and nuclear power plants, etc. Consequently, enormous studies have already been carried out to analyze various aspects of FGM beams, cylinders, spheres and plates. For instance, Xiang and Yang [8] considered thermal load for the analysis of free and forced vibration of a laminated functionally graded Timoshenko beam of variable thickness. A Timoshenko beam of FGMs was also considered to investigate the post-buckling behavior in response to the thermal load [9]. FGM circular cylinders were considered by Obata and Noda [10] and Liew *et al.* [11] to analyze the thermal stresses. FGM circular cylinders were also considered by Afsar *et al.* [12] for the analysis of brittle fracture characteristics by taking into account the effect of incompatibility of eigenstrain developed in the cylinder due to nonuniform CTE as a result of temperature change. Loghman *et al.* [13] investigated the magnetothermoelastic creep behavior of thick-walled spheres made of functionally graded materials(FGM) placed in uniform magnetic and distributed temperature fields and subjected to an internal pressure using method of successive elastic solution.

Among various geometrics of FGM bodies, FGM plates have received wide attention for the analysis of various aspects as FGM plates have potential application in different branches of engineering. A huge amount of works are available in literature that performed evaluation

of thermomechanical behavior of functionally gradient material plates using finite element techniques. It includes both linearity and non linearity in various areas. A number of approaches have been employed to study the static bending problems of FGM plates. The assessment of thermo-mechanical deformation behavior of functionally graded plate structures considerably depends on the plate model kinematics. For instance, Praveen and Reddy reported theoretical formulations and finite element analysis of the thermomechanical, transient response of functionally graded cylinders and plates with nonlinearity [14]. Qian *et al* [15] analyzed static deformations, free and forced vibrations of a thick rectangular functionally graded elastic plate by using a higher order shear and normal deformable plate theory and a meshless local Petrov–Galerkin (MLPG) method. Chung, Chang [16] studied the mechanical behavior of rectangular plates with functionally graded coefficient of thermal expansion subjected to thermal loading. Ashraf and Daoud [17] determined the thermal buckling response of functionally graded plates using sinusoidal shear deformation plate theory (SPT).

It is seen that although various aspects of FGM plates have been analyzed, analysis of fracture characteristics has received only a little attention.Systems of bearing and shaft with a lubricant between them are common components of almost all engines, turbines and other devices with relative motion. FGM coatings around the bearing surfaces can be used to prevent wear and oxidation, and at the same time substantially reduce the mismatch thermal stresses, whereby providing strong bonding between substrates and coatings. However, using liquid lubricant exerts considerably high pressure at the bearing surfaces due to which surface cracking may occur from initial flaws or other defects and propagate into the coatings. Since the thickness of the coatings around the bearing surfaces is small, the systems can be considered as infinite FGM plates with a circular hole.

Afsar and Sekine[18] carried out an analysis of fracture characteristics of such an infinite plate with an FGM coating around a circular hole. However, they confined their attention only to a single crack emanating from the circular hole. It is well known that two diametrically opposed edge cracks emanating from a hole is the worst case than a single crack. Thus, it is important to carry out the analysis of fracture characteristics for two diametrically opposed edge cracks. This motivates the author to consider the case of two diametrically opposed edge cracks emanating from a circular hole with an FGM coating in an infinite plate in order to understand, quantify, and improve the fracture characteristics.

1.3 Objectives

Two diametrically-opposed edge cracks emanating from a circular hole with an FGM coating in an infinite plate are considered for the analysis of brittle fracture characteristics.

The specific objectives of the study are

a) To modify an existing method developed for a single edge crack with view to applying it to the case of two diametrically-opposed edge cracks.
b) To analyze fracture characteristics corresponding to prescribed material distributions in the FGM coating around a circular hole in the plate.
c) To analyze the effects of temperature gradient, coating thickness, and strength factor on the fracture characteristics.
d) To evaluate and analyze apparent fracture toughness as a function of material distribution, temperature gradient, and coating thickness.
e) To compare the results of two diametrically-opposed cracks with those of the single crack.

It is expected that the modified method to be developed here in this study and the results to be presented would be helpful in designing with bearings having an FGM coating at the inner surface from the viewpoint of fracture characteristics. It is also expected that the outcome of the present research will provide important information to the academicians and industrialists for further research in the similar field.

Chapter 2 : LITERATURE REVIEW

Over the past few years, there have been a number of works, both theoretical [19-21]and experimental[22], to study the responses of FGMs to mechanical and thermal loads for various geometries in various fracture mechanisms. Putting concern on the effects of material nonhomogeneities on the stress field at crack tips Cook and Erdogan [23], and Erdogan and Cook [24] showed that the stress field around a crack tip terminating at the interface has a behavior of the form r^{α}, where r is the distance from the crack tip and $-1<\alpha<0$. By further research, an important conclusion is given that the nature of the stress singularity at a crack tip in nonhomogeneous materials would remain to be the standard square-root type as homogeneous solids, provided that the spatial distribution of the material properties are continuous and piecewise continuously differentiable [25-29].Hence the stress intensity factor concept can still be used to study the fracture behavior of FGMs as long as the crack-tip nonlinear deformations and process zones are completely included within the region dominated by the stress intensity factors.

Extensive investigations have been carried out to analyze the effects of nonhomogeneities of FGMs on the stress intensity factor (SIF) for various geometries and loading conditions. However, mathematical difficulties due to nonhomogeneous properties have made analytical studies for cracked nonhomogeneous bodies inappropriate. Therefore, it is often conventional to regard the material properties to be some certain assumed functions of space variable such as exponential and power functions.

A series of papers on the crack problems of nonhomogeneous materials have appeared in the literature in which the material properties have been assumed to vary following an exponential function [30-34]or a power function[35-37] . Delale and Erdogan [34] solved the crack problem of nonhomogeneous infinite plate assuming constant Poisson's ratio and exponentially varying Young's modulus. They found that the Poisson's ratio did not have much effect on the resulting stress intensity factors. They also found that the strain-energy release rate of the crack embedded in the portion of the medium with higher stiffness is lower than that corresponding to the crack tip in the less stiff side of the material. Gu and Asaro [31] considered a semi-infinite crack in a strip of an isotropic, functionally graded material under edge loading and in-plane deformation conditions. Their results showed that the fracture modes of the cracks in FGMs are inherently mixed when they are not parallel to the direction of material property variation, i.e. there are

typically both normal and shear tractions ahead of the crack tips because of the non-symmetry in the material properties. The crack problems of FGMs with the exponential variation of material properties and involving various geometries discussed above were solved for mechanical loadings. Numerous researchers have also carried out a number of studies for cracked FGM bodies subjected to thermal loadings assuming the same exponential function for the material properties. Jin and Noda [38], Noda and Jin [39] have studied crack problems of FGMs under steady thermal loading in order to reduce the thermal stresses and the thermal stress intensity factors. All of these authors, in their research work, conclude that the appropriate selection of the mechanical and the thermal nonhomogeneous parameters of the material reduces the thermal stresses and, hence, the thermal stress intensity factors. Bao and Wang [35] studied multiple cracking in functionally graded ceramic/metal coatings and considered both mechanical and thermal loads. The gradation in the FGM coating was taken to be of a power function, both linear and nonlinear. It was found that the gradation of the coating could significantly reduce the crack driving force. It was also found that under mechanical loading the effect of different gradations on the crack driving force was relatively small. However, under thermal loading, the influence of coating gradation could be significant.
Dynamic fracture of FGMs and experimental investigations into the fracture of FGMs, due to the high cost and elaborate facilities required for preparing FGM specimens has received very little attention. Nakagaki et al. [40] addressed a numerical treatment of fracture occurring in an FGM under dynamic loading.

From the above reviews discussed so far, it can be summarized that the various aspects of crack problems of functionally graded materials have been studied, both analytically and experimentally, under various mechanical and thermal loading conditions, and for various geometries. However, these studies are concerned with the direct problems in which the fracture characteristics of FGM bodies can be analyzed only for certain assumed functions of the material properties e.g. exponential and power functions.

An important aspect of FGM bodies still remaining to be dealt with is the inverse problems in which the improved characteristics of FGM bodies under mechanical and thermal loadings can be prescribed and the corresponding material composition profiles via the material properties can be obtained by inverse calculation [41-46]. A general inverse design procedure for FGMs was addressed by Hirano and Wakashima [47] to determine both the basic material combination and optimum material distribution profile with respect to the objective structural shape and the

thermomechanical boundary conditions. Markworth and Saunders [48] considered the inverse problem of optimizing an assumed functional form for the spatially dependent material distributions subject to certain constraints such as maximizing or minimizing the heat flux across the material. In all the references mentioned above, the inverse problems were considered in order to design FGMs optimally from the viewpoint of thermal characteristics. The analytical solution to the inverse problems of designing FGMs from the viewpoint of fracture characteristics turns out to be very complicated due to their nonhomogenous material properties. Obviously, the inverse problems cannot be restricted to certain assumed functions for the material property distributions as Zuiker [49] pointed out that these assumed property distributions are not physically realizable for certain material composition profiles which may be obtained by the inverse problems. Afsar and Sekine [18] dealt with the inverse problem of calculating material distribution for prescribed apparent fracture toughness in FGM coatings around a circular hole in infinite elastic media. They also considered semi-infinite FGM media with a single [50] and periodic [51] edge cracks and computed material distribution profiles for improved fracture characteristics. In another work [52], they calculated the optimum material distribution in a thick-walled FGM circular pipe with a single edge crack for desired apparent fracture toughness.

It is found that some of the above mentioned studies were concern about the presence of a single crack in an infinite elastic medium under different loading conditions. However, for an infinite plate, two diametrically opposed cracks emanating from a circular hole with an FGM coating have not been considered so far. Since the case of two diametrically-opposed cracks is the worst case than that of a single crack, this should be addressed to understand, quantify and improve the brittle fracture characteristics. Therefore, the present study focuses on the analysis of brittle fracture characteristics of an infinite plate with two diametrically opposed edge cracks emanating from a circular hole with an FGM coating.

Chapter 3 : APPROXIMATION METHOD OF STRESS INTENSITY FACTOR FOR INFINITE PLATE WITH FGM COATING

3.1 Method of Homogenization

Functionally graded materials being nonhomogeneous solids, their nonhomogeneities complicate the analytical study of fracture characteristics due to mathematical difficulties. This complexity gives rise to a trend of assuming the material properties as certain assumed functions of space variable, for instance, exponential and power functions, in order to simplify the problems. However, in designing with FGMs *i.e.* in the inverse problems, in which material composition profiles have to be determined to achieve desired fracture characteristics, special functional forms of the properties cannot be assumed. Since these assumed functional forms of the properties may not be physically realizable for some material composition profiles obtained by inverse calculation. Therefore, in this study, as an alternate approach, an approximation method to calculate the stress intensity factor (SIF) developed by Sekine and Afsar [50] is adopted for a crack in FGMs, which is not restricted to any specific property distributions, but can treat any arbitrary distributions of the properties. The concept of the approximation method is explained below.

First, the FGM bodies are homogenized by simulating the material nonhomogeneities by a distribution of equivalent eigenstrain. The distribution of the equivalent eigenstrain to be determined is such that the elastic fields are identical in both the FGM and the homogenized bodies under the same loading conditions. Then a method is formulated to calculate the stress intensity factor for cracks in the homogenized bodies subjected to external loadings. Since the equivalent eigenstrain is determined from the condition of identical elastic fields in the uncracked FGM and homogenized bodies, the elastic filed in the cracked homogenized bodies cannot exactly represent the elastic field in the cracked FGM bodies. Therefore, the stress intensity factors calculated for cracks in the homogenized bodies with the equivalent eigenstrain represent the approximate values of the stress intensity factors for the same crack in the corresponding FGM bodies and hence it is referred to the approximation method.

The resultant stress field in the cracked homogenized bodies can be obtained by the principle of superposition. Initially, the stress field in the uncracked bodies is determined due to external loadings, and incompatible and equivalent eigenstrains. The disturbed stress field due to the presence of two diametrically opposed radial edge cracks is then determined. Finally, the resultant stress field in the cracked homogenized bodies is obtained by superposing the disturbed stress field and the one obtained for the uncracked bodies. Thus the following boundary condition along the crack surfaces is satisfied for the disturbed stress field

$$\sigma_s^d + \sigma_s^h = T_s \ , \tag{3.1}$$

where σ_s^h is the stress component along the prospective crack line in the uncracked homogeneous bodies, σ_s^d is the stress component of the disturbed field due to the presence of a crack, and T_s is the traction applied to the crack surface. The disturbed stress field can be determined by representing the crack by a continuous distribution of edge dislocations.

3.2 Apparent Fracture Toughness of FGMs

There are possibilities of three independent kinematic movements of the crack surfaces with respect to each other [3]. Depending on this relative movement of crack surfaces, crack propagation is classified as Mode I, Mode II, and Mode III as shown in Fig.3.1. Of these three basic modes of deformation Mode I resemble the characteristics of the present problem as the stress is normal to the crack surface. So we will consider Mode I deformation.

The stress intensity factors for a crack in homogeneous materials without any initial stresses or eigenstrains can be expressed, in general, for the Mode I as [53]

$$K_I = Fp\sqrt{\pi l} \ , \tag{3.2}$$

where F is a geometric factor that depends on the geometry of the crack and the cracked body and the loading configuration, l is the crack length, and p is the applied pressure.

For a specific crack length l, the above expression gives the intrinsic fracture toughness of homogeneous materials when the applied pressure p approaches its critical value p_c, because p_c alone contributes to the crack driving force.

In contrast, the effective crack driving force in the case of FGMs is obtained due to the resultant effects of the applied critical pressure p_c and the induced incompatible eigenstrain resulting from non-uniform CTE when FGMs are cooled from sintering temperature. However, apparently it seems that the crack extension in FGMs occurs due to the applied critical pressure p_C alone. Therefore, the above expression gives the apparent fracture toughness in the case of FGMs when p is substituted by p_C.

Thus the apparent fracture toughness K_{IC}^a of FGMs can be defined by,

$$K_{IC}^a = Fp_c\sqrt{\pi l}\,. \tag{3.3}$$

Since the factor F is a function of the geometry and the loading configuration, the apparent fracture toughness K_{IC}^a is also a function of the same. Thus in calculating the apparent fracture toughness of FGM bodies, it is necessary to consider crack geometries as well as loading configuration.

3.3 Intrinsic Fracture Toughness of FGMs

The intrinsic fracture toughness of FGMs represents the fracture resistance that a FGM actually possesses. It is related to the effective critical stress acting at the crack tip. Therefore, in determining the intrinsic fracture toughness of FGMs, the stress arising from the incompatible eigenstrain will also have to be considered along with the applied critical pressure.

Again, the intrinsic fracture toughness of FGMs can be determined from their effective properties. If a material A is distributed in a matrix material B and forms an A/B FGM, the intrinsic fracture toughness of the FGM can be determined from equation [54],

$$K_C = \frac{E}{E_0} K_C^B\,, \tag{3.4}$$

where K_C^B is the intrinsic fracture toughness of the material B, E_0 is the Young's modulus of the material B, and E is the effective Young's modulus of the A/B FGM, which can be obtained by using an appropriate model of mixture rule.

3.4 Effective Properties of FGMs

To calculate the effective properties of FGMs, an appropriate and reliable model of mixture rule is required. In fact, the mixture rule developed for conventional composites cannot be used for FGMs as the microstructure in FGMs varies with the volume fractions of the constituents. Moreover, a dispersive phase at one side of FGMs transforms to matrix phase at the other side. Therefore, a special attention is necessary to give while deriving a mixture rule for FGMs. Among various models of mixture rules, which are developed giving emphasis on different aspects of their interests, the mixture rule introduced by Nan *et al.* [55] is adopted in this study, as it appears to be more accurate for the entire range of volume fractions of the constituents. For an FGM whose constituents are *A* and *B*, this mixture rule is given by,

$$V_A \frac{K_A - K}{3K_A + 4\mu} + V_B \frac{K_B - K}{3K_B + 4\mu} = 0, \tag{3.5a}$$

$$V_A \frac{\mu_A - \mu}{\mu_A + Y} + V_B \frac{\mu_B - \mu}{\mu_B + Y} = 0, \tag{3.5b}$$

$$\alpha = V_A \alpha_A \frac{K_A(3K + 4\mu)}{K(3K_A + 4\mu)} + V_B \alpha_B \frac{K_B(3K + 4\mu)}{K(3K_B + 4\mu)}, \tag{3.5c}$$

$$Y = \frac{\mu(9K + 8\mu)}{(6K + 12\mu)}, \tag{3.5d}$$

$$E = \frac{9K\mu}{(3K + \mu)}, \tag{3.5e}$$

where *V* is the volume fraction, *K* is the bulk modulus, *E* is the Young's modulus and μ is the shear modulus of elasticity, α is the coefficient of thermal expansion. The subscripts *A* and *B* denote the respective properties of the constituent materials, and the non-subscripted variables are used to denote the effective properties of the FGM.

Chapter 4 : THEORETICAL FORMULATION OF THE CRACK PROBLEM

Application of FGM as coating around a bearing surface helps preventing wear and oxidation as well as reduce the mismatch thermal stresses, whereby providing strong bondage between substrates and coatings. However, due to inherent imperfections introduced while manufacturing, surface cracking may occur and propagate into the coatings when liquid lubricant exerts considerably high pressure. With small coating thickness around the bearing surface, the system can be considered as infinite plate with FGM coating around a circular hole.

4.1 Modeling of the Problem

In the present model of the problem, consider an FGM coating around a circular hole of radius R in an infinite plate as shown in Fig.4.1, which is referred to the Cartesian coordinate system x-y and the polar coordinate system r-θ having the same origin located at the center of the circular hole. The constituents of the FGM coating are denoted by the materials A and B, and their volume fractions V_A and V_B are assumed to vary in the radial direction only. The FGM coating extends upto the radius R_f. Thus, the region $R \le r \le R_f$ has a gradation of the properties while the infinite region $r > R_f$ is homogeneous consisting of the material B. The continuously and arbitrarily varying Young's modulus, Poisson's ratio and the coefficient of thermal expansion of the FGM coating are represented by E, ν and α, respectively while the corresponding properties of the homogeneous region are, respectively, denoted by E_0, ν_0 and α_0. An incompatible eigenstrain $\varepsilon^*(r)$, which is a function of r only, is induced in the FGM coating due to mismatch in coefficients of thermal expansion when it is cooled from the sintering temperature. The incompatible eigenstrain $\varepsilon^*(r)$ can be defined by

$$\varepsilon^*(r) = (\alpha_0 - \alpha)\Delta T\,, \tag{4.1}$$

where, ΔT is temperature difference between sintering and room temperatures, α is the coefficient of thermal expansion which is determined by using the mixture rule in Eq. (3.5).

For this model of the problem, fracture characteristics will be examined by considering two diametrically opposed radial edge crack emanating from the circular hole and assuming that the surfaces of the hole and the crack are subjected to a uniform pressure p.

4.2 Equivalent Eigenstrain to Simulate Nonhomogeneities

The FGM coating around the circular hole shown in Fig.4.1 is homogenized by a distribution of equivalent eigenstrain. As stated earlier, the equivalent eigenstrain is determined from the condition of identical elastic fields in the uncracked FGM and homogenized coatings subjected to the same loading condition. To determine the elastic fields, we first consider the FGM coating subjected to a uniform applied pressure p around the circular hole. For this purpose, a special technique is adopted in which the FGM coating is radially divided into layers of infinitesimal thickness as shown in Fig. 4.2, which exhibits one half of the elastic medium. Each layer is assumed to have constant material properties but different from those in the other layers. The inner and the outer radii of the ith layer are, respectively, denoted by r_{i-1} and r_i, where $r_0 = R$ and $r_n = R_f$. The region $r > R_f$ is homogeneous. The pressures at the inner and the outer surfaces of the ith layer are, respectively, P_{i-1}^f and P_i^f which are the resultant of the pressures due to the uniform applied pressure p and the incompatible eigenstrain ε^*. For this layered FGM coating, it can be easily shown that the resultant stress components in the ith layer, in axisymmetric case and plane stress condition [50], are

$$\sigma_{r,f}^i = \frac{c_i^2 P_{i-1}^f}{1-c_i^2}\left[1-\frac{r_i^2}{r^2}\right] - \frac{P_i^f}{1-c_i^2}\left[1-c_i^2\frac{r_i^2}{r^2}\right], \tag{4.2a}$$

$$\sigma_{\theta,f}^i = \frac{c_i^2 P_{i-1}^f}{1-c_i^2}\left[1+\frac{r_i^2}{r^2}\right] - \frac{P_i^f}{1-c_i^2}\left[1+c_i^2\frac{r_i^2}{r^2}\right], \tag{4.2b}$$

where

$$c_i = \frac{r_{i-1}}{r_i}, \tag{4.3a}$$

$$P_i^f = p_i^f + p_i^{*,f}. \tag{4.3b}$$

At the right hand side of Eq. (4.3b), the first term appears due to the uniform applied pressure p while the second term appears due to the incompatible eigenstrain ε^*.

The strain and the displacement components in the *i*th layer are derived as

$$\varepsilon^i_{r,f} = \frac{1-\nu_i}{E_i(1-c_i^2)}\left[(c_i^2 P^f_{i-1} - P^f_i) - \frac{1+\nu_i}{1-\nu_i}\frac{r_i^2}{r^2}c_i^2(P^f_{i-1} - P^f_i)\right] + \varepsilon^*_i \,, \tag{4.4a}$$

$$\varepsilon^i_{\theta,f} = \frac{1-\nu_i}{E_i(1-c_i^2)}\left[(c_i^2 P^f_{i-1} - P^f_i) + \frac{1+\nu_i}{1-\nu_i}\frac{r_i^2}{r^2}c_i^2(P^f_{i-1} - P^f_i)\right] + \varepsilon^*_i \,, \tag{4.4b}$$

$$\varepsilon^i_{z,f} = -\frac{2\nu_i}{E_i(1-c_i^2)}\left[c_i^2 P^f_{i-1} - P^f_i\right] + \varepsilon^*_i \,, \tag{4.4c}$$

$$u^f_i = \frac{(1-\nu_i)r_i}{E_i(1-c_i^2)}\left[c_i^2 P^f_{i-1}\left\{\frac{r}{r_i} + \frac{1+\nu_i}{1-\nu_i}\frac{r_i}{r}\right\} - P^f_i\left\{\frac{r}{r_i} + \frac{1+\nu_i}{1-\nu_i}\frac{r_i}{r}c_i^2\right\}\right] + r\varepsilon^*_i \,. \tag{4.5}$$

In deriving the above equations, it has been assumed that all the components of the incompatible eigenstrain are equal *i.e.* $\varepsilon^*_i = \varepsilon^*_{r,i} = \varepsilon^*_{\theta,i} = \varepsilon^*_{z,i}$.

The unknown pressures p^f_i and $p^{*,f}_i$ are determined from the condition that the displacements at $r = r_i$ are identical for the *i*th and the (*i*+1) th layers, which gives

$$\delta^f_{i,i-1} r_{i-1} p^f_{i-1} + \delta^f_{i,i} r_i p^f_i + \delta^f_{i,i+1} r_{i+1} p^f_{i+1} = 0 \quad ; \quad i = 1,2,.....,n-1 \,, \tag{4.6a}$$

$$\delta^f_{i,i-1} r_{i-1} p^{*,f}_{i-1} + \delta^f_{i,i} r_i p^{*,f}_i + \delta^f_{i,i+1} r_{i+1} p^{*,f}_{i+1} = r_i(\varepsilon^*_{i+1} - \varepsilon^*_i) \quad ; \quad i = 1,2,.....,n-1 \,, \tag{4.6b}$$

where

$$\delta^f_{i,i-1} = \frac{2c_i}{E_i(1-c_i^2)} \,, \tag{4.7a}$$

$$\delta^f_{i,i} = -\frac{1}{E_i}\left[\frac{1+c_i^2}{1-c_i^2} - \nu_i\right] - \frac{1}{E_{i+1}}\left[\frac{1+c_{i+1}^2}{1-c_{i+1}^2} + \nu_{i+1}\right], \tag{4.7b}$$

$$\delta^f_{i,i+1} = \frac{2c_{i+1}}{E_{i+1}(1-c_{i+1}^2)} \,, \tag{4.7c}$$

and

$$p^f_0 = p \,, \tag{4.8a}$$

$$p^{*,f}_0 = 0. \tag{4.8b}$$

The stress and displacement components in the region $r > R_f$ are derived as

$$\sigma_{r,f} = -\frac{R_f^2 P_n^f}{r^2}; \ , \tag{4.9a}$$

$$\sigma_{\theta,f} = \frac{R_f^2 P_n^f}{r^2}; \ , \tag{4.9b}$$

$$u^f = \frac{R_f^2 P_n^f}{2\mu_0 r}; \ . \tag{4.10}$$

To solve Eq. (4.6), it is necessary to know the pressures p_n^f and $p_n^{*,f}$ at the outer surface of the *n*th layer. These are determined from the condition that the displacements u_n^f of the *n*th layer and u^f of the homogeneous region are equal at $r = R_f$. From this condition, we obtain

$$p_n^f = \frac{2E_0 c_n^2 p_{n-1}^f}{(1+\nu_0)E_n(1-c_n^2) + E_0\{(1-\nu_n)+(1+\nu_n)c_n^2\}}, \tag{4.11a}$$

$$p_n^{*,f} = \frac{E_0 E_n \varepsilon_n^* (1-c_n^2) + 2E_0 c_n^2 p_{n-1}^{*,f}}{(1+\nu_0)E_n(1-c_n^2) + E_0\{(1-\nu_n)+(1+\nu_n)c_n^2\}}. \tag{4.11b}$$

Now we consider a homogeneous infinite medium with the same geometry and determine the elastic field in the region of the coating following the same procedure as FGM coating. In this case, the pressure at the outer surface of the *n*th layer is taken same as FGM coating so as to achieve the same elastic field in the region $r > R_f$. The equivalency in the elastic fields of the region $R \le r \le R_f$ is achieved by assuming a distribution of equivalent eigenstrain. First, we determine the elastic field in the *i*th layer of the coating region due to the uniform applied pressure *p* and the incompatible eigenstrain ε^* as,

$$\sigma_{r,h_0}^i = \frac{c_i^2 P_{i-1}^h}{1-c_i^2}\left[1-\frac{r_i^2}{r^2}\right] - \frac{P_i^h}{1-c_i^2}\left[1-c_i^2\frac{r_i^2}{r^2}\right], \tag{4.12a}$$

$$\sigma_{\theta,h_0}^i = \frac{c_i^2 P_{i-1}^h}{1-c_i^2}\left[1+\frac{r_i^2}{r^2}\right] - \frac{P_i^h}{1-c_i^2}\left[1+c_i^2\frac{r_i^2}{r^2}\right], \tag{4.12b}$$

$$\varepsilon_{r,h_0}^i = \frac{1-\nu_0}{E_0(1-c_i^2)}\left[(c_i^2 P_{i-1}^h - P_i^h) - \frac{1+\nu_0}{1-\nu_0}\frac{r_i^2}{r^2}c_i^2(P_{i-1}^h - P_i^h)\right] + \varepsilon_i^*, \tag{4.13a}$$

$$\varepsilon^{i}_{\theta,h_0} = \frac{1-\nu_0}{E_0(1-c_i^2)}\left[(c_i^2 P^h_{i-1} - P^h_i) + \frac{1+\nu_0}{1-\nu_0}\frac{r_i^2}{r^2}c_i^2(P^h_{i-1} - P^h_i)\right] + \varepsilon^*_i \,, \tag{4.13b}$$

$$\varepsilon^{i}_{z,h_0} = -\frac{2\nu_0}{E_0(1-c_i^2)}\left[c_i^2 P^h_{i-1} - P^h_i\right] + \varepsilon^*_i \,, \tag{4.13c}$$

$$u^{h_0}_i = \frac{(1-\nu_0)r_i}{E_0(1-c_i^2)}\left[c_i^2 P^h_{i-1}\left\{\frac{r}{r_i} + \frac{1+\nu_0}{1-\nu_0}\frac{r_i}{r}\right\} - P^h_i\left\{\frac{r}{r_i} + \frac{1+\nu_0}{1-\nu_0}\frac{r_i}{r}c_i^2\right\}\right] + r\varepsilon^*_i \,, \tag{4.14}$$

where,

$$P^h_i = p^h_i + p^{*,h}_i. \tag{4.15}$$

The unknown pressures p^h_i and $p^{*,h}_i$ are, respectively, determined from the following equations:

$$\delta^h_{i,i-1} r_{i-1} p^h_{i-1} + \delta^h_{i,i} r_i p^h_i + \delta^h_{i,i+1} r_{i+1} p^h_{i+1} = 0 \quad ; \quad i = 1,2,.....,n-1 \,, \tag{4.16a}$$

$$\delta^h_{i,i-1} r_{i-1} p^{*,h}_{i-1} + \delta^h_{i,i} r_i p^{*,h}_i + \delta^h_{i,i+1} r_{i+1} p^{*,h}_{i+1} = r_i(\varepsilon^*_{i+1} - \varepsilon^*_i) \quad ; \quad i = 1,2,.....,n-1 \,, \tag{4.16b}$$

where,

$$\delta^h_{i,i-1} = \frac{2c_i}{E_0(1-c_i^2)} \,, \tag{4.17a}$$

$$\delta^h_{i,i} = -\frac{1}{E_0}\left[\frac{1+c_i^2}{1-c_i^2} + \frac{1+c_{i+1}^2}{1-c_{i+1}^2}\right], \tag{4.17b}$$

$$\delta^h_{i,i+1} = \frac{2c_{i+1}}{E_0(1-c_{i+1}^2)} \,, \tag{4.17c}$$

and,

$$p^h_0 = p \,, \tag{4.18a}$$

$$p^h_n = p^f_n \,, \tag{4.18b}$$

$$p^{*,h}_0 = 0 \,, \tag{4.18c}$$

$$p^{*,h}_n = p^{*,f}_n. \tag{4.18d}$$

Now we assume a distribution of equivalent eigenstrain $\varepsilon_{j,e}^{i}$ in the ith layer of the coating region, where $j = r,\ \theta$ and z. From the equivalency of the stress fields in the coating regions, we can write

$$\sigma_{r,f}^{i} = \sigma_{r,h_0}^{i} + \sigma_{r,e}^{i}\ , \tag{4.19a}$$

$$\sigma_{\theta,f}^{i} = \sigma_{\theta,h_0}^{i} + \sigma_{\theta,e}^{i}\ , \tag{4.19b}$$

where $\sigma_{r,e}^{i}$ and $\sigma_{\theta,e}^{i}$ are, respectively, the radial and the circumferential stress components in the ith layer of the coating region of the homogeneous medium due to the equivalent eigenstrain $\varepsilon_{j,e}^{i}$.

From the equivalency of the total strains, we can write,

$$\varepsilon_{r,f}^{i} = \varepsilon_{r,h_0}^{i} + e_{r,e}^{i} + \varepsilon_{r,e}^{i}\ , \tag{4.20a}$$

$$\varepsilon_{\theta,f}^{i} = \varepsilon_{\theta,h_0}^{i} + e_{\theta,e}^{i} + \varepsilon_{\theta,e}^{i}\ , \tag{4.20b}$$

$$\varepsilon_{z,f}^{i} = \varepsilon_{z,h_0}^{i} + e_{z,e}^{i} + \varepsilon_{z,e}^{i}\ , \tag{4.20c}$$

where $e_{j,e}^{i}$ is the elastic strain associated with the equivalent eigenstrain $\varepsilon_{j,e}^{i}$ in the ith layer of the coating region of the homogeneous medium.

The elastic strain $e_{j,e}^{i}$ is related to the stress $\sigma_{j,e}^{i}$ by Hooke's law as follows

$$e_{r,e}^{i} = \frac{1}{E_0}\left[\sigma_{r,e}^{i} - \nu_0 \sigma_{\theta,e}^{i}\right], \tag{4.21a}$$

$$e_{\theta,e}^{i} = \frac{1}{E_0}\left[\sigma_{\theta,e}^{i} - \nu_0 \sigma_{r,e}^{i}\right], \tag{4.21b}$$

$$e_{z,e}^{i} = -\frac{\nu_0}{E_0}\left[\sigma_{r,e}^{i} + \sigma_{\theta,e}^{i}\right]. \tag{4.21c}$$

Combining Eqs. (4.2), (4.3), (4.12), (4.13) and (4.19)-(4.20), the expressions for the equivalent eigenstrains in the ith layer can be derived as

$$\varepsilon_{r,e}^{i} = \frac{1-\nu_i}{E_i(1-c_i^2)}\left[(c_i^2 P_{i-1}^f - P_i^f) - \frac{1+\nu_i}{1-\nu_i}\frac{r_i^2}{r^2}c_i^2(P_{i-1}^f - P_i^f)\right]$$
$$-\frac{1-\nu_0}{E_0(1-c_i^2)}\left[(c_i^2 P_{i-1}^h - P_i^h) - \frac{1+\nu_0}{1-\nu_0}\frac{r_i^2}{r^2}c_i^2(P_{i-1}^h - P_i^h)\right]$$
$$+\frac{1}{E_0(1-c_i^2)}\left[c_i^2\left(1-\frac{r_i^2}{r^2}\right)(P_{i-1}^h - P_{i-1}^f) - \left(1-c_i^2\frac{r_i^2}{r^2}\right)(P_i^h - P_i^f)\right]$$
$$-\frac{\nu_0}{E_0(1-c_i^2)}\left[c_i^2\left(1+\frac{r_i^2}{r^2}\right)(P_{i-1}^h - P_{i-1}^f) - \left(1+c_i^2\frac{r_i^2}{r^2}\right)(P_i^h - P_i^f)\right], \tag{4.22a}$$

$$\varepsilon_{\theta,e}^{i} = \frac{1-\nu_i}{E_i(1-c_i^2)}\left[(c_i^2 P_{i-1}^f - P_i^f) + \frac{1+\nu_i}{1-\nu_i}\frac{r_i^2}{r^2}c_i^2(P_{i-1}^f - P_i^f)\right]$$
$$-\frac{1-\nu_0}{E_0(1-c_i^2)}\left[(c_i^2 P_{i-1}^h - P_i^h) + \frac{1+\nu_0}{1-\nu_0}\frac{r_i^2}{r^2}c_i^2(P_{i-1}^h - P_i^h)\right]$$
$$+\frac{1}{E_0(1-c_i^2)}\left[c_i^2\left(1+\frac{r_i^2}{r^2}\right)(P_{i-1}^h - P_{i-1}^f) - \left(1+c_i^2\frac{r_i^2}{r^2}\right)(P_i^h - P_i^f)\right]$$
$$-\frac{\nu_0}{E_0(1-c_i^2)}\left[c_i^2\left(1-\frac{r_i^2}{r^2}\right)(P_{i-1}^h - P_{i-1}^f) - \left(1-c_i^2\frac{r_i^2}{r^2}\right)(P_i^h - P_i^f)\right], \tag{4.22b}$$

$$\varepsilon_{z,e}^{i} = \frac{2\nu_0}{E_0(1-c_i^2)}(c_i^2 P_{i-1}^h - P_i^h) - \frac{2\nu_i}{E_i(1-c_i^2)}(c_i^2 P_{i-1}^f - P_i^f)$$
$$-\frac{2\nu_0}{E_0(1-c_i^2)}\left[c_i^2(P_{i-1}^h - P_{i-1}^f) - (P_i^h - P_i^f)\right]. \tag{4.22c}$$

Although the equivalent eigenstrains derived above and the incompatible eigenstrain ε_i^* are stepwise continuous, discontinuities in their values occur at the interfaces between the layers, which are physically inadmissible for an FGM with continuously varying material properties. Therefore, for physically admissible results, we obtain continuous distributions of the equivalent and the incompatible eigenstrains for the non-layered coating region of the homogeneous medium, as shown in Fig. 4.3, by spline interpolation of the stepwise continuous eigenstrains. Including this equivalent eigenstrain, the resultant stress components in the non-layered homogeneous medium as shown in Fig. 4.3 are derived as,

$$\sigma_r^h = \frac{pR^2}{R_f^2 - R^2}\left[1 - \frac{R_f^2}{r^2}\right] - \frac{R_f^2(p_n^f + p_n^{*,f})}{R_f^2 - R^2}\left[1 - \frac{R^2}{r^2}\right]$$
$$+E_0\left[-\frac{1}{r^2}\int_R^r r\varepsilon^* dr + \left(1 - \frac{R^2}{r^2}\right)\frac{1}{R_f^2 - R^2}\int_R^{R_f} r\varepsilon^* dr\right]$$
$$+\frac{E_0}{2}\left[-\frac{1}{r^2}\int_R^r r(\varepsilon_r^e + \varepsilon_\theta^e)dr + \int_R^r \frac{1}{r}(\varepsilon_r^e - \varepsilon_\theta^e)dr + C\left\{1 - \frac{R^2}{r^2}\right\}\right]; R \le r \le R_f \tag{4.23a}$$

$$\sigma_\theta^h = \frac{pR^2}{R_f^2 - R^2}\left[1 + \frac{R_f^2}{r^2}\right] - \frac{R_f^2(p_n^f + p_n^{*,f})}{R_f^2 - R^2}\left[1 + \frac{R^2}{r^2}\right]$$
$$+E_0\left[-\varepsilon^* + \frac{1}{r^2}\int_R^r r\varepsilon^* dr + \left(1 + \frac{R^2}{r^2}\right)\frac{1}{R_f^2 - R^2}\int_R^{R_f} r\varepsilon^* dr\right]$$
$$+\frac{E_0}{2}\left[-2\varepsilon_\theta^e + \frac{1}{r^2}\int_R^r r(\varepsilon_r^e + \varepsilon_\theta^e)dr + \int_R^r \frac{1}{r}(\varepsilon_r^e - \varepsilon_\theta^e)dr + C\left\{1 + \frac{R^2}{r^2}\right\}\right]; R \le r \le R_f, \tag{4.23b}$$

$$\sigma_r^h = -\frac{p_n^f R_f^2}{r^2} - \frac{p_n^{*,f} R_f^2}{r^2}; r \ge R_f, \tag{4.23c}$$

$$\sigma_\theta^h = \frac{p_n^f R_f^2}{r^2} + \frac{p_n^{*,f} R_f^2}{r^2}; r \ge R_f, \tag{4.23d}$$

where,

$$C = \frac{1}{R_f^2 - R^2}\left\{\int_R^{R_f} r(\varepsilon_r^e + \varepsilon_\theta^e)dr - R_f^2\int_R^{R_f}\frac{1}{r}(\varepsilon_r^e - \varepsilon_\theta^e)dr\right\}, \tag{4.24}$$

and ε^* and ε_j^e represent, respectively, the incompatible and the equivalent eigenstrain distributions which are continuous over the entire range of interest.

4.3 Formulation for Stress Intensity Factor

The stress field in the uncracked homogeneous infinite medium shown in Fig. 4.3 has been determined in the preceding section. Now let us consider two diametrically opposed radial edge cracks of equal length *l* each emanating from the circular hole in this homogeneous infinite plate as shown in Fig. 4.4. The surfaces of the hole and the crack are subjected to the uniform applied pressure *p*. In this case, the boundary condition along the crack surface given by Eq. (3.1) reduces to

Crack I : $\sigma_\theta^d = -\sigma_\theta^h - p$; $R \le r \le l + R, \theta = 0^0$. (4.25a,b)

Crack II : $\sigma_\theta^d = -\sigma_\theta^h - p$; $R \le r \le l + R, \theta = 180^0$

The stress component σ_θ^h in the uncracked homogenized plate has been determined in the previous section. The disturbed stress field σ_θ^d can be determined by representing the crack by a continuous distribution of edge dislocations. The method of complex potential functions is used to calculate the stress field due to the edge dislocations. The complex potential functions for an edge dislocation making an angle β with the positive x axis and passing through a point $z = h$ in an infinite medium with a circular hole of radius R as shown in Fig. 4.5, are given by[50]

$$\Phi(z) = \frac{i\mu_0(b_1 + ib_2)}{\pi(\kappa_0 + 1)} e^{i\beta} \frac{1}{z - h} + \sum_{k=0}^{\infty} a_k z^{-k} \tag{4.26a}$$

$$\Psi(z) = -\frac{i\mu_0(b_1 - ib_2)}{\pi(\kappa_0 + 1)} e^{-i\beta} \frac{1}{z - h} + \frac{i\mu_0(b_1 + ib_2)}{\pi(\kappa_0 + 1)} \frac{\bar{h}}{(z - h)^2} e^{i\beta} + \sum_{k=0}^{\infty} a_k' z^{-k} , \tag{4.26b}$$

where $h = R+s, b_1$ and b_2 are the components of Burgers vector, and κ_0 is Kolosov's constant which is equal to $(3-\nu_0)/(1+\nu_0)$ for plane stress condition and $z = x + iy = re^{i\theta}$

and,

$a_0, a_0' = 0$, for dislocation only as it represent stress distribution at infinity (4.27a)

$a_1 = -B_p$, (4.27b)

$a_1' = -\overline{B_P}$, (4.27c)

$a_2 = -\overline{B_p} \frac{R^4}{\bar{h}^3} + \overline{B_p} \frac{hR^2}{\bar{h}^2} + \overline{B_m} \frac{R^2}{\bar{h}}$, (4.27d)

$a_2' = B_m \frac{R^2}{\bar{h}} - B_p \frac{R^2}{h}$, (4.27e)

$a_k = \overline{B_p}(k-1)[\frac{hR^{2(k-1)}}{\bar{h}^k} - \frac{R^{2k}}{\bar{h}^{k+1}}] + \overline{B_m} \frac{R^{2(k-1)}}{\bar{h}^{k-1}}; k \ge 3$, (4.27f)

$a_k' = \overline{B_p}(k-1)(k-3)[\frac{hR^{2(k-2)}}{\bar{h}^{(k-2)}} - \frac{R^{2(k-1)}}{\bar{h}^{(k-1)}}] + \overline{B_m}(k-1)\frac{R^{2k}}{\bar{h}^{(k-1)}} + B_m \frac{R^{2(k-1)}}{\bar{h}^{(k-1)}}$, (4.27g)

$$B_p = Pi(b_1 + ib_2)e^{i\beta} \ , \tag{4.27h}$$

$$\overline{B_p} = -Pi(b_1 - ib_2)e^{-i\beta} \ , \tag{4.27i}$$

$$B_m = Pi(b_1 - ib_2)e^{-i\beta} \ , \tag{4.27j}$$

$$\overline{B}_m = -Pi(b_1 + ib_2)e^{i\beta} \ , \tag{4.27k}$$

In the present study, two diametrically opposed radial edge cracks, crack I and crack II emanating from the surface of a circular hole are considered. For crack I the disturbed stress component is first determined. Now we consider that, for this crack, the discrete edge dislocation is located on the *x* axis and at a distance $h=R+s$. For this configuration of the dislocation β=-90^o,so $e^{i\beta} = \cos 90^0 - i\sin 90^0 = -i$.

Also, for the orientation shown, the crack tip experiences mode I deformation only. So, $b_2 = 0$

Now, the complex potential functions of Eqs.(4.26a) and(4.26b)can be written as

$$\Phi(z) = \frac{\mu_0 b}{\pi(\kappa_0 + 1)}\left[\frac{1}{z-h} - \frac{1}{z} - \frac{R^4}{h^3}\frac{1}{z^2} + \sum_{k=3}^{\infty} A_k z^{-k}\right] \ , \tag{4.28a}$$

$$\Psi(z) = \frac{\mu_0 b}{\pi(\kappa_0 + 1)}\left[\frac{1}{z-h} - \frac{1}{z} + \frac{h}{(z-h)^2} - \frac{2R^2}{h}\frac{1}{z^2} + \sum_{k=3}^{\infty} A'_k z^{-k}\right] \ , \tag{4.28b}$$

where,

$$a_k = \frac{\mu_0 b}{\pi(k_0 + 1)} A_K \ , \tag{4.29a}$$

$$a'_k = \frac{\mu_0 b}{\pi(k_0 + 1)} A'_K , \tag{4.29b}$$

$$A_k = (k-2)\frac{R^{2(k-1)}}{h^{k-1}} - (k-1)\frac{R^{2k}}{h^{k+1}}; \quad k \geq 3, \tag{4.29c}$$

$$A'_k = (k-1)(k-4)\frac{R^{2(k-2)}}{h^{k-3}} - (k-2)^2\frac{R^{2(k-1)}}{h^{k-1}}; \quad k \geq 3. \tag{4.29d}$$

If the crack is represented by a continuous distribution of edge dislocation, the potential functions are rewritten as [53]

$$\Phi(z)=\frac{\mu_0}{\pi(\kappa_0+1)}\int_0^l\left[\frac{1}{z-h}-\frac{1}{z}-\frac{R^4}{h^3}\frac{1}{z^2}+\sum_{k=3}^{\infty}A_k z^{-k}\right]b(s)ds\,, \tag{4.30a}$$

$$\Psi(z)=\frac{\mu_0}{\pi(\kappa_0+1)}\int_0^l\left[\frac{1}{z-h}-\frac{1}{z}+\frac{h}{(z-h)^2}-\frac{2R^2}{h}\frac{1}{z^2}+\sum_{k=3}^{\infty}A'_k z^{-k}\right]b(s)ds\,. \tag{4.30b}$$

The stresses can be expressed in terms of the complex potentials $\Phi(z)$, $\Psi(z)$ and their complex conjugates as below [56]**:**

$$\sigma_\theta^d+i\sigma_{r\theta}^d=\Phi(z)+\overline{\Phi(z)}+\left[\bar{z}\Phi'(z)+\Psi(z)\right]e^{2i\theta}, \tag{4.31a}$$

$$\sigma_r^d-i\sigma_{r\theta}^d=\Phi(z)+\overline{\Phi(z)}-\left[\bar{z}\Phi'(z)+\Psi(z)\right]e^{2i\theta}\,. \tag{4.31b}$$

By using Eqs. (4.30) and (4.31), we can easily obtain the circumferential stress component along the crack line of crack I ($\theta=0^{\circ}, z=re^{i\theta}=r=\bar{z}$, r= R+x, for horizontal orientation of cracks h=R+s) as follows

$$\begin{aligned}[\sigma_\theta^d+i\sigma_{r\theta}^d]_{\mathrm{I}}=\frac{2\mu_0}{\pi(\kappa_0+1)}\int_0^l\Bigg[&\frac{1}{x-s}-\frac{1}{R+x}-\frac{R^2}{R+s}\frac{1}{(R+x)^2}+\frac{1}{2}\sum_{k=3}^{\infty}(2-k)A_k(R+x)^{-k}\\&+\frac{1}{2}\sum_{k=3}^{\infty}A'_k(R+x)^{-k}\Bigg]b(s)ds,\end{aligned} \tag{4.32}$$

where,

$$A_k=(k-2)\frac{R^{2(k-1)}}{(R+s)^{k-1}}-(k-1)\frac{R^{2k}}{(R+s)^{k+1}};\quad k\geq 3\,, \tag{4.33a}$$

$$A'_k=(k-1)(k-4)\frac{R^{2(k-2)}}{(R+s)^{k-3}}-(k-2)^2\frac{R^{2(k-1)}}{(R+s)^{k-1}};\quad k\geq 3\,. \tag{4.33b}$$

Now, crack II is considered and the discrete edge dislocation for this crack is shown in Fig. 4.6. For the configuration of the dislocation shown, $\beta=+90^0$,

So, $e^{i\beta} = \cos 90^0 + i \sin 90^0 = +i$.

This crack is also represented by a continuous distribution of edge dislocations. Following the similar procedure as crack I, the stresses along the crack line of crack I due to crack II is determined by setting $\theta = -180^0$ and considering b_1 as negative in Eq. (4.26). Finally, one obtains,

$$[\sigma_\theta^d + i\sigma_{r\theta}^d]_{II} = -\frac{2\mu_0}{\pi(\kappa_0+1)}\int_0^l \left[\frac{1}{2R+x+s} - \frac{1}{R+x} + \frac{R^2}{R+s}\frac{1}{(R+x)^2} + \frac{1}{2}\sum_{k=3}^{\infty}(2-k)A_k(R+x)^{-k} + \frac{1}{2}\sum_{k=3}^{\infty}A_k'(R+x)^{-k}\right] b(s)ds, \tag{4.34}$$

where,

$$A_k = (k-2)\frac{R^{2(k-1)}}{(-1)^{k-1}(R+s)^{k-1}} - (k-1)\frac{R^{2k}}{(-1)^{k+1}(R+s)^{k+1}}; \quad k \geq 3, \tag{4.35a}$$

$$A_k' = (k-1)(k-4)\frac{R^{2(k-2)}}{(-1)^{k-3}(R+s)^{k-3}} - (k-2)^2\frac{R^{2(k-1)}}{(-1)^{k-1}(R+s)^{k-1}}; \quad k \geq 3. \tag{4.35b}$$

Now, superposition of Eqs. (4.32) and (4.34) gives the resultant circumferential stress component of the disturbed stress field along the crack line of crack I as:

$$\sigma_\theta^d = \frac{2\mu_0}{\pi(k_0+1)}\int_0^l \left[\frac{1}{x-s} + f_1(r,h) - \frac{1}{2R+x+s} - f_2(r,h)\right] b(s)ds, \tag{4.36}$$

where,

$$f_1(r,h) = -\frac{1}{R+x} - \frac{R^2}{R+s}\frac{1}{(R+x)^2} + \frac{1}{2}\sum_{k=3}^{\infty}(2-k)A_k(R+x)^{-k} + \frac{1}{2}\sum_{k=3}^{\infty}A_k'(R+x)^{-k}, \tag{4.37a}$$

$$f_2(r,h) = -\frac{1}{R+x} + \frac{R^2}{R+s}\frac{1}{(R+x)^2} + \frac{1}{2}\sum_{k=3}^{\infty}(2-k)A_k(R+x)^{-k} + \frac{1}{2}\sum_{k=3}^{\infty}A_k'(R+x)^{-k}. \tag{4.37b}$$

The boundary condition along the crack line of crack I given by Eq. (4.25) reduce to

$$\frac{2\mu_0}{\pi(k_0+1)}\int_0^l[\frac{1}{x-s}+f_1(r,h)-\frac{1}{2R+x+s}-f_2(r,h)]b(s)ds=-p(S_f\frac{\sigma_\theta^h}{\sigma_u}+1);R_i\le r\le R_i+l,\theta=0^0.$$

(4.38)

Where S_f is the strength factor defined by the ratio of the ultimate strength σ_u of the base material B to the applied internal pressure p. Equation (4.38) is the singular integral equations for the unknown density function $b(s)$, which is normalized over the interval [-1,+1] by using the substitutions,

$$H=\frac{2t}{l}-1, \tag{4.39a}$$

$$T=\frac{2s}{l}-1, \tag{4.39b}$$

$$D=\frac{2R}{l}. \tag{4.39c}$$

Finally, we obtain

$$\frac{2\mu_0}{\pi(\kappa_0+1)}\int_{-1}^1[\frac{1}{H-T}+G_1(H,T)+G_2(H,T)+G_1'(H,T)+G_2'(H,T)+G_3'(H,T)]B(T)dT$$
$$=-\sigma_\theta^h-p;-1\le H\le 1.$$

(4.40)

where,

$$B(T)=b\left(\frac{l}{2}T\right), \tag{4.41a}$$

$$G_1(H,T)=-\frac{1}{D+H+1}-\frac{D^2}{(D+T+1)(D+H+1)^2}, \tag{4.41b}$$

$$G_2(H,T)=\frac{1}{2}\sum_{k=3}^{\infty}(2-k)B_k(D+H+1)^{-k}+\frac{1}{2}\sum_{k=3}^{\infty}B_k'(D+H+1)^{-k}, \tag{4.41c}$$

$$G_1'(H,T)=-\frac{1}{2D+H+T+2}, \tag{4.41d}$$

$$G_2'(H,T)=\frac{1}{D+H+1}-\frac{D^2}{(D+T+1)(D+H+1)^2}, \tag{4.41e}$$

$$G_3'(H,T)=-\frac{1}{2}\sum_{k=3}^{\infty}(2-k)C_k(D+H+1)^{-k}-\frac{1}{2}\sum_{k=3}^{\infty}C_k'(D+H+1)^{-k}, \tag{4.41f}$$

$$B_k=(k-2)\frac{D^{2(k-1)}}{(D+T+1)^{k-1}}-(k-1)\frac{D^{2k}}{(D+T+1)^{k+1}}, \tag{4.41g}$$

$$B_k'=(k-1)(k-4)\frac{D^{2(k-2)}}{(D+T+1)^{k-3}}-(k-2)^2\frac{D^{2(k-1)}}{(D+T+1)^{k-1}},. \tag{4.41h}$$

$$C_k=(k-2)\frac{D^{2(k-1)}}{(-1)^{k-1}(D+T+1)^{k-1}}-(k-1)\frac{D^{2k}}{(-1)^{k+1}(D+T+1)^{k+1}}, \tag{4.41i}$$

$$C_k'=(k-1)(k-4)\frac{D^{2(k-2)}}{(-1)^{k-3}(D+T+1)^{k-3}}-(k-2)^2\frac{D^{2(k-1)}}{(-1)^{k-1}(D+T+1)^{k-1}}. \tag{4.41j}$$

The density function $B(T)$ can be expressed as the product of a fundamental function $w(T)$ which characterizes the bounded-singular behavior of $B(T)$ and a bounded continuous function $\varphi(T)$ in the closed interval $-1 \le T \le +1$. Thus, we can formulate

$$B(T)=w(T)\varphi(T). \tag{4.42}$$

In the present case, the fundamental function can be given by

$$w(T)=\sqrt{\frac{(1+T)}{(1-T)}}. \tag{4.43}$$

Using the Gauss-Jacobi integral formula corresponding to the weight function in Eq. (4.42) in the manner developed by Erdogan et al. [57] Eq. (4.40) can be converted to a system of algebraic equations to determine the unknowns $\varphi(T_j)$ as follows

$$\frac{2\mu_0}{(\kappa_0+1)}\sum_{j=1}^{N}(1+T_j)\left[\frac{1}{H_i-T_j}+G_1(H_i,T_j)+G_2(H_i,T_j)+G_1'(H_i,T_j)+G_2'(H_i,T_j)+G_3'(H_i,T_j)\right]\phi(T_j)$$
$$=-\frac{2N+1}{2}\left[\sigma_\theta^h(H_i)+p\right];\ i=1,2,3,...,N;\ -1\le H\le 1. \tag{4.44}$$

The integration and collocation points are given by

$$T_j=\cos\left(\frac{2j-1}{2N+1}\pi\right);\ j=1,2,3,...,N, \tag{4.45a}$$

$$H_i=\cos\left(\frac{2\pi i}{2N+1}\right);\ i=1,2,3,...,N. \tag{4.45b}$$

It can be readily shown that the stress intensity factor can be derived as[58]

$$K_I=\sqrt{2\pi l}\,\frac{2\mu_0}{(\kappa_0+1)}\varphi(+1), \tag{4.46}$$

where $\varphi(+1)$ is computed by Krenk's interpolation formula [59] given by

$$\varphi(+1)=\frac{2}{2N+1}\sum_{j=1}^{N}\frac{\sin\left(\frac{2j-1}{2N+1}N\pi\right)}{\tan\left(\frac{2j-1}{2N+1}\frac{\pi}{2}\right)}\varphi(T_j). \tag{4.47}$$

The solution of Eq. (4.43) provides the unknowns $\varphi(T_j)$ which are used in Eq. (4.47) to determine the value of $\varphi(+1)$ and then the stress intensity factor can be computed from Eq. (4.46).

4.4 Approach of Evaluating Apparent Fracture Toughness

In this section, an approach is introduced to evaluate apparent fracture toughness (AFT) using the formulations of SIFs discussed in the article 4.2. Equations (4.44) to (4.47) determine the SIF due to combined effect of the eigenstrain and applied internal pressure. Therefore, the critical value of SIF

at the crack tip determined from Eqs (4.44) to (4.47) must be equal to the intrinsic fracture toughness, determined form the Eq (3.4) of the point of crack tip position. It is noted that the right hand side of Eq. (4.44) is the function of eigenstrains and applied internal pressure. It is noted that, the eigenstrain is considered to be a function of material composition. Therefore, for a prescribed material composition and crack length, this equation can be solved in terms of unknown internal pressure p in the form of

$$K_I = k_e + k_p p \,. \tag{4.48}$$

where k_e is the SIF associated with the eigenstrain and k_p is the factor associated with the coefficient of p in Eq. (4.44). Then, Eqs. (3.2) and (4.48) are equated to determine the critical value of internal pressure p_c corresponding to given crack length. Note that the right hand side of Eq. (3.2) is known as the material composition is already prescribed from which E can be determined by using the mixture rule formula given by Nan et al.[56]. The critical value of internal pressure p_c is then used in Eq. (3.3) to determine the AFT of the point of the crack tip position. Equations (4.44) to (4.47) are repeatedly solved by varying the crack length and the AFT is determined at the position of crack tip following the above procedure.

4.5 Direct Problem

In direct problems, the fracture characteristics of cylinders with an FGM coating are analyzed for assumed functions of the material properties. To calculate the stress intensity factors, first, the effective properties of the FGM cylinder are determined for an assumed material composition in the FGM cylinder by using the mixture rule given by Eqs. (3.5a) to (3.5e). Then, we can calculate the equivalent eigenstrain by using Eq. (4.22) and the resultant stress σ_θ^h from Eq. (4.23b). From Eqs. (4.44) to (4.47), we can then determine the stress intensity factor for the FGM cylinder.

Chapter 5 : NUMERICAL RESULTS AND DISCUSSIONS

Numerical results are obtained for a TiC/Al_2O_3 FGM coating around a hole in an infinite plate in which the constituents TiC and Al_2O_3 correspond to the materials A and B, respectively. The characteristic dimensions R and R_f are taken as 10 mm and 11 mm, respectively. In numerical calculations, the number of layers of infinitesimal thickness shown in Fig. 4-2 is chosen as 50.The mechanical and thermal properties of the constituent as displayed in Table.5.1.

5.1 Verification of the Method

The approximation method of calculating stress intensity factors of an infinite plate with two diametrically-opposed radial edge cracks emanating from the inner surface of a circular hole with an FGM coating is first verified by applying the method for a homogeneous plate. By setting $V_A = 0$ or uniform distribution of V_A throughout the FGM coating, one obtains a homogeneous plate with a circular hole. The normalized stress intensity factors $F_I = K_I / p\sqrt{\pi(cl + R)}$ are calculated for such a homogeneous plate for R/R_f=1.1 and compared with those available in literatures as shown in Fig. 5.1. The solid line represents the results obtained by the present method while the dotted line represents the results obtained using Boundary-Collocation Method by Newman [60]. The results correspond to nl=10 in Eqs.(4.44).It is observed that the results obtained by the present method agree well with those obtained by Newman for the entire range of normalized crack length $(cl + R) / R$. This satisfies the validity of the present approximation method of evaluating SIFs.

5.2 Stress Intensity Factors for Prescribed Material Compositions

In this study, the stress intensity factors are calculated for an infinite plate with two diametrically-opposed radial edge cracks emanating from the inner surface of a circular hole with an FGM coating for four different prescribed material distributions as shown by the curves in Fig. 5.2. The volume fraction of material A varies only in the FGM coating. Although any material distribution can be considered, these four distributions are considered here merely for examples. For these prescribed material distributions and Rf/R= 1.1, strength factor S_f=1.0, normalized stress intensity factor F_1 versus normalized crack length $(cl+R)/R$ is plotted in Fig. 5.3. For all the cases with the increase of the crack length cl. This reflects the usual characteristic of SIFs of conventional

materials. The lowest value of SIF is obtained for the uniform material distribution. However, the uniform distribution is not recommended as it has a sharp interface that causes the problem of delamination. Further, among three other distributions, the stress intensity factor for parabolic upward distribution is the minimum for the lower range of crack length. This is due to the fact that this material distribution has the higher gradient near surface of the plate which produces more incompatibility in the eigenstrain giving higher magnitude of compressive eigenstress. This compressive eigenstress attributes to the reduction in the stress intensity factor. Thus, it can be said that the FGM coating having the higher gradient would have the lower stress intensity factor.

The effect of the FGM coating thickness in the plate are shown in Fig. 5.4 and Fig. 5.5. In Fig. 5.4 the stress intensity factors are plotted for different values of R_f/R for linear material composition and S_f=1.0. Here, the layer thinness has been varied by keeping the number of layers fixed, nl=10. On the other hand, in Fig. 5.5 the same plot is done varying the number of layers and keeping the layers thickness $(R_f-R)/nl$ fixed at 0.2.In both the cases, it is observed that for higher coating thickness the stress intensity factor is less, thus has more toughness against crack propagation. Furthermore, it is found that the layer thickness or the number of layers have little effect on the overall pattern or value of stress intensity factors.

The effects of strength factor S_f on the stress intensity factor are also examined and shown in Fig. 5.6. The results correspond to the linear material distribution and R_f/R=1.1. The stress intensity factor decreases as the strength factor increases. This is because the higher value of strength factor represents the lower value of applied load p.

The effect of ΔT , that represents the difference between sintering and application temperatures of the plate with FGM coating on the stress intensity factor can also be examined by the present method. If the FGM coated plate is used in an application of elevated temperature (higher than the room temperature), the value of ΔT will be smaller. Its effect is shown in Fig. 5.7 which is plotted for the linear material distribution shown in Fig. 5.2. It is observed that the stress intensity factor rises as the value of ΔT decreases, i.e. at higher application temperature of the FGM coated plate. This conforms to the physical phenomenon that at lower value of ΔT, the eigenstrain developed in the plate becomes lower.

A comparison between the stress intensity factors for a single radial edge crack and two diametrically opposed edge cracks is depicted in Fig.5.8. The stress intensity factors for a single

radial edge crack can be calculated by setting $G_1'(H_i,T_j)+G_2'(H_i,T_j)+G_3'(H_i,T_j)=0$ in Eq. (4.38). The results are obtained for S_f=1.0, R_f/R = 1.1. Note that the stress intensity factor is higher in the case of two diametrically-opposed cracks for any of the material distributions especially for a larger crack length. The comparison of stress intensity factors for a single and two diametrically-opposed edge cracks around a circular hole of an infinite plate with FGM coating for linear material distribution are shown in Fig.5.9. The stress intensity factors calculated for R_f/R = 2.5 and S_f=1.0. For single and double edge cracks SIF are very close over the inner region of the plate. It shows that the stress intensity factors of the plate with two diametrically-opposed edge cracks are much higher than those with a single radial edge crack over the outer region. So, the infinite pate with two diametrically-opposed edge cracks is more critical than that with a single radial edge crack.

5.3 Apparent Fracture Toughness for Prescribed Material Distribution

The apparent fracture toughness for prescribed material distributions of Fig. 5.2 is also evaluated numerically. The apparent fracture toughness K_{IC}^a is normalized by the intrinsic fracture toughness K_C^B of Al_2O_3. This normalized apparent fracture toughness K_{IC}^a / K_C^B is plotted in Fig. 5.10 for R_f/R=1.1, ΔT = 1000°C. For all the cases of material distributions, the AFT initially increases over certain inner region of the plate. Then it decreases over rest of the region. The incompatible eigenstrain induces an eigenstress, which is a self-equilibrated internal stress. The compressive eigenstress reduces the crack driving force that eventually increases the apparent fracture toughness. On the other hand, the tensile eigenstress has the reverse effects on the apparent fracture toughness. The composition profiles shown in Fig. 5.2 induce compressive eigenstress over certain portion at the inner side of the plate and a balancing tensile eigenstress over the remaining portion of the outer side. That is why the apparent fracture toughness increases from the inner surface up to a certain length and then it decreases as seen from Fig. 5.10. This type of fracture characteristic is desirable as it ensures the protection of catastrophic failure. Once the crack starts to propagate under a certain pressure, it immediately stops propagating as the region ahead of the crack tip has a higher toughness. For its further propagation, the internal pressure should be increased. The maximum peak value of AFT is obtained for the uniform material distribution. However, the uniform material distribution is not recommended as it has sharp interface that causes delimitation. Among other three other three material distributions, it is noted that parabolic upward distribution in Fig. 5.2 gives the maximum peak value of apparent fracture toughness. This is due to the fact that parabolic

upward material distribution is steeper near the inner surface that induces compressive eigenstress with a higher absolute magnitude than those obtained for the other two profiles. It is also noted that apparent fracture toughness for all material distributions has the value, which is significantly higher than the intrinsic fracture toughness K_C^B of the base material of Al_2O_3 except those at and near the outer region of the plate.

The effect of the FGM coating thickness around a circular hole of an infinite plate on AFT are shown in Fig. 5.11 and Fig. 5.12. In Fig. 5.11, the AFT are plotted for different values of R_f/R for linear material distribution. Here, the layer thinness has been varied by keeping the number of layers fixed, nl=10.On the other hand, in Fig. 5.12, the same plot is done varying the number of layers and keeping the layers thickness $(R_f-R)/nl$ fixed at 0.2. In both the cases, it is observed that for higher coating thickness the AFT is high, thus has more toughness against crack propagation. Furthermore, it is found that the layer thickness or the number of layers have little effect on the overall pattern or value of apparent fracture toughness.

Figure 5.13 shows AFT as a function of application temperature. The parameter ΔT refers to the difference between the sintering and the application temperature. Thus, a lower value of ΔT indicates the higher application temperature. It is evident from Fig. 5.13 that the plate has better fracture resistance at low application temperature.

Shown in Fig. 5.14 is the comparison of AFT for a single and two diametrically-opposed edge cracks. The results correspond to the linear material distribution of Fig. 5.2, R_f/R=1.1, ΔT = 1000°C. For both the cases of single and double cracks, the AFT is same over the inner region of the plate. However, it only differs significantly over the outer region.

Chapter 6 : CONCLUSION

6.1 Concluding Remarks

An approach is developed to analyze brittle fracture characteristics of an infinite plate having an FGM coating around a circular hole. The analysis is done considering the arbitrary variation of material properties instead of some presumed functional forms of material properties. The effect of eigenstrain developed in the plate as a result of cooling from sintering temperature due to nonuniform coefficient of thermal expansion is taken into account. The method is formulated to calculate the stress intensity factor for two diametrically-opposed edge cracks emanating from a circular hole of an infinite plate. This method is equally suitable for a single edge crack. Further, it can also be applied to a homogenous cylinder with a single as well as two diametrically opposed edge cracks. To demonstrate the method, some numerical results are obtained for an infinite plate with TiC/Al_2O_3 FGM coating around a circular hole. From the numerical results the following salient points can be noted:

i. The stress intensity factors of an infinite plate with FGM coating depend on the material distribution. The SIF is less for material distribution with higher gradient.

ii. The coating thickness around the circular hole has also significant influence on the SIF and AFT.

iii. The strength factor S_f has reverse effect on the SIF, i.e. the SIF decreases as S_f increases.

iv. Like a homogeneous cylinder, two diametrically-opposed edge cracks are more critical than a single edge crack in an infinite plate with FGM coating.

v. Infinite plate with FGM coating has better fracture resistance at low application temperature.

vi. The apparent fracture toughness of an Infinite plate with FGM coating is a function of material distribution. Thus the desired apparent fracture toughness can be introduced in an infinite plate with FGM coating by choosing the material distribution appropriately.

6.2 Recommendations for Future Work

Some recommendations for further work are given below:

i. Investigation of the effect of unequal crack size of two diametrically opposed edge cracks can be carried out.

ii. Investigation of the effect of relative crack position of two radial edge cracks on the fracture characteristics of infinite plates with FGM coating around a circular hole can be carried out.

iii. Investigation of the effect of multiple radial edge cracks (more than two cracks) on the fracture characteristics of infinite plates with FGM coating around a circular hole can be carried out.

REFERENCES

[1] Yamanouchi, M., Koizumi, M., Hirai, T., and Shiota, I., Proc. of the First Int. Sympos. on Functionally Gradient Materials, Sendai, Japan, 1990.

[2] Holt, J.B., Koizumi, M., Hirai, T., and Munir, Z. A., Ceramic Transactions, Functionally Gradient Materials, The American Ceramic Society, vol. 34, pp.157-164.1993.

[3] Gdoutos, E. E., "Fracture Mechanics: An Introduction, Solid Mechanics and its Applications", Kluwer Academic Publishers, Dordrecht, The Netherlands, vol. 14, 1993.

[4] Erdogan, F., "Fracture Mechanics", Int J. Solids Struct., vol. 37, pp. 171-183, 2000.

[5] Gu, P. and Asaro, R. J., "Crack Deflection in Functionally Graded Materials", Int J. Solids Struct., vol. 34, pp. 3085-3098, 1997.

[6] Kolednik, O., "The Yield Stress Gradient Effect in Inhomogeneous Materials", Int J. Solids Struct., vol. 37, pp.781-808, 2000.

[7] Mura, T., "Micromechanics of Defects in Solids: Mechanics of Elastic and Inelastic Solids", Kluwer Academic Publishers, Dordrecht, The Netherlands, 1987.

[8] Xiang, H. J., and Yang, J., "Free and Forced Vibration of a Laminated FGM Timoshenko Beam of Variable Thickness Under Heat Conduction," Compos.*: Part B,* vol. 39, pp. 292–303, 2008.

[9] Li, S.R., Zhang, J.H., and Zhao, Y.G.,"Thermal Post-buckling of Functionally Graded Material Timoshenko Beams," Appl. Math. Mech., vol. 27, pp. 803–810, 2006.

[10] Obata, Y., and Noda, N., "Steady Thermal Stresses in a Hollow Circular Cylinder and a Hollow Sphere of a Functionally Graded Material", J. Thermal Stresses, vol.17, pp. 471–487, 1994.

[11] Liew, K. M., Kitipornchai, S., Zhang, X. Z. and Lim, C. W., "Analysis of the Thermal Stress Behavior of Functionally Graded Hollow Circular Cylinders", Int. J. Solids Struct., vol.40, pp. 2355–2380, 2003.

[12] Afsar, A. M. and Anisuzzaman, M., "Stress Intensity Factors of Two Diametrically Opposed Edge Cracks in a Thick-Walled Functionally Graded Material Cylinder", Engng. Fract. Mech., vol. 74, pp. 1617–1636, 2007.

[13] Loghman, A., Aleayoub, SMA., “Hasani, Sadi M. Time-dependent Magnetothermoelastic Creep Modeling of FGM Spheres using Method of Successive Elastic Solution”, Appl Math Model, vol.36: 836–845, 2012.

[14] Praveen, G. N., Reddy, J. N., “Nonlinear Transient Thermoelastic Analysis of Functionally Graded Ceramic-Metal Plates,” Int. J. Solids Struct.,vol. 35, pp. 4457–76, 1998.

[15] Qian, L.F., Batra, R. C. and Chen, L. M.,“Static and Dynamic Deformations of Thick Functionally Graded Elastic Plates by using Higher Order Shear and Normal Deformable Plate Theory and Meshless Local Petrov-Galerkin Method”, Compos.: Part B, vol.35, pp. 685−697,2004.

[16] Chung, Y. N., and Chang, H. X., “Mechanical Behavior of Rectangular Plates with Functionally Graded Coefficient of Thermal Expansion Subjected to Thermal Loading”, J. Therm. Stresses, vol. 31, pp. 368-88, 2008.

[17] Zenkour, A. M. and Mashat, D. S. ,“Thermal Buckling Analysis of Ceramic-Metal Functionally Graded Plates”, Nat. Sci., 2, vol.9, pp.968-978, 2010.

[18] Afsar, A. M., and Sekine, H., “Inverse Problems of Material Distributions for Prescribed Apparent Fracture Toughness in FGM Coatings around a Circular Hole in Infinite Elastic Media”, Compos. Sci. and Tech., vol. 62, pp. 1063-1077, 2002.

[19] Cheng Z., Gao D., and Zhong Z., "Crack Propagating in Functionally Graded Coating with Arbitrarily Distributed Material Properties Bonded to Homogeneous Substrate", Acta Mech, vol.23 (5), pp.437-46, 2010.

[20] Rousseau, C-E. , and Tippur, H. V., "Influence of Elastic Gradient Profiles on Dynamically Loaded Functionally Graded Materials: Cracks Along the Gradient", Int J. Solids Stuct., vol.38 (44-45), pp.7839-56, 2001.

[21] Monfared, M.M., Ayatollahi, M., "Dynamic Stress Intensity Factors of Multiple Cracks in a Functionally Graded Orthotropic Half Plane", Theor Appl Fract Mec, vol.56, pp.49–57, 2011.

[22] Jin X., Wu L., Guo L., Yu H., and Sun Y.," Experimental Investigation of the Mixed-mode Crack Propagation in ZrO2/NiCr Functionally Graded Materials", Eng Fract Mech,vol.76(12), pp.1800-10, 2009.

[23] Cook, T. S. and Erdogan F., “Stresses in Bonded Materials with a Crack Perpendicular to the Interface”, Int J. Solids Stuct, vol.10, pp. 667-697,1972.

[24] Erdogan, F. and Cook, T. S., "Antiplane Shear Cracks Terminating at and Going Through a Bimaterial Interface", Int J. Fracture, vol. 10, pp. 227-240, 1974.

[25] Erdogan, F., "The Crack Problem for Bonded Nonhomogeneous Materials Under Antiplane Shear Loading", ASME J. Appl Mech., vol. 52, pp. 823-828, 1985.

[26] Schovanec, L. and Walton, J. R., "On the Order of Stress Singularity for an Antiplane Shear Crack at the Interface of Two Bonded Inhomogeneous Elastic Materials", ASME J. Appl Mech., vol. 55, pp. 234-236, 1988.

[27] Konda, N., and Erdogan, F., "The Mixed Mode Crack Problem in a Nonhomogeneous Elastic Medium", Eng Fract Mech, vol. 47, pp. 533-545,1994.

[28] Jin, Z. H. and Noda, N., "Crack-Tip Singular Fields in Nonhomogeneous Materials", ASME J. Appl Mech., vol. 61, pp. 738-740, 1994.

[29] Erdogan, F. and Wu, B. H., "The Surface Crack Problem for a Plate with Functionally Graded Properties", ASME J. Appl Mech. , vol. 64, pp. 449-456, 1997.

[30] Chen, Y. F., Erdogan F., "The Interface Crack Problem for a Nonhomogenous Coatings Bonded to a Homogenous Substrate", J. Mech. Phys. Solids, vol. 44, pp. 771-87, 1996.

[31] Gu, P. and Asaro, R. J., "Cracks in Functionally Graded Materials", Int. J. Solids Struct., vol. 34, pp. 1-17, 1997.

[32] Ozturk, M., Erdogan, F., " Axisymmetric Crack Problem in Bonded Materials with a Graded Interfacial Region", Int. J. Solids Struct., vol. 33, pp. 4101-17, 1996.

[33] Choi, H. J., "Bonded Dissimilar Strips with a Crack Perpendicular to the Functionally Graded Interface", Int. J. Solids Struct., vol. 32, pp. 2853-71, 1995.

[34] Delale, F., and Erdogan, F., "The Crack Problem for a Nonhomogeneous Plane", ASME J. Appl. Mech., vol. 50, pp. 609-614, 1983.

[35] Bao, G. and Wang, L., "Multiple Cracking in Functionally Graded Ceramic/Metal Coatings", Int. J. Solids Struct., vol. 32, pp. 2853-2871, 1995.

[36] Hassan, H. A. Z., "Torsion of a Nonhomogeneous Infinite Elastic Cylinder Slackened by a Circular Cut", J. Engng. Math.,vol. 30, pp. 547-55, 1996.

[37] Zou, Z. Z., Wang, X. Y., Wang, D., "On the Modelling of Interfacial Zone Containing a Griffith Crack: Plane Problem", Key Engng. Mater, vol. 145, pp. 489-94, 1998.

[38] Jin, Z-H., and Noda, N., "An Internal Crack Parallel to the Boundary of a Nonhomogenous Half Plane Under Thermal Loading". Int. J. Engng. Sci.,vol. 31, pp. 793-806, 1993.

[39] Noda, N., and Jin, Z. H., "A Crack in Functionally Graded Materials Under Thermal Shock", Arch. Appl. Mech., vol. 64, pp. 99-110, 1994.

[40] Nakagaki, M., Sasaki, H. and Hagihara, S., "A Study of Crack in Functionally Graded Material Under Dynamic Loading", PVP-Dynamic Fracture Failure and Deformation, ASME 300, pp. 1-6, 1995.

[41] Nadeau, J. C., and Ferrari, M., "Microstructural Optimization of a Functionally Graded Transversely Isotropic Layer", Mech. Mater, vol. 31, pp. 637-51, 1999.

[42] Nadeau, J. C., and Meng, X. N., " Microstructural Optimization of a Functionally Graded Layer", Compos.:Part B, vol. 31, pp. 285-97, 2000.

[43] Nakamura, T., Wang, T., and Sampath, S., "Determination of Properties of Graded Materials by Inverse Analysis and Instrumented Indentation", Acta Mater, vol. 48, pp. 4293-306, 2000.

[44] Oatao, Y., Kawamura, R., Tanigawa Y., and Imamura, R., " Optimization of Material Composition of Nonhomogenous Hollow Sphere for Thermal Stress Relaxation Making use of Neural Network", Comput. Meth. Appl. Mech. Engng., vol. 180, pp. 185-201, 1999.

[45] Oatao, Y., Tanigawa Y., and Nakaura, T., "Optimization of Material Composition of FGM Hollow Circular Cylinder under Thermal Loading: A Neural Network Approach", Compos.:Part B, vol. 30, pp. 415-22, 1999.

[46] Oatao, Y., Kawamura, R., Tanigawa Y., and Imamura, R., " Optimization of Material Composition of Nonhomogenous Hollow Circular Cylinder for Thermal Stress Relaxation Making use of Neural Network", J. Thermal Stresses., vol. 22, pp. 1-22, 1999.

[47] Hirano, T., Wakashima, K., "Mathematical Modeling and Design", Mater Res. Soc, vol. 20, pp. 40-2, 1995.

[48] Makworth, A. J., and Saunders, J. H., "A Model of Structure Optimization for a Functionally Graded Material", Matter Lett., vol. 22, pp. 103-7, 1995.

[49] Zuikar, J.R., "Functionally Graded Materials: Choice of Micromechanics Model and Limitations in Property Variation", Compos. Engng., vol. 5, pp. 807-19, 1996.

[50] Sekine, H., and Afsar, A. M., "Composition Profile for Improving the Brittle Fracture Characteristics in Semi-Infinite Functionally Graded Materials", JSME Int. J., vol. 42, pp. 592-600. 1999.

[51] Afsar, A. M. and Sekine H., "Crack Spacing Effect on the Brittle Fracture Characteristics of Semi-Infinite Functionally Graded Materials with Periodic Edge Cracks". Int. J. of Fracture, vol. 102, pp. L61- L66. 2000.

[52] Afsar, A. M. and Sekine H., "Optimum Material Distributions for Prescribed Apparent Fracture Toughness in Thick-Walled FGM Circular Pipes". Int. j. of Press. vessels and piping, vol. 78, pp. 471-484, 2001.

[53] Wu, Xue-Ren., and Janne, A., "Weight Functions and Stress Intensity factors Solutions", Pergamon Press PIC, Headington Hill, Oxford OX3OBW, England, 1991.

[54] Nair, S. V., "Crack-Wake Debonding and Toughness in Fiber-or Whisker-Reinforced Brittle-Matrix Composites", J. Am Ceram. Soc., vol 73, pp. 2839-2847, 1990.

[55] Nan, C. W., Yuan, R. Z., and Zhang, L. M., "The Physics of Metal/Ceramic Functionally Gradient Materials" ,Ceramic Transaction: Functionally Gradient Materials, Edited by J.B.Holt et al., Am Ceram Soc., Westerville, OH, vol 34, pp.75-82, 1993.

[56] Muskhelishvili, N.I., "Some Basic Problems of the Mathematical Theory of Elasticity" (Translated from the Russian by J.R.M.Radok), 2nd edition, Noordhoff International Publishers, The Netherlands, 1975.

[57] Erdogan, F., Gupta, G.D, Cook, T.S., "Numerical Solution of Singular Integral Equations", In. Sith GC, vol. 1, pp. 368-425, 1973.

[58] Hills, D.A., Kelly, P.A., Dai, D.N., and Korsunsky, A.M., "Solution of Crack Problems: The Distributed Dislocation Technique", Kluwer Academic Publishers, 1996.

[59] Krenk, S., “On the Use of the Interpolation Polynomial for Solution of Singular Integral Equation”, Quarterly of Appl. Math., vol. 32, pp. 479-484, 1975.

[60] Newman, J.C. Jr., “An Improved Method of Collocation for the Stress Analysis of Cracked plates with Various Shaped Boundaries”, NASA TND-6376, pp.1-45, 1971.

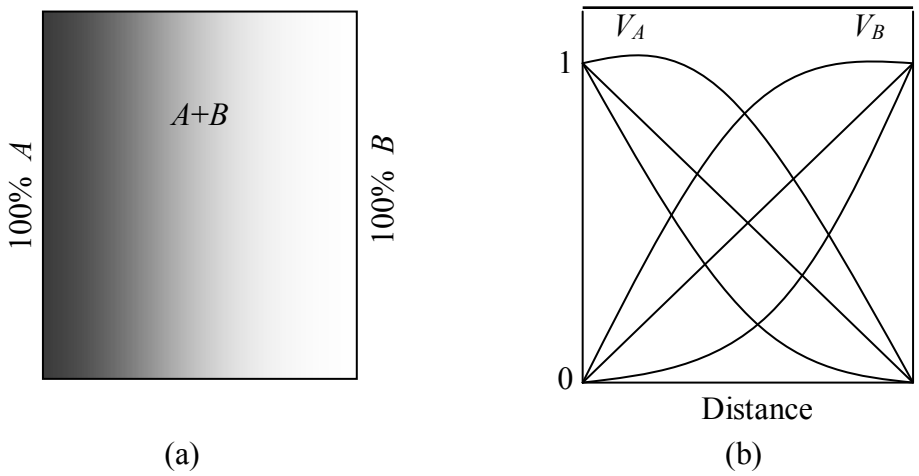

Figure 1.1 Concept of FGM: (a) an FGM plate, (b) material distribution in the FGM plate.

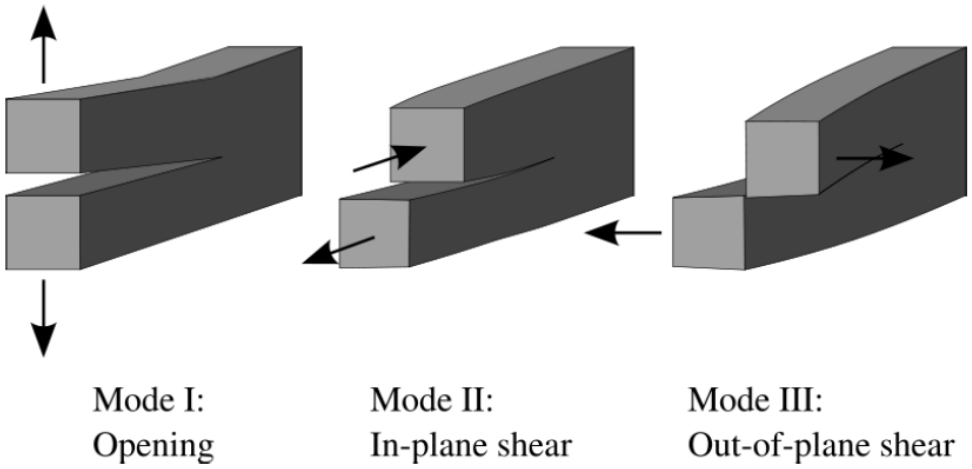

Figure 3.1 The three basic fracture modes.

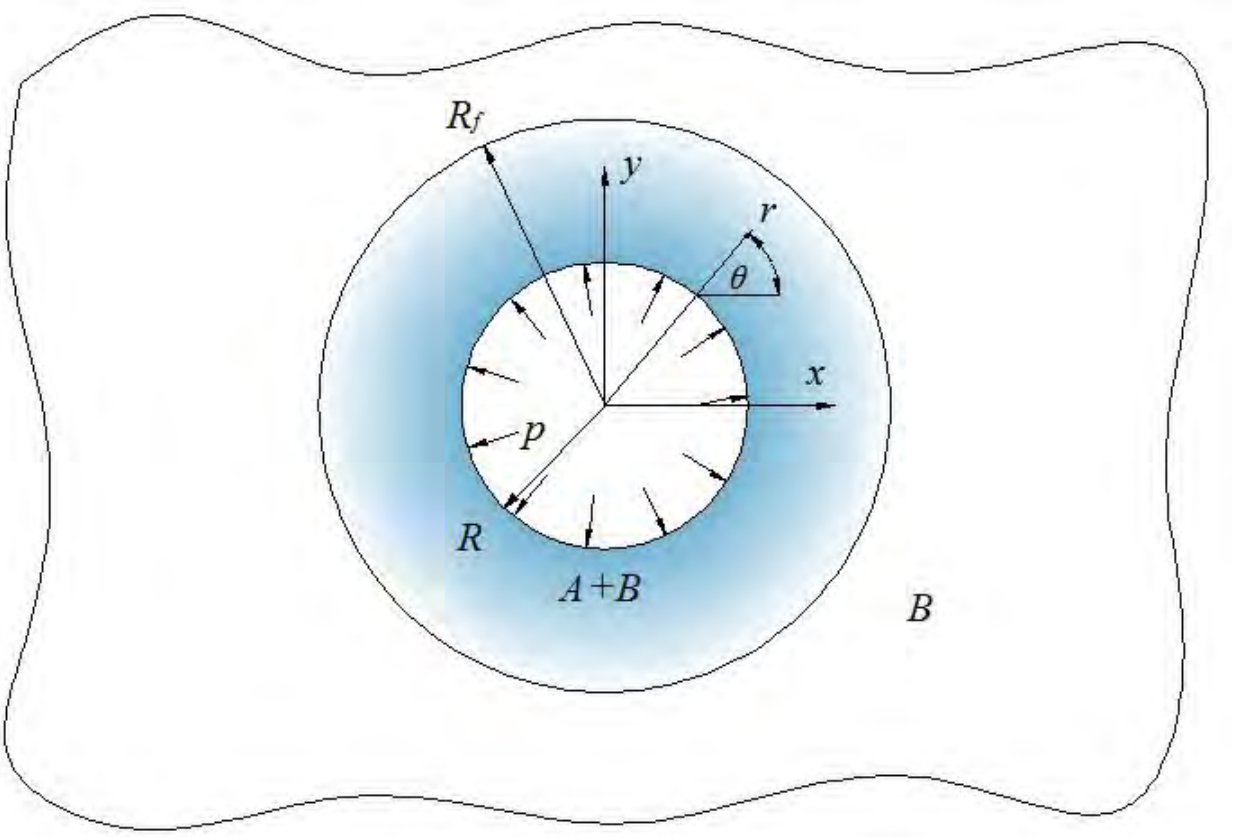

Figure 4.1 Analytical model of an infinite FGM plate with a circular hole.

.

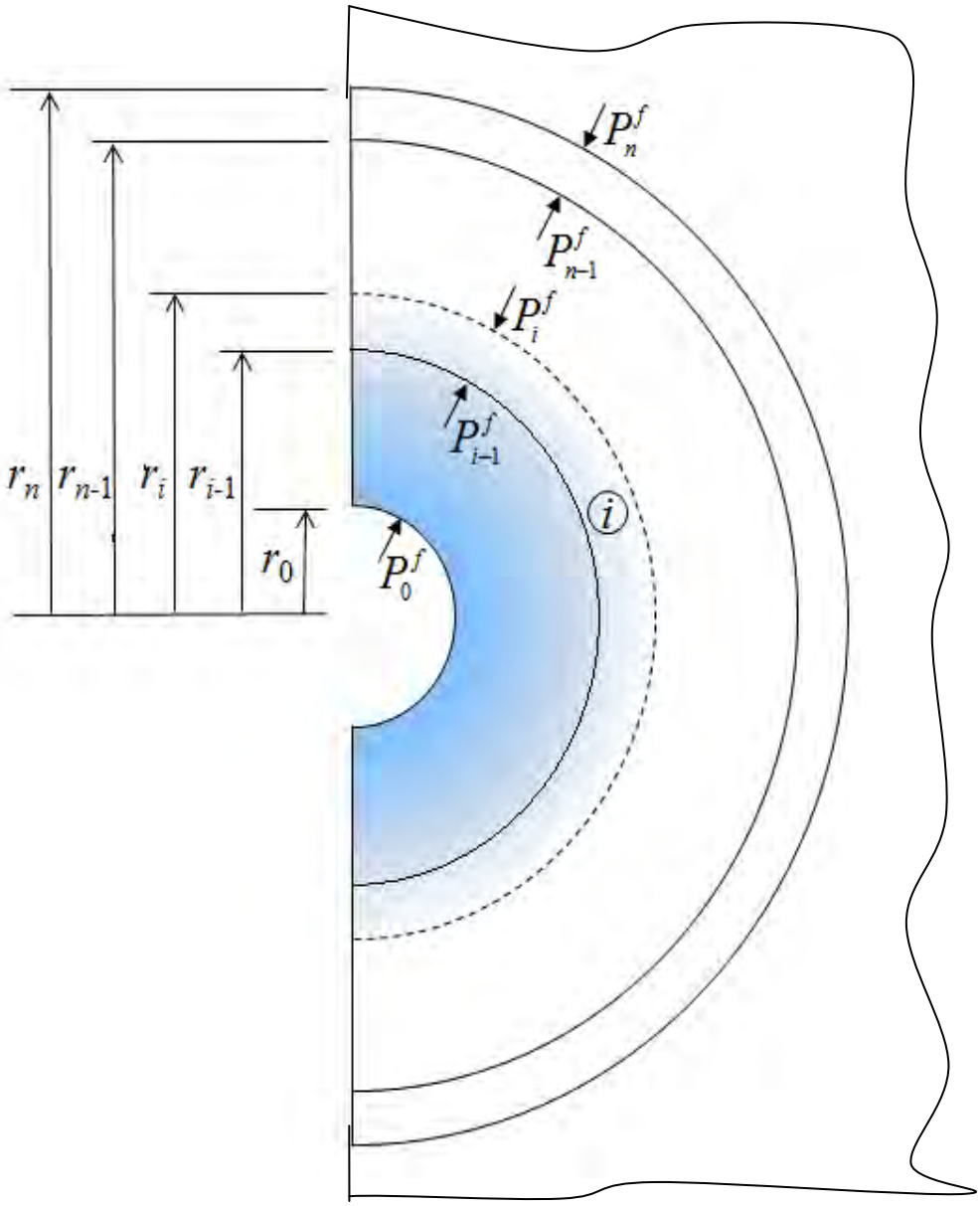

Figure 4.2 Layering of the FGM region around the circular hole in an infinite plate.

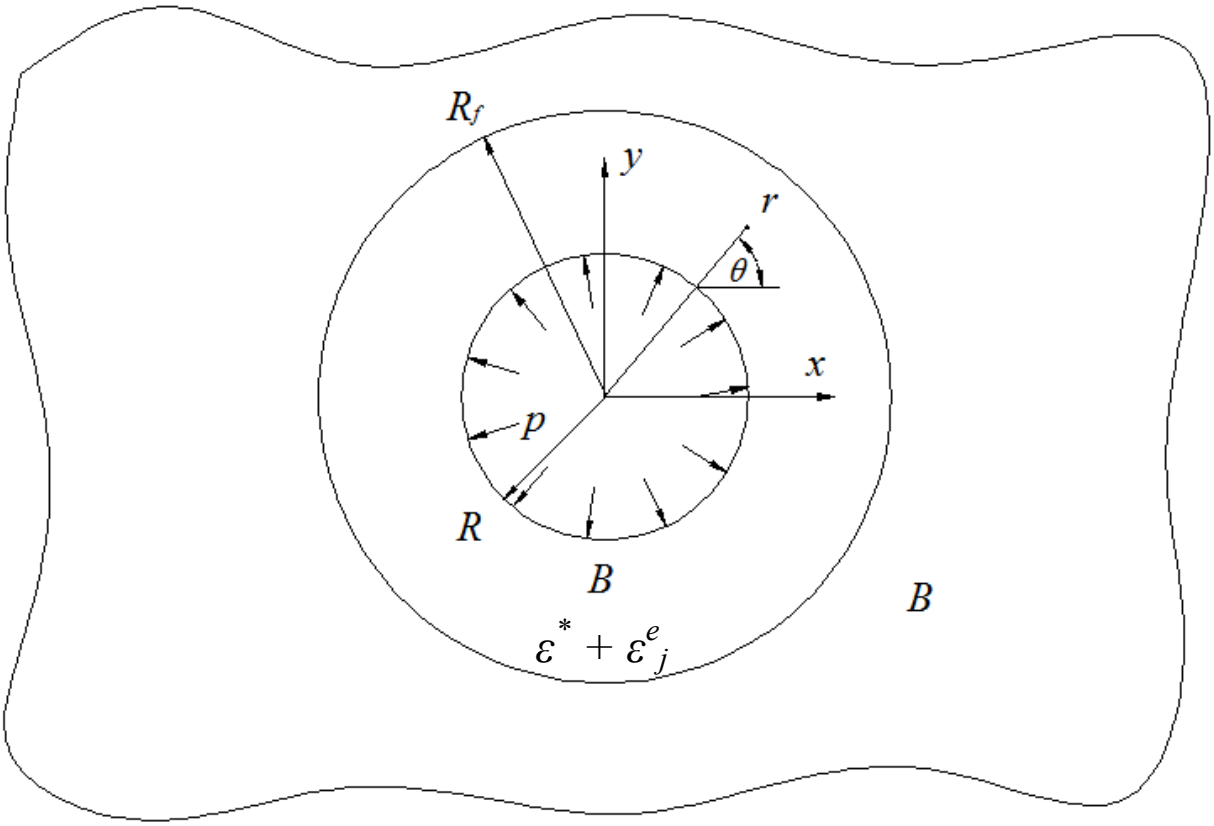

Figure 4.3 Infinite homogenized plate containing a circular hole with distributed incompatible and equivalent eigenstrains under a uniformly applied internal pressure.

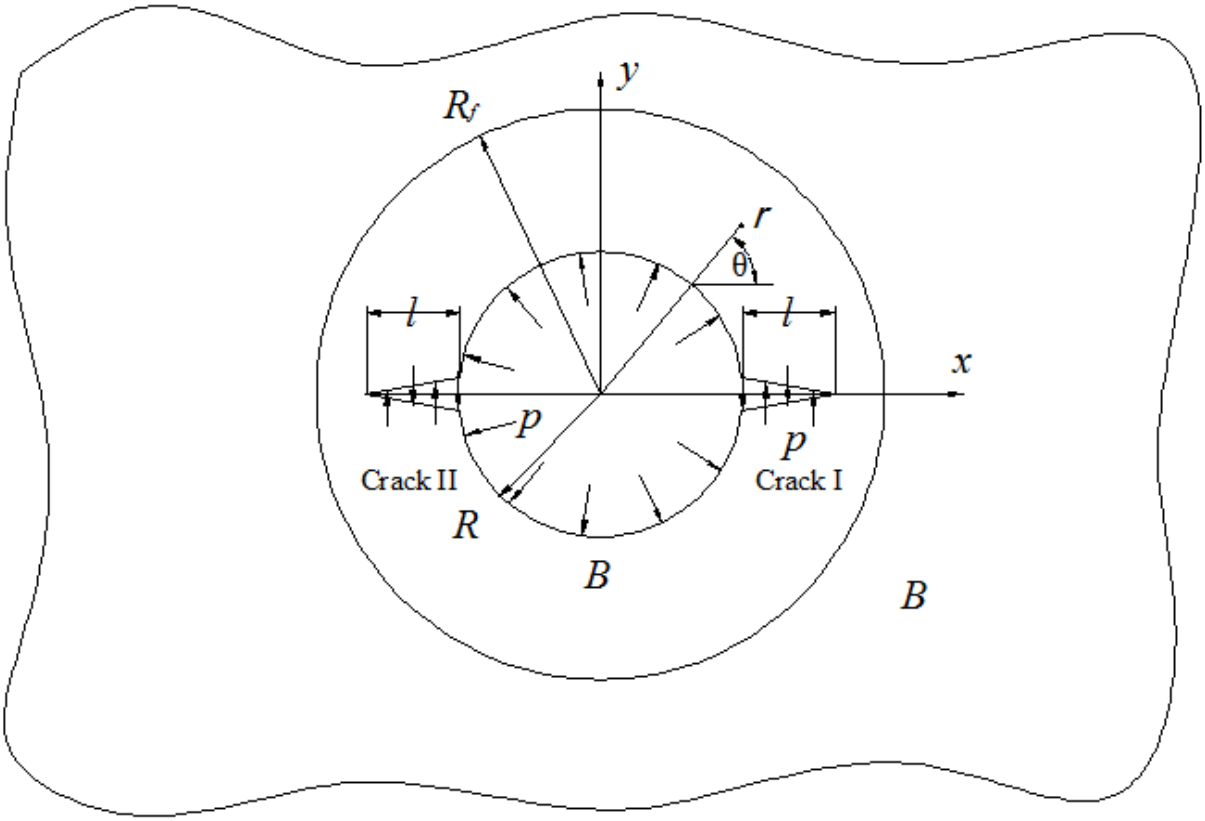

Figure 4.4 Two diametrically-opposed edge cracks emanating from a circular hole in an infinite homogenized plate with distributed incompatible and equivalent eigenstrains under a uniformly applied internal pressure.

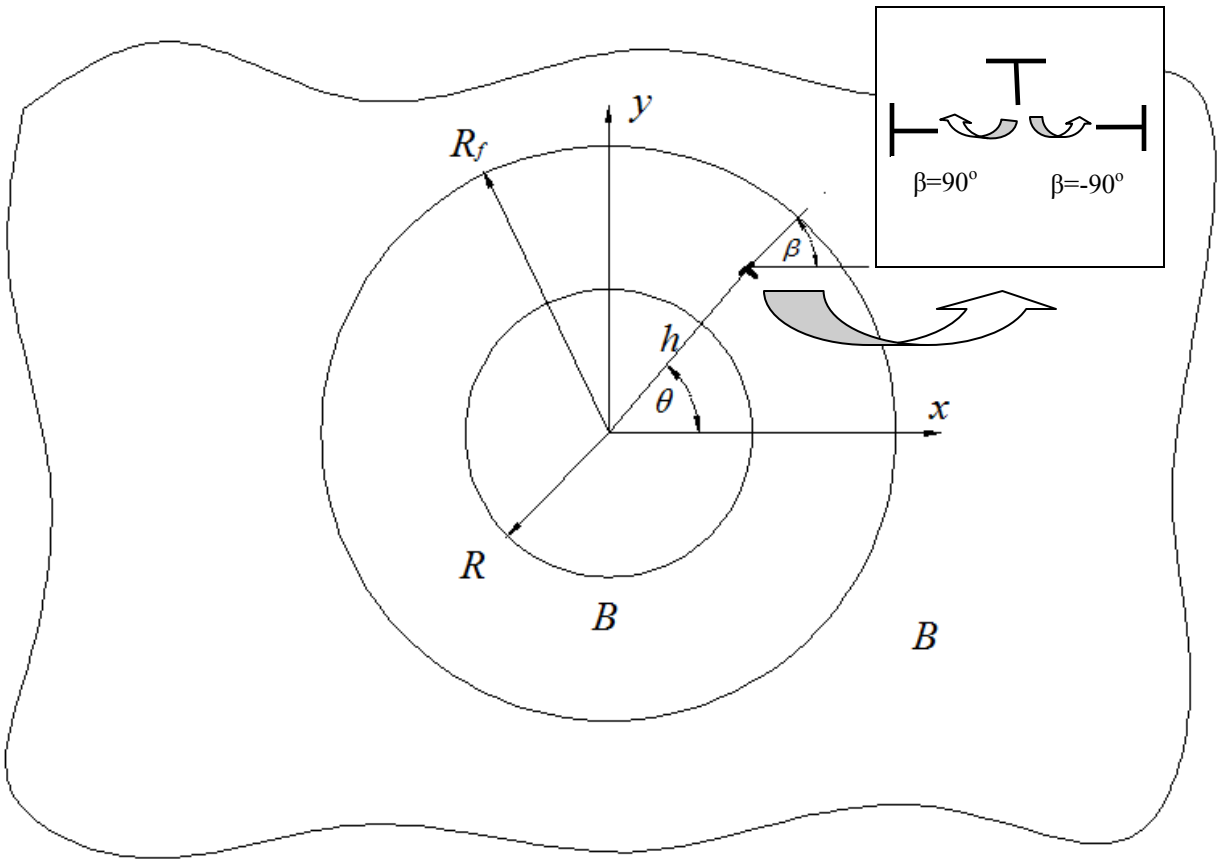

Figure 4.5 A discrete edge dislocation at $z=h$.

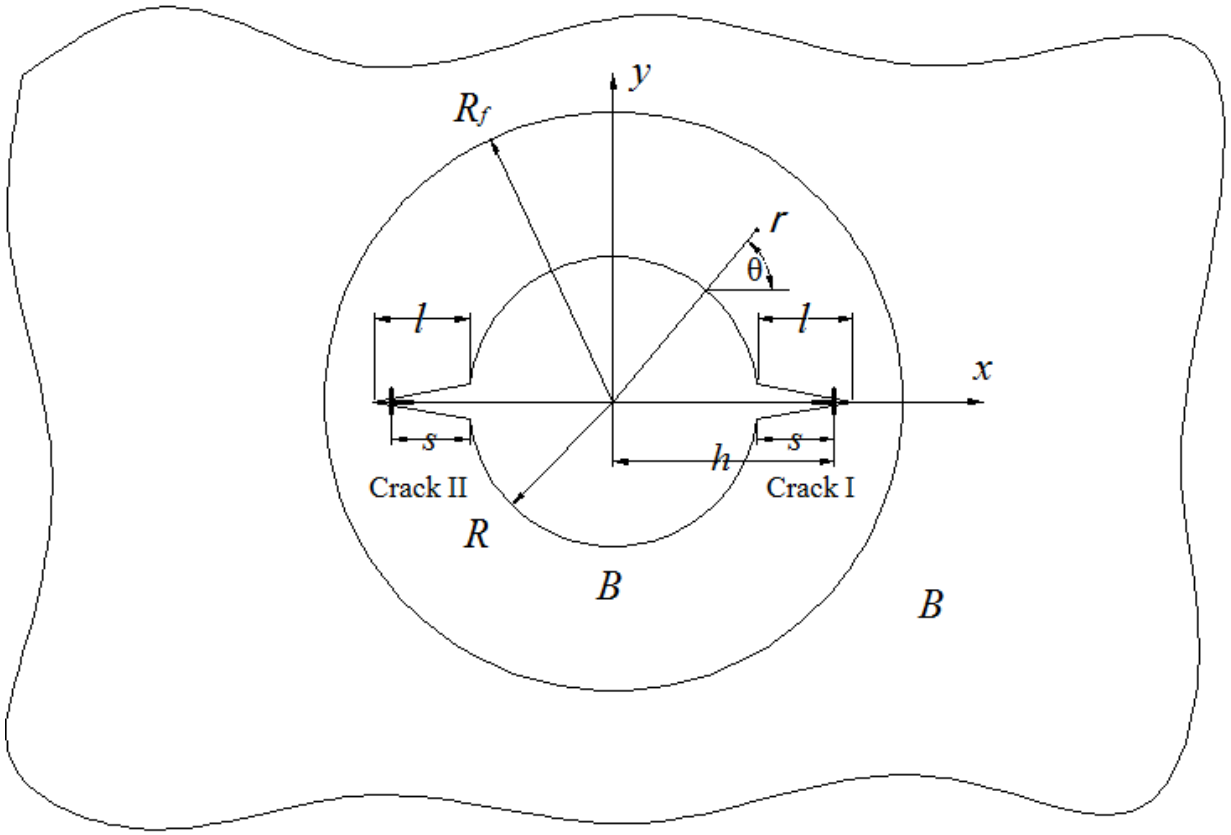

Figure 4.6 Two discrete edge dislocations at $z = \pm h$ measured from the center of a circular hole in a homogenized infinite plate.

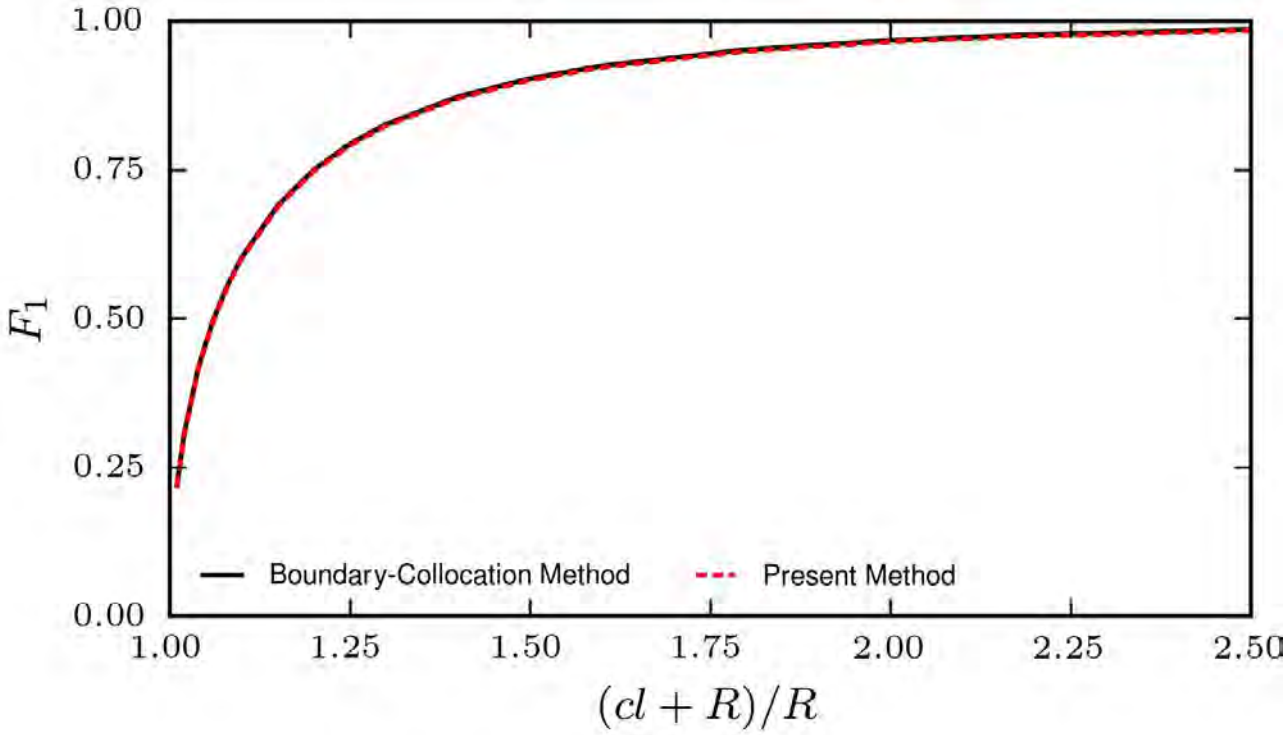

Figure 5.1 Comparison of normalized stress intensity factors for two diametrically opposed edge cracks at a circular hole in a homogeneous infinite plate obtained by the present method and by Boundary-Collocation method [60].

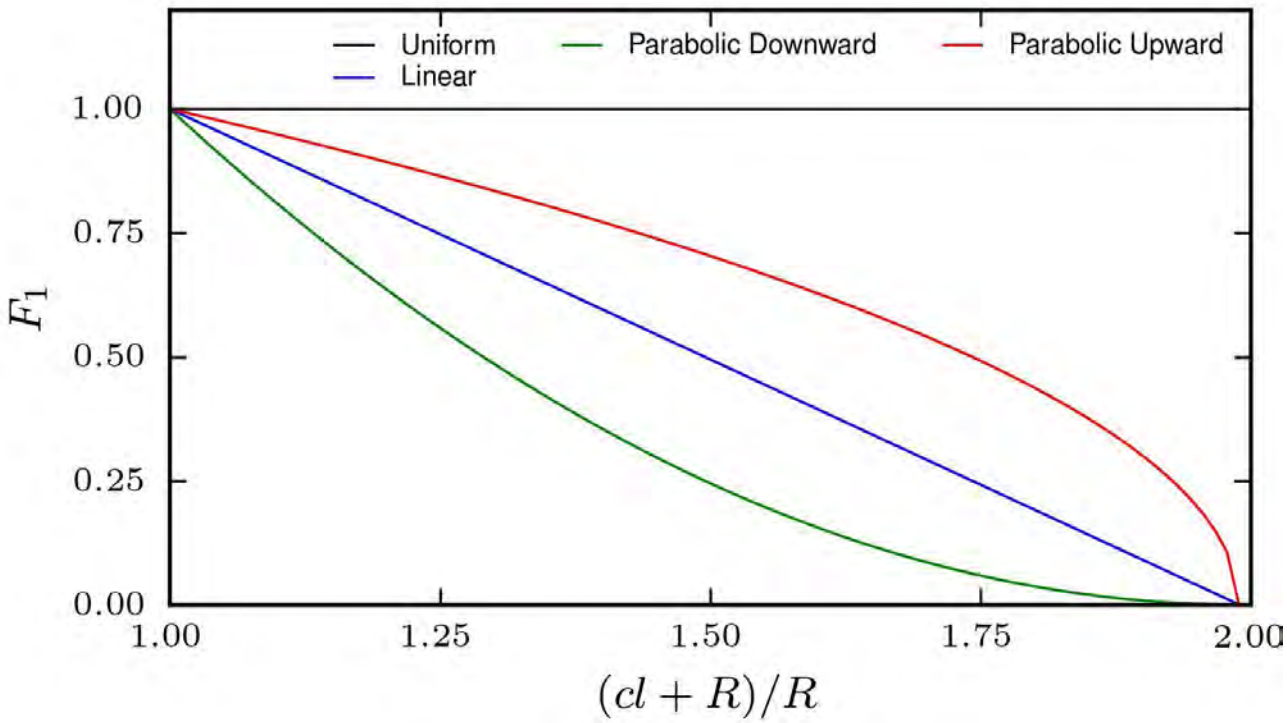

Figure 5.2 Prescribed material distributions of TiC in TiC/Al_2O_3 FGM coating.

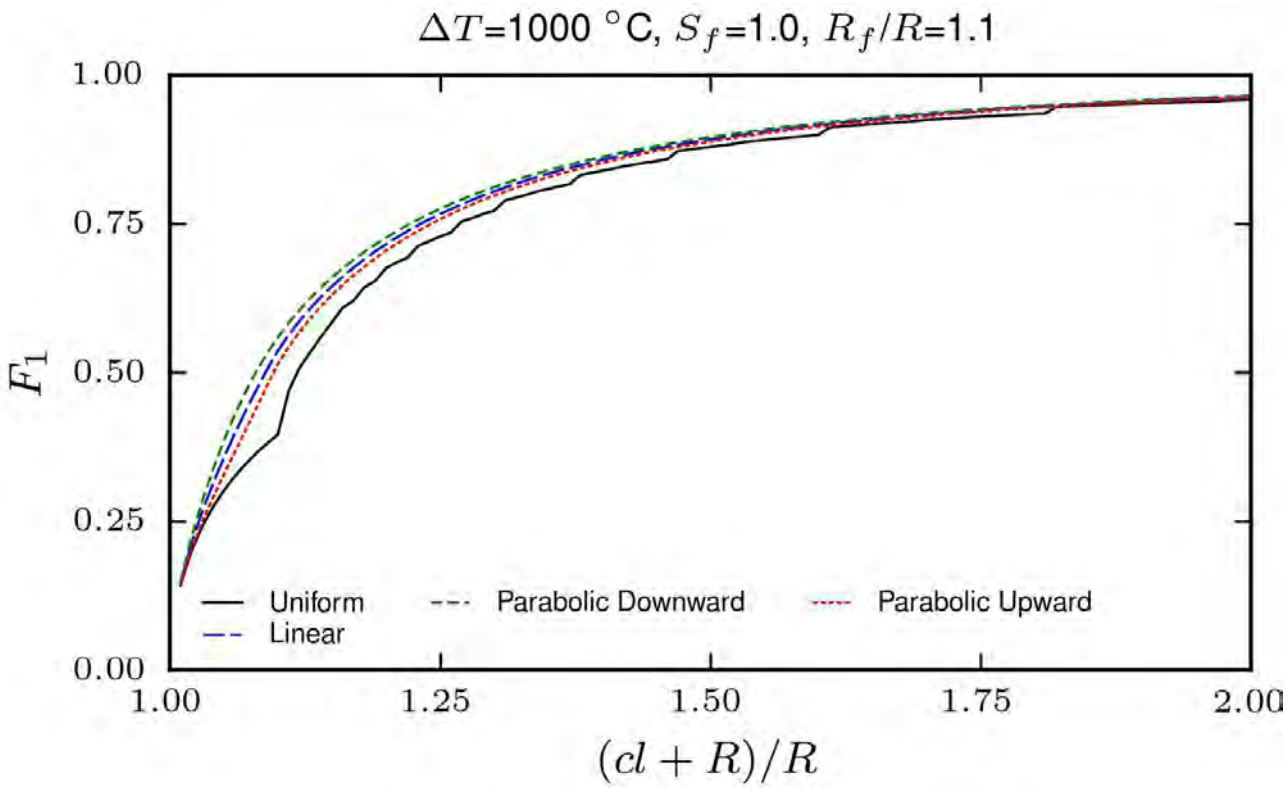

Figure 5.3 Effect of material distribution on normalized stress intensity factors.

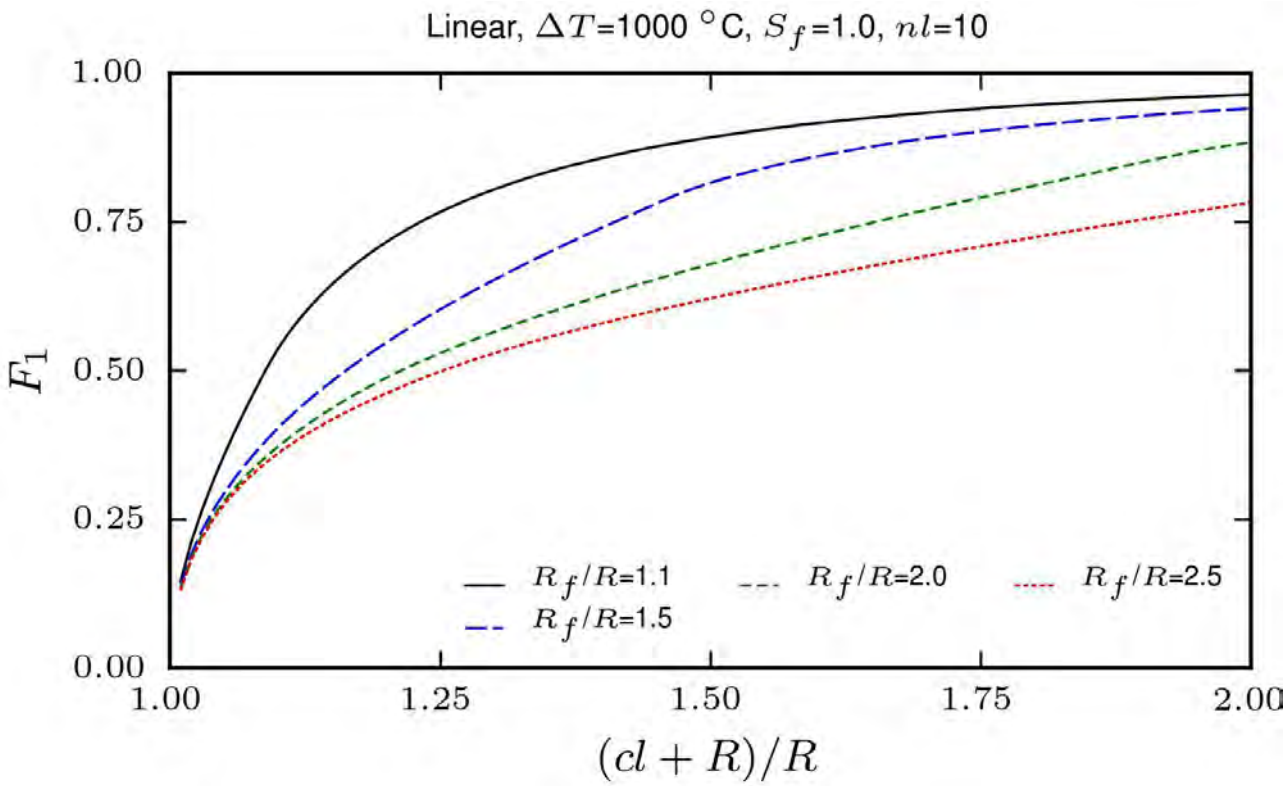

Figure 5.4 Normalized stress intensity factors as a function of FGM coating thickness around a circular hole of an infinite plate for same number of layers.

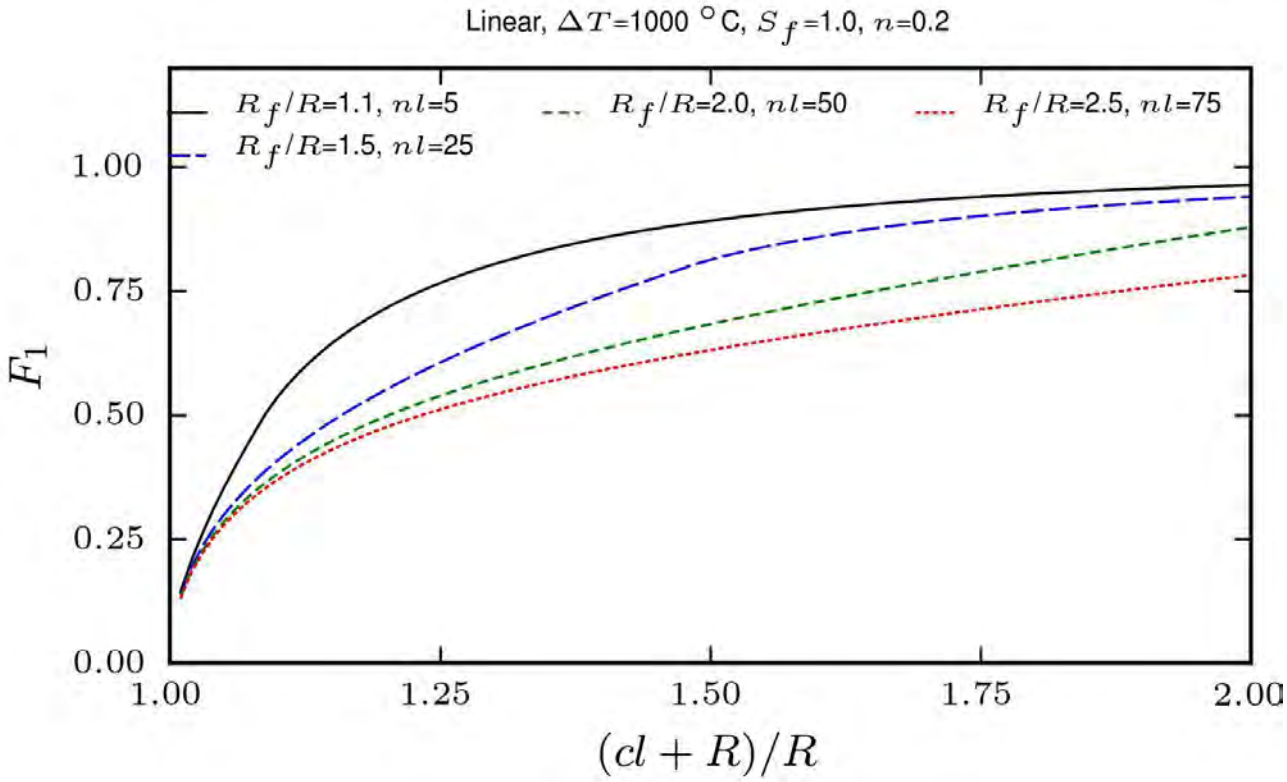

Figure 5.5 Normalized stress intensity factors as a function of FGM coating thickness around a circular hole of an infinite plate for same layer thickness.

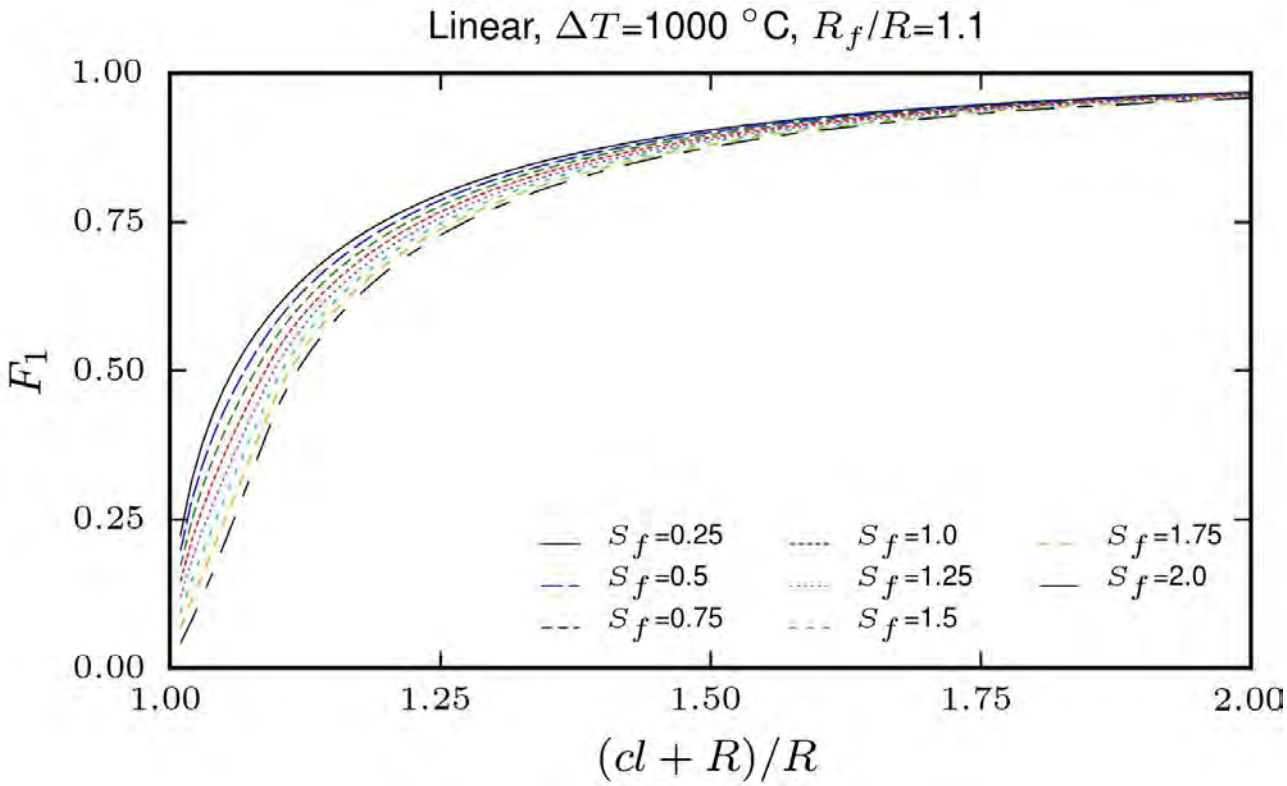

Figure 5.6 Normalized stress intensity factors as a function of strength factor.

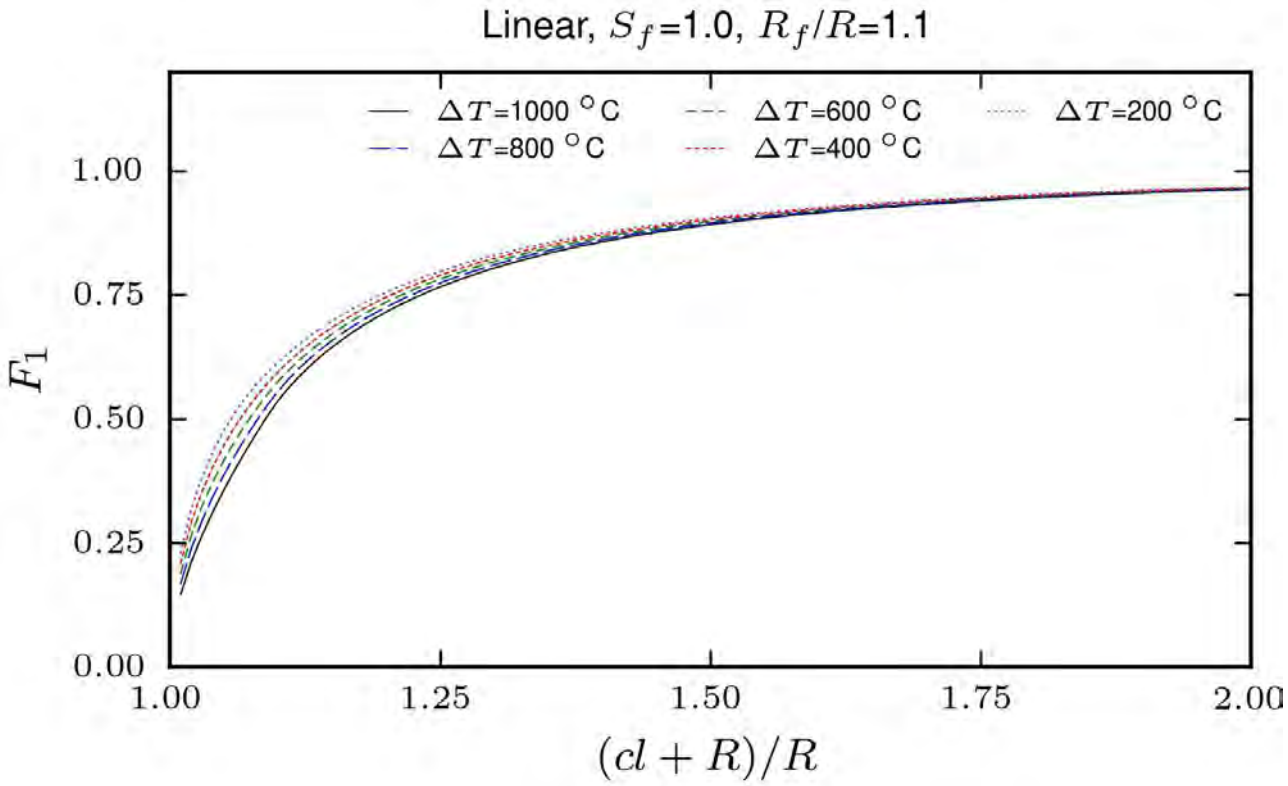

Figure 5.7 Normalized stress intensity factors as function of difference in sintering and application temperature.

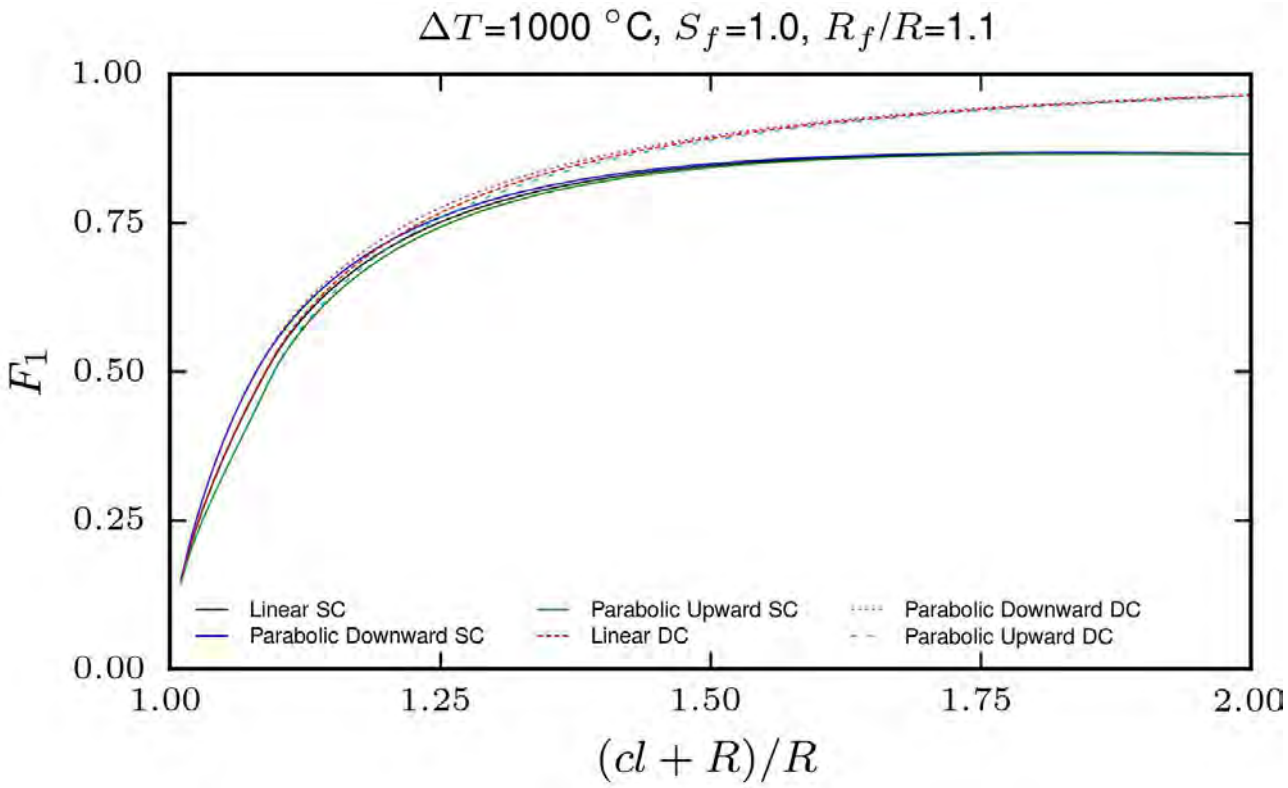

Figure 5.8 Comparison of normalize stress intensity factors for a single and two diametrically opposed cracks considering different prescribed material distributions.

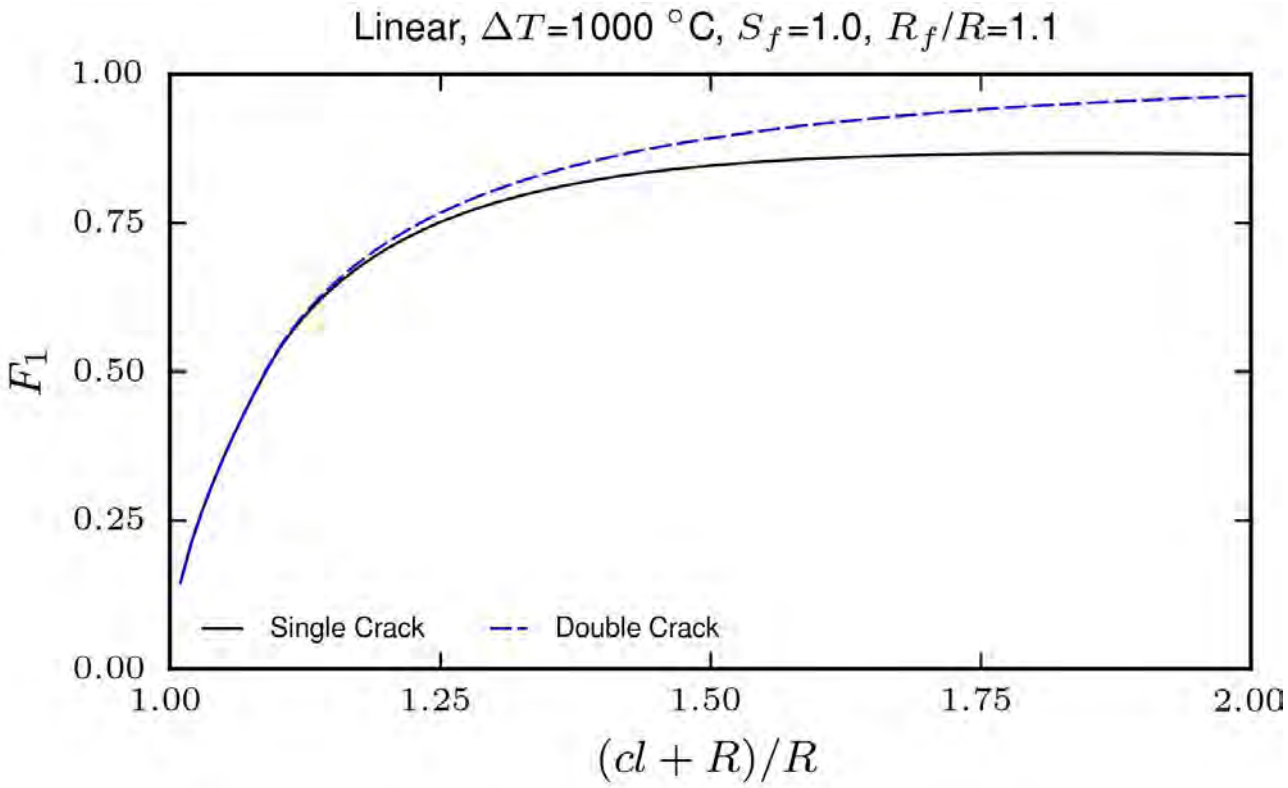

Figure 5.9 Comparison of normalized stress intensity factors for a single and two diametrically-opposed edge cracks.

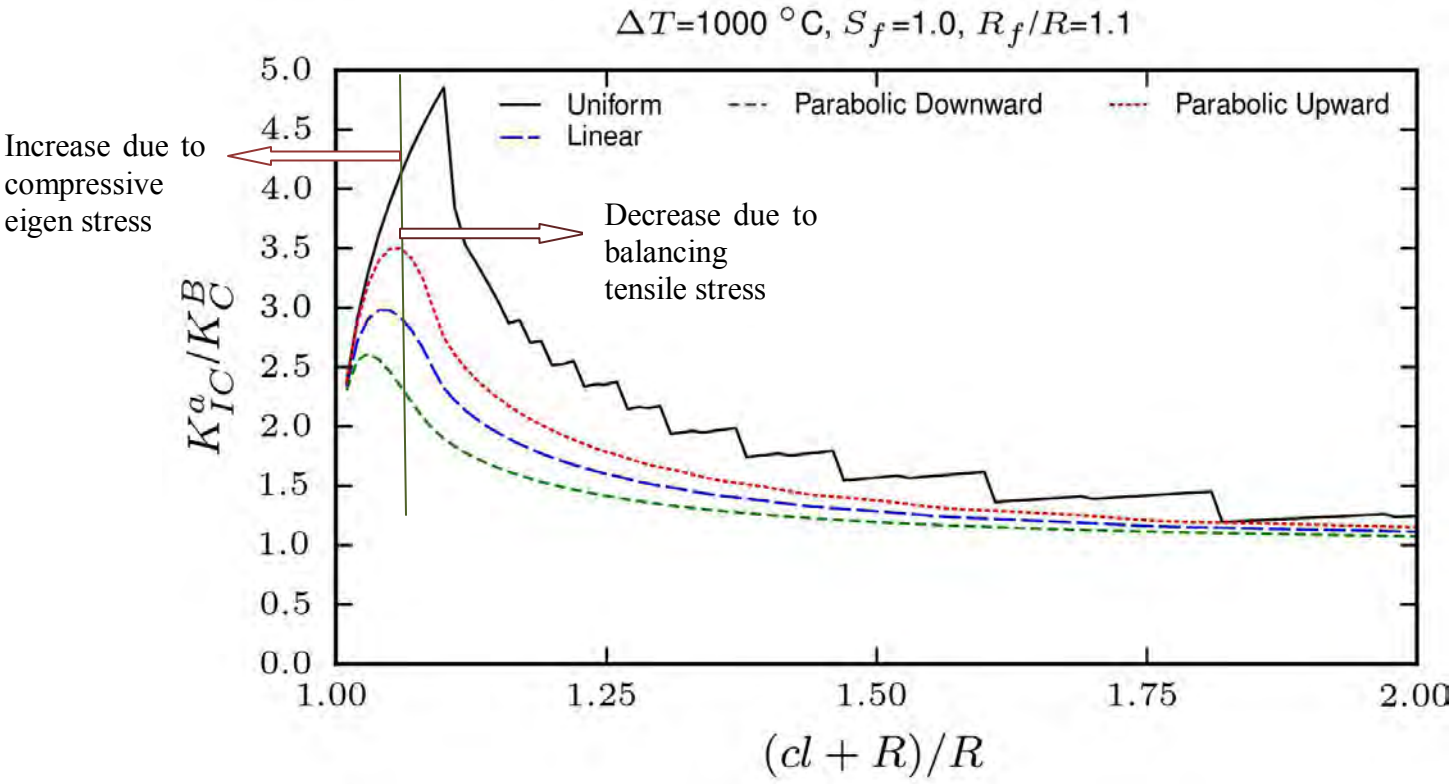

Figure 5.10 Effect of material distribution on apparent fracture toughness.

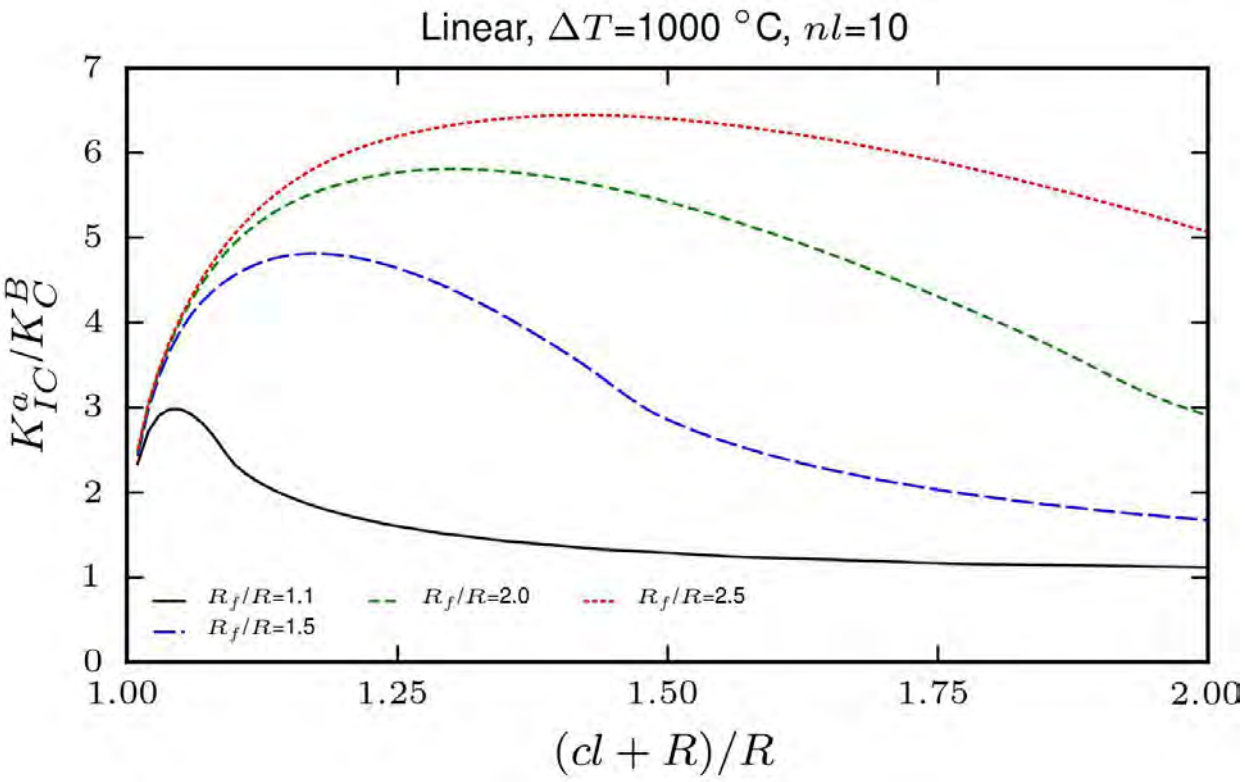

Figure 5.11 Effect of FGM coating thickness around a circular hole of an infinite plate on the apparent fracture toughness for same number of layers.

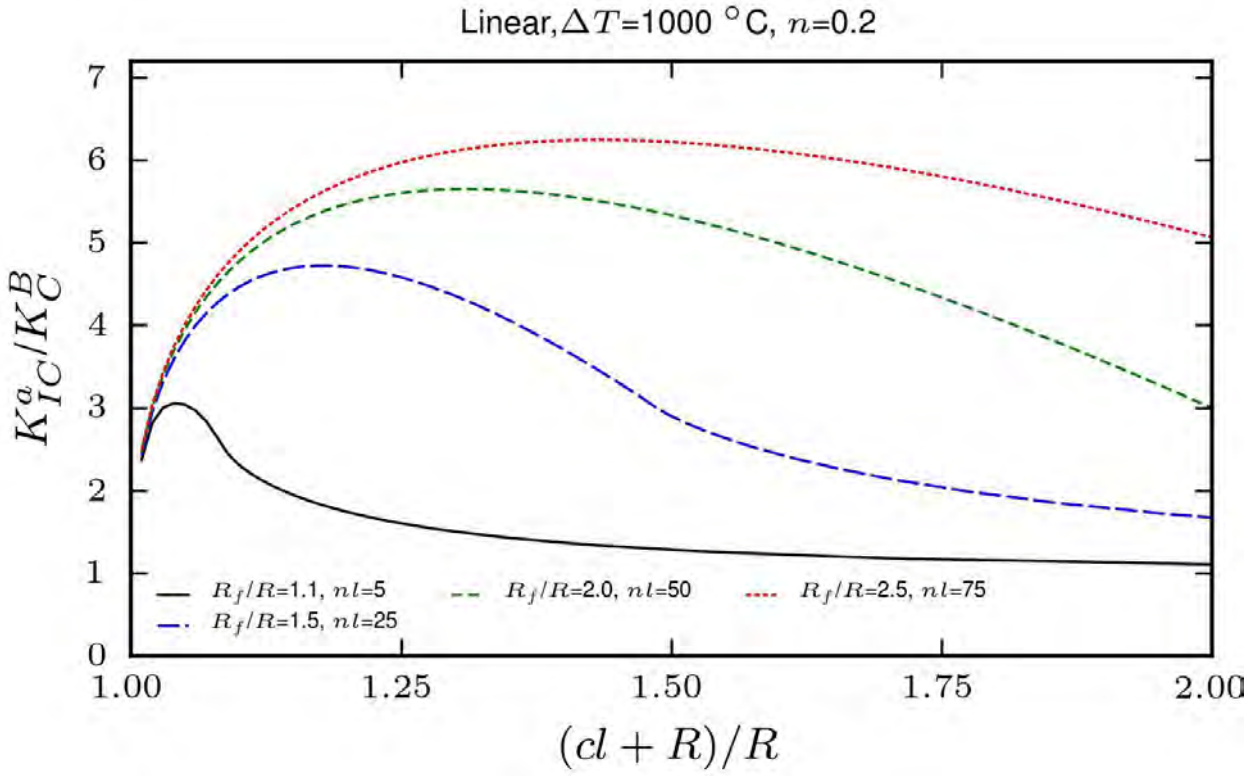

Figure 5.12 Effect of FGM coating thickness around a circular hole of an infinite plate on the apparent fracture toughness for same layer thickness.

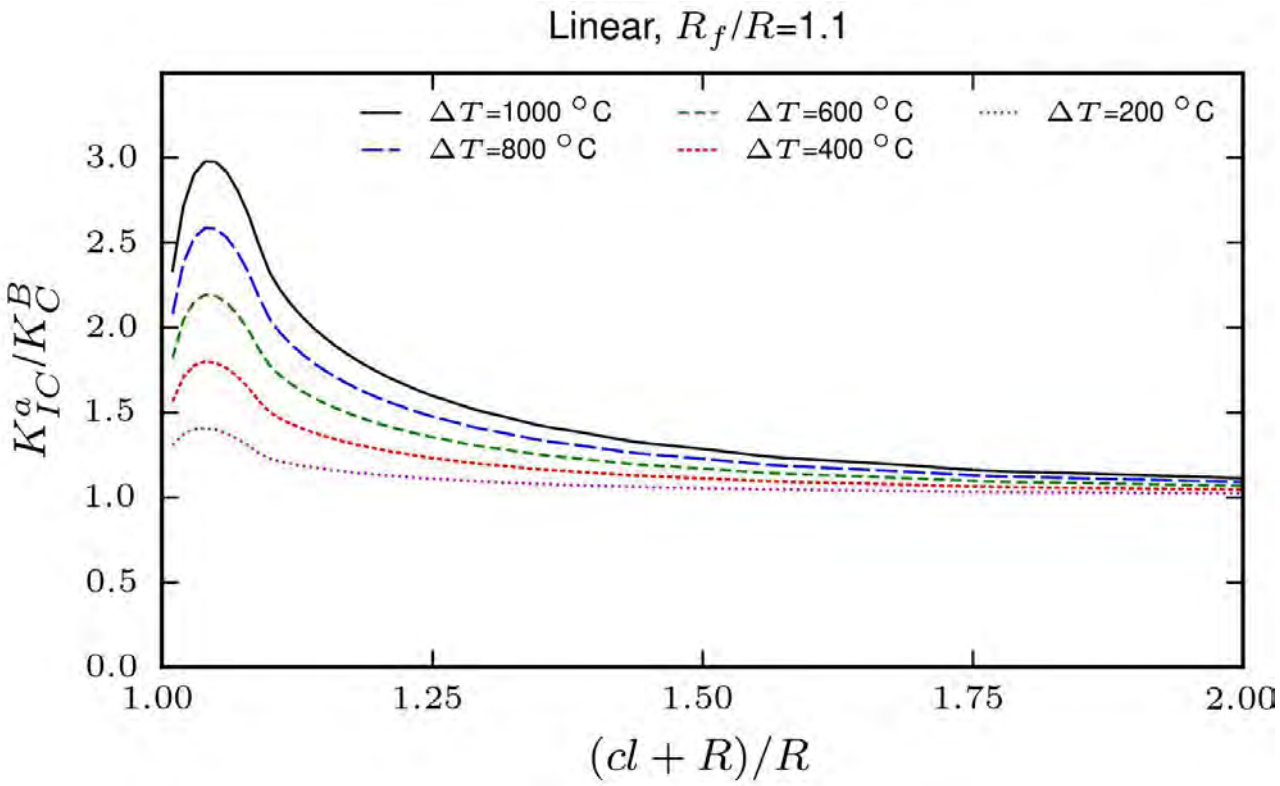

Figure 5.13 Effect of application temperature on the apparent fracture toughness.

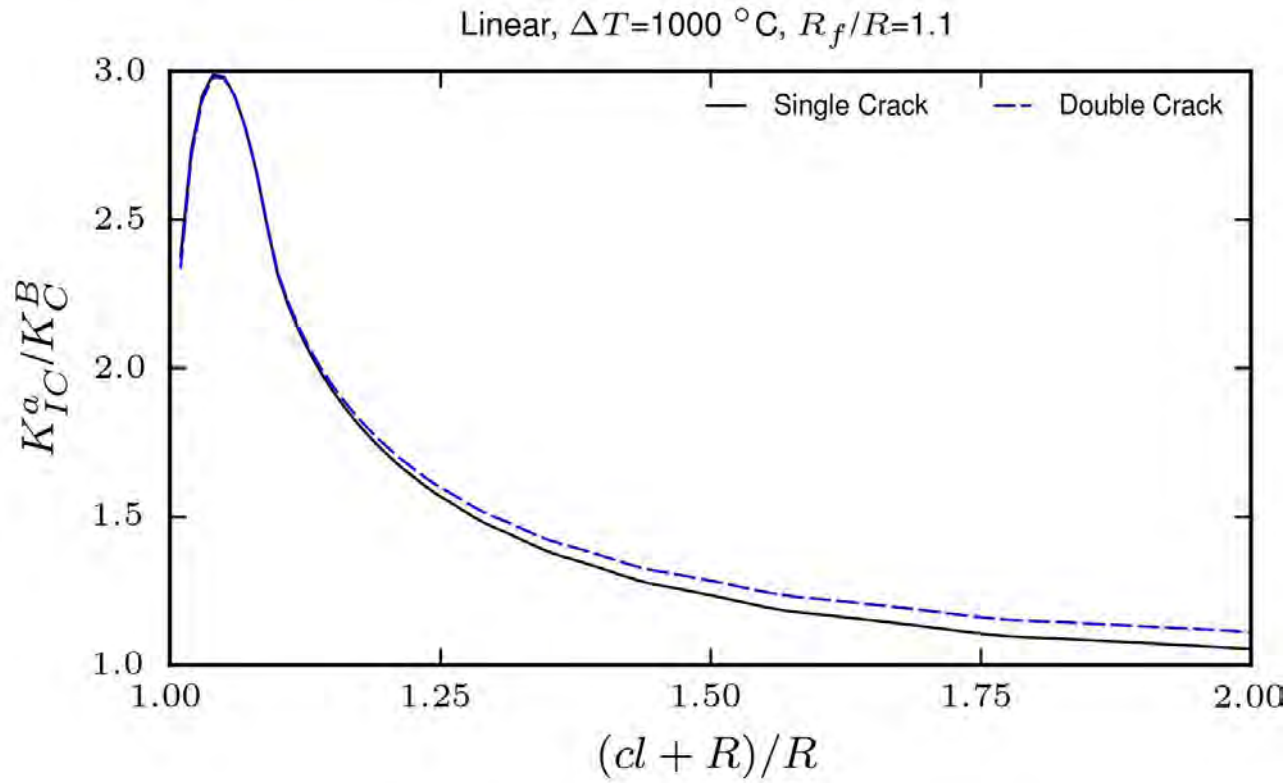

Figure 5.14 Comparison of apparent fracture toughness for a single and two diametrically-opposed edge cracks.

Table 5.1 Material properties of TiC and Al_2O_3

Material	Young's Modulus (GPa)	Shear Modulus (GPa)	Poisson's Ratio	CTE (/°C)	Ultimate Tensile Strength (GPa)	Intrinsic Apparent Fracture Toughness K_{IC} (MPa $m^{1/2}$)
TiC	462	194.12	0.19	7.4×10^{-6}	-	4.1
Al_2O_3	380	150.79	0.26	8.0×10^{-6}	0.28	3.5

APPENDIX

Deriving simultaneous algebraic equations from singular integral equations

The complex potential functions for an edge dislocation making an angle β with the positive x axis and passing through a point $z = h$ in an infinite medium with a circular hole of radius R

$$\Phi(z) = \frac{i\mu_0(b_1 + ib_2)}{\pi(\kappa_0 + 1)} e^{i\beta} \frac{1}{z-h} + \sum_{k=0}^{\infty} a_k z^{-k} \tag{1a}$$

$$\Psi(z) = -\frac{i\mu_0(b_1 - ib_2)}{\pi(\kappa_0 + 1)} e^{-i\beta} \frac{1}{z-h} + \frac{i\mu_0(b_1 + ib_2)}{\pi(\kappa_0 + 1)} \frac{\bar{h}}{(z-h)^2} e^{i\beta} + \sum_{k=0}^{\infty} a_k' z^{-k} \tag{1b}$$

where $h = R+s, b_1$ and b_2 are the components of Burgers vector, and κ_0 is Kolosov's constant which is equal to (3-ν_0)/(1+ν_0) for plane stress condition and $z = x + iy = re^{i\theta}$

Now for k=0, 1 and integrating Eqs. 1(a, b) we get

$$\Phi(z) = \frac{i\mu_0(b_1 + ib_2)}{\pi(\kappa_0 + 1)} e^{i\beta} \log(z-h) + a_o z + a_1 \log z + \sum_{k=2}^{\infty} a_k \frac{z^{-k+1}}{-k+1} \tag{2a}$$

$$\Psi(z) = \frac{-i\mu_0(b_1 - ib_2)}{\pi(\kappa_0 + 1)} e^{-i\beta} \log(z-h) - \frac{i\mu_0(b_1 + ib_2)}{\pi(\kappa_0 + 1)} e^{i\beta} \frac{\bar{h}}{(z-h)} + a_o' z + a_1' \log z + \sum_{k=2}^{\infty} \frac{a_k' z^{-k+1}}{-k+1} \tag{2b}$$

The increment in displacement due to moving around a closed curve is given by
$[2\mu(u+iv)]_c = [\kappa_0 \Phi(z) - z\bar{\Phi}'(z) - \Psi(z)]_c = 0$; for single valuedness

Putting the values we get,

$$\kappa_0 \{\frac{i\mu_0(b_1 + ib_2)e^{i\beta}}{\pi(\kappa_0 + 1)} 2\pi i + 2\pi i a_1\} - \{\frac{i\mu_0(b_1 + ib_2)e^{i\beta}}{\pi(\kappa_0 + 1)} (-2\pi i) + (-2\pi i)\bar{a}_1' = 0$$

$$\kappa_0 \frac{i\mu_0(b_1 + ib_2)e^{i\beta}}{\pi(\kappa_0 + 1)} + \kappa_0 a_1 + \frac{i\mu_0(b_1 + ib_2)e^{i\beta}}{\pi(\kappa_0 + 1)} + \bar{a}_1' = 0$$

$$\kappa_0 a_1 + \bar{a}_1' = (\kappa_0 + 1) \frac{i\mu_0(b_1 + ib_2)e^{i\beta}}{\pi(\kappa_0 + 1)} \tag{3}$$

Stress components are related by,

$$\sigma_r^d + i\sigma_{r\theta}^d = \Phi(z) + \overline{\Phi(z)} + \left[\bar{z}\Phi'(z) + \Psi(z)\right]e^{2i\theta} \tag{4a}$$

$$\sigma_r^d - i\sigma_{r\theta}^d = \Phi(z) + \overline{\Phi(z)} - \left[\bar{z}\Phi'(z) + \Psi(z)\right]e^{2i\theta} \tag{4b}$$

Eq(1) can be rewritten as

$$\Phi(z) = pi(b_1 + ib_2)e^{i\beta}\frac{1}{z-h} + \sum_{k=0}^{\infty} a_k z^{-k} \tag{5a}$$

$$\Psi(z) = -pi(b_1 - ib_2)e^{-i\beta}\frac{1}{z-h} + pi(b_1 + ib_2)e^{i\beta}\frac{\bar{h}}{(z-h)^2} + \sum_{k=0}^{\infty} a_k z^{-k} \tag{5b}$$

$$\Phi'(z) = -pi(b_1 + ib_2)e^{i\beta}\frac{1}{(z-h)^2} + \sum_{k=1}^{\infty} a_k z^{-(k+1)}(-k) \tag{5c}$$

$$\bar{\Phi}(z) = -pi(b_1 - ib_2)e^{-i\beta}\frac{1}{\bar{z}-\bar{h}} + \sum_{k=0}^{\infty} \bar{a}_k \bar{z}^{-k};\ p = \frac{\mu}{\pi(\kappa_0 + 1)} \tag{5d}$$

Substituting Eqs 5(a-d) into equation (4b), we obtain

$$\sigma_r^d - i\sigma_{r\theta}^d = Pi(b_1 + ib_2)e^{i\beta}\frac{1}{z-h} + \sum_{k=0}^{\infty} a_k z^{-k} + \sum_{k=0}^{\infty} \bar{a}_k \bar{z}^{-k} - Pi(b_1 - ib_2)e^{-i\beta}\frac{1}{\bar{z}-\bar{h}} - e^{2i\theta}\left[-Pi(b_1 + ib_2)e^{i\beta}\frac{\bar{z}}{(z-h)^2} + \right.$$
$$\left. \sum_{k=1}^{\infty}(-k)\bar{z}a_k z^{-(k+1)} - Pi(b_1 - ib_2)e^{-i\beta}\frac{1}{z-h} + Pi(b_1 + ib_2)e^{i\beta}\frac{\bar{h}}{(z-h)^2} + \sum_{k=0}^{\infty} a_k' z^{-k}\right] \tag{6}$$

Along the boundary of the circle, $\sigma_r^d - i\sigma_{r\theta}^d = 0$; $z = x + iy = R*e^{i\theta}$ and $\bar{z} = R*e^{-i\theta}$; Thus equation (6) reduces to,

$$Pi(b_1 + ib_2)e^{i\beta}\frac{1}{R*e^{i\theta} - h} + \sum_{k=0}^{\infty} a_k R^{-k} e^{-ki\theta} + \sum_{k=0}^{\infty} \bar{a}_k R^{-k} e^{ki\theta} - Pi(b_1 - ib_2)e^{-i\beta}\frac{1}{R*e^{-i\theta} - \bar{h}} - e^{2i\theta}\left[-Pi(b_1 + ib_2)e^{i\beta}\frac{R*e^{-i\theta}}{(R*e^{i\theta} - h)^2} + \right.$$
$$\left. \sum_{k=1}^{\infty}(-k)R*e^{-i\theta}a_k R^{-(k+1)}e^{-(k+1)i\theta} - Pi(b_1 - ib_2)e^{-i\beta}\frac{1}{R*e^{i\theta} - h} + Pi(b_1 + ib_2)e^{i\beta}\frac{\bar{h}}{(R*e^{i\theta} - h)^2} + \sum_{k=0}^{\infty} a_k' R^{-k} e^{-ki\theta}\right] = 0 \tag{7}$$

Now,

$$\text{R.H.S} = -Pi(b_1 + ib_2)e^{i\beta}\frac{1}{R*e^{i\theta} - h} + Pi(b_1 - ib_2)e^{-i\beta}\frac{1}{R*e^{-i\theta} - \bar{h}} - e^{2i\theta}Pi(b_1 + ib_2)e^{i\beta}\frac{R*e^{-i\theta}}{(R*e^{i\theta} - h)^2} - e^{2i\theta}$$
$$Pi(b_1 - ib_2)e^{-i\beta}\frac{1}{R*e^{i\theta} - h} + e^{2i\theta}Pi(b_1 + ib_2)e^{i\beta}\frac{\bar{h}}{(R*e^{i\theta} - h)^2}$$

$$= Pi(b_1 + ib_2)e^{i\beta}\frac{1}{h}(1-\frac{R*e^{i\theta}}{h})^{-1} - Pi(b_1 - ib_2)e^{-i\beta}\frac{1}{\bar{h}}(1-\frac{R*e^{-i\theta}}{\bar{h}})^{-1} - Pi(b_1 + ib_2)e^{i\beta}\frac{R*e^{(2i\theta - i\theta)}}{h^2}(1-\frac{R*e^{i\theta}}{h})^{-2} + e^{2i\theta}$$

$$Pi(b_1 - ib_2)e^{-i\beta}\frac{1}{h}(1-\frac{R*e^{i\theta}}{h})^{-1} + e^{2i\theta}Pi(b_1 + ib_2)e^{i\beta}\frac{\bar{h}}{h^2}(1-\frac{R*e^{i\theta}}{h})^{-2}$$

$$= Pi(b_1 + ib_2)e^{i\beta}\frac{1}{h}\sum_{k=0}^{\infty}\frac{R^k e^{ki\theta}}{h^k} - Pi(b_1 - ib_2)e^{-i\beta}\frac{1}{\bar{h}}\sum_{k=0}^{\infty}\frac{R^k e^{-ki\theta}}{\bar{h}^k} - Pi(b_1 + ib_2)e^{i\beta}\frac{R*e^{i\theta}}{h^2}\sum_{k=0}^{\infty}\frac{R^k e^{ki\theta}}{h^k}(k+1) +$$

$$Pi(b_1 - ib_2)e^{-i\beta}\frac{e^{2i\theta}}{h}\sum_{k=0}^{\infty}\frac{R^k e^{ki\theta}}{h^k} + Pi(b_1 + ib_2)e^{i\beta}\frac{\bar{h}*e^{2i\theta}}{h^2}\sum_{k=0}^{\infty}\frac{R^k e^{ki\theta}}{h^k}(k+1)$$

$$= Pi(b_1 + ib_2)e^{i\beta}\sum_{k=0}^{\infty}\frac{R^k e^{ki\theta}}{h^{k+1}} - Pi(b_1 - ib_2)e^{-i\beta}\sum_{k=0}^{\infty}\frac{R^k e^{-ki\theta}}{\bar{h}^{k+1}} - Pi(b_1 + ib_2)e^{i\beta}\sum_{k=0}^{\infty}\frac{R^{k+1}}{h^{k+2}}e^{(k)i\theta}(k+1) +$$

$$Pi(b_1 - ib_2)e^{-i\beta}\sum_{k=0}^{\infty}\frac{R^k e^{(k+2)i\theta}}{h^{k+1}} + Pi(b_1 + ib_2)e^{i\beta}\sum_{k=0}^{\infty}\frac{\bar{h}R^k}{h^{k+2}}e^{(k+2)i\theta}(k+1)$$

$$= B_p\frac{1}{h}\sum_{k=0}^{\infty}\frac{R^k e^{ki\theta}}{h^k} - B_m\frac{1}{\bar{h}}\sum_{k=0}^{\infty}\frac{R^k e^{-ki\theta}}{\bar{h}^k} - B_p\frac{R*e^{i\theta}}{h^2}\sum_{k=0}^{\infty}\frac{R^k e^{ki\theta}}{h^k}(k+1) +$$

$$B_m\frac{e^{2i\theta}}{h}\sum_{k=0}^{\infty}\frac{R^k e^{ki\theta}}{h^k} + B_p\frac{\bar{h}*e^{2i\theta}}{h^2}\sum_{k=0}^{\infty}\frac{R^k e^{ki\theta}}{h^k}(k-1)$$

where,

$$B_p = Pi(b_1 + ib_2)e^{i\beta}$$

$$B_m = Pi(b_1 - ib_2)e^{-i\beta}$$

$$\text{L.H.S} = \sum_{k=0}^{\infty}a_k R^{-k}e^{-ki\theta} + \sum_{k=0}^{\infty}\bar{a}_k R^{-k}e^{ki\theta} + e^{2i\theta}\sum_{k=1}^{\infty}kR*e^{-i\theta}a_k R^{-(k+1)}e^{-(k+1)i\theta} - e^{2i\theta}\sum_{k=0}^{\infty}a'_k R^{-k}e^{-ki\theta}$$

$$= \sum_{k=0}^{\infty}a_k R^{-k}e^{-ki\theta} + \sum_{k=0}^{\infty}\bar{a}_k R^{-k}e^{ki\theta} + \sum_{k=1}^{\infty}ke^{-i\theta}a_k R^{-k}e^{-ki\theta} - \sum_{k=0}^{\infty}a'_k R^{-k}e^{-(k-2)i\theta}$$

$$= \sum_{k=0}^{\infty}\frac{k+1}{R^k}a_k e^{-ki\theta} + \sum_{k=0}^{\infty}\frac{\bar{a}_k}{R^k}e^{ki\theta} - a'_0 e^{2i\theta} - \frac{a'_1}{R}e^{i\theta} - \sum_{k=0}^{\infty}\frac{a'_{k+2}}{R^{k+2}}e^{-ki\theta}$$

Now, Equation (7) can be written as,

$$\sum_{k=0}^{\infty}\frac{k+1}{R^k}a_k e^{-ki\theta} + \sum_{k=0}^{\infty}\frac{\bar{a}_k}{R^k}e^{ki\theta} - a'_0 e^{2i\theta} - \frac{a'_1}{R}e^{i\theta} - \sum_{k=0}^{\infty}\frac{a'_{k+2}}{R^{k+2}}e^{-ki\theta} = B_p\frac{1}{h}\sum_{k=0}^{\infty}\frac{R^k e^{ki\theta}}{h^k} - B_m\frac{1}{\bar{h}}\sum_{k=0}^{\infty}\frac{R^k e^{-ki\theta}}{\bar{h}^k} - B_p\frac{R*e^{i\theta}}{h^2}\sum_{k=0}^{\infty}\frac{R^k e^{ki\theta}}{h^k}$$

$$B_m\frac{e^{2i\theta}}{h}\sum_{k=0}^{\infty}\frac{R^k e^{ki\theta}}{h^k} + B_p\frac{\bar{h}*e^{2i\theta}}{h^2}\sum_{k=0}^{\infty}\frac{R^k e^{ki\theta}}{h^k}(k-1) \qquad (8)$$

For, k=0;

$$a_0 + \bar{a}_0 - \frac{a'_2}{R^2} - a'_0 e^{2i\theta} - \frac{a'_1}{R}e^{i\theta} = \frac{B_p}{h} - \frac{B_m}{\bar{h}} - \frac{B_p}{h^2}R*e^{i\theta} + \frac{B_m}{h}e^{2i\theta} + \frac{B_p\bar{h}}{h^2}e^{2i\theta}$$

Equating constant terms ,we obtain(terms without $e^{i\theta}$)

$$a_0 + \bar{a}_0 - \frac{a_2'}{R^2} = \frac{B_p}{h} - \frac{B_m}{\bar{h}}$$

$$2a_0 - \frac{a_2'}{R^2} = \frac{B_p}{h} - \frac{B_m}{\bar{h}}; a_0 = real$$

$$a_2' = \frac{B_p}{h} R^2 - \frac{B_m}{\bar{h}} R^2 + 2a_0 R^2 \tag{9}$$

For k=1,

$$\frac{2a_1}{R} e^{-i\theta} + \frac{\bar{a}_1}{R} e^{i\theta} - a_0' e^{2i\theta} - \frac{a_1'}{R} e^{i\theta} - \frac{a_3'}{R^3} e^{-i\theta} = \frac{B_p}{h^2} R * e^{i\theta} - \frac{B_m}{\bar{h}^2} R * e^{-i\theta} - \frac{B_p}{h^2} R * e^{i\theta} + \frac{B_m}{h} e^{2i\theta} + \frac{B_p \bar{h}}{h^2} e^{2i\theta}$$

Equating co efficient of $e^{i\theta}$,we get

$$\frac{\bar{a}_1}{R} - \frac{a_1'}{R} = \frac{B_p}{h^2} R - \frac{B_p}{h^2} R$$

$$\bar{a}_1 - a_1' = 0 \tag{10}$$

Now ,Equating co efficient of $e^{2i\theta}$ for k=2,we get

$$\frac{\bar{a}_2}{R^2} - a_0' = B_p \frac{R^2}{h^3} - 2B_p \frac{R^2}{h^3} + \frac{B_m}{h} + B_p \frac{\bar{h}}{h^2}$$

$$\frac{\bar{a}_2}{R^2} - a_0' = -B_p \frac{R^2}{h^3} + \frac{B_m}{h} + B_p \frac{\bar{h}}{h^2}$$

$$\bar{a}_2 = -B_p \frac{R^4}{h^3} + \frac{B_m R^2}{h} + B_p \frac{\bar{h} R^2}{h^2} + a_0' R^2$$

So,

$$a_2 = -B_p \frac{R^4}{\bar{h}^3} + \frac{B_m R^2}{\bar{h}} + B_p \frac{h R^2}{\bar{h}^2} + \bar{a}_0' R^2 \tag{11}$$

Thus, co efficient of $e^{ki\theta}$ with $k \geq 3$

$$\frac{\bar{a}_k}{R^k} = B_p \frac{R^k}{h^{k+1}} - B_p \frac{kR^k}{h^{k+1}} + B_m \frac{R^{k-2}}{h^{k-1}} + (k-1) B_p \frac{\bar{h} R^{k-2}}{h^k}$$

$$= -(k-1) B_p \frac{R^k}{h^{k+1}} + (k-1) B_p \frac{\bar{h} R^{k-2}}{h^k} + B_m \frac{R^{k-2}}{h^{k-1}}$$

$$\bar{a}_k = (k-1) B_p [\frac{\bar{h} R^{2(k-1)}}{h^k} - \frac{R^{2k}}{h^{k+1}}] + B_m \frac{R^{2(k-1)}}{h^{k-1}}$$

So,

$$a_k = (k-1) \bar{B}_p [\frac{h R^{2(k-1)}}{\bar{h}^k} - \frac{R^{2k}}{\bar{h}^{k+1}}] + B_m \frac{R^{2(k-1)}}{\bar{h}^{k-1}}; k \geq 3 \tag{12}$$

Co efficient of $e^{-ki\theta}$ with $k \geq 1$ will be,

$$\frac{1+k}{R^k} a_k - \frac{1}{R^{k+1}} a'_{k+2} = -B_m \frac{R^k}{\bar{h}^{k+1}}$$

$$a'_{k+2} = B_m \frac{R^{2(k+1)}}{\bar{h}^{k+1}} + \frac{1+k}{R^{k+2}} R^2 a_k$$

$$= B_m \frac{R^{2(k+1)}}{\bar{h}^{k+1}} + (k+1) R^2 a_k, k \geq 1 \ ;$$

So,

$$a'_k = B_m \frac{R^{2(k-1)}}{\bar{h}^{k-1}} + (k-1) R^2 a_{k-2}, k \geq 3 \tag{13}$$

Solving Eqs.(3) and (10),we get

$$a_1 = -B_p \tag{14}$$

So, $a'_1 = -\bar{B}_p$ (15)

The co efficient a_0 and a'_0 represent the stress distribution at infinity. For present case(dislocation only), they are zero.

Thus the coefficient a_2 and a'_2 reduce to

$$a_2 = -B_p \frac{R^4}{\bar{h}^3} + \frac{B_m R^2}{\bar{h}} + B_p \frac{hR^2}{\bar{h}^2} \tag{16a}$$

$$a'_2 = -B_p \frac{R^2}{h} + \frac{B_m R^2}{\bar{h}} \tag{16b}$$

Now we can write the potential functions for edge dislocation in a plane with hole or radius R as follows

$$\Phi(z) = \frac{i\mu_0 (b_1 + ib_2)}{\pi(\kappa_0 + 1)} e^{i\beta} \frac{1}{z-h} - \frac{i\mu_0 (b_1 + ib_2)}{\pi(\kappa_0 + 1)} e^{i\beta} \frac{1}{z} + a_2 \frac{1}{z^2} + \sum_{k=3}^{\infty} a_k z^{-k} \tag{17a}$$

$$\Psi(z) = \frac{-i\mu_0 (b_1 - ib_2)}{\pi(\kappa_0 + 1)} e^{-i\beta} \frac{1}{z-h} + \frac{i\mu_0 (b_1 + ib_2)}{\pi(\kappa_0 + 1)} e^{i\beta} \frac{\bar{h}}{(z-h)^2} + \frac{i\mu_0 (b_1 - ib_2)}{\pi(\kappa_0 + 1)} e^{-i\beta} \frac{1}{z} + a'_2 \frac{1}{z^2} + \sum_{k=3}^{\infty} a'_k z^{-k} \tag{17b}$$

Now, we consider that the dislocation is located on the x axis and at a distance $h=R+s$. Here $h = \bar{h} = \text{Real}$ .For this dislocation we set b_2 =0 and β=-90°. So b_1=b

$$e^{i\beta} = \cos\beta + i\sin\beta = \cos 90 - i\sin 90 = -i$$

$$e^{-i\beta} = \cos\beta - i\sin\beta = \cos 90 + i\sin 90 = i$$

Equation (17) reduces to

$$\Phi(z)=\frac{i\mu_0 b(-i\,|)}{\pi(\kappa_0+1)}\frac{1}{z-h}-\frac{i\mu_0 b(-i)}{\pi(\kappa_0+1)}\frac{1}{z}+a_2\frac{1}{z^2}+\sum_{k=3}^{\infty}a_k z^{-k}$$

$$=\frac{\mu_0 b}{\pi(\kappa_0+1)}[\frac{1}{z-h}-\frac{1}{z}]+a_2\frac{1}{z^2}+\sum_{k=3}^{\infty}a_k z^{-k}$$

$$\Psi(z)=\frac{-i\mu_0 b(i)}{\pi(\kappa_0+1)}\frac{1}{z-h}+\frac{i\mu_0 b(i)}{\pi(\kappa_0+1)}\frac{h}{(z-h)^2}+\frac{i\mu_0 b(i)}{\pi(\kappa_0+1)}\frac{1}{z}+a_2'\frac{R^2}{h}\frac{1}{z^2}+\sum_{k=3}^{\infty}a_k' z^{-k}$$

$$=\frac{\mu_0 b}{\pi(\kappa_0+1)}\frac{1}{z-h}+\frac{\mu_0 b}{\pi(\kappa_0+1)}\frac{h}{(z-h)^2}-\frac{\mu_0 b}{\pi(\kappa_0+1)}\frac{1}{z}+a_2'\frac{R^2}{h}\frac{1}{z^2}+\sum_{k=3}^{\infty}a_k' z^{-k}$$

Again,

$$B_m=Pi(b_1-ib_2)e^{-i\beta}=-Pb=-\frac{\mu_0 b}{\pi(\kappa_0+1)}$$

$$B_p=Pi(b_1+ib_2)e^{i\beta}=Pb=\frac{\mu_0 b}{\pi(\kappa_0+1)}$$

$$a_2=-B_p\frac{R^4}{\bar{h}^3}+\frac{B_m R^2}{\bar{h}}+B_p\frac{hR^2}{\bar{h}^2}$$

$$=-\frac{\mu_0 b}{\pi(\kappa_0+1)}\frac{R^4}{\bar{h}^3}-\frac{\mu_0 b}{\pi(\kappa_0+1)}\frac{R^2}{h}+\frac{\mu_0 b}{\pi(\kappa_0+1)}\frac{R^2}{h}$$

$$=-\frac{\mu_0 b}{\pi(\kappa_0+1)}\frac{R^4}{h^3}\ ;$$

$$a_2'=-B_p\frac{R^2}{h}+\frac{B_m R^2}{\bar{h}}$$

$$=-\frac{\mu_0 b}{\pi(\kappa_0+1)}\frac{R^2}{h}-\frac{\mu_0 b}{\pi(\kappa_0+1)}\frac{R^2}{h}$$

$$=-\frac{2\mu_0 b}{\pi(\kappa_0+1)}\frac{R^2}{h}\ .$$

$$a_k=(k-1)\bar{B}_p[\frac{hR^{2(k-1)}}{\bar{h}^k}-\frac{R^{2k}}{\bar{h}^{k+1}}]+B_m\frac{R^{2(k-1)}}{\bar{h}^{k-1}};k\geq 3$$

$$=(k-1)\frac{\mu_0 b}{\pi(\kappa_0+1)}[\frac{R^{2(k-1)}}{h^{k-1}}-\frac{R^{2k}}{h^{k+1}}]-\frac{\mu_0 b}{\pi(\kappa_0+1)}\frac{R^{2(k-1)}}{h^{k-1}}$$

$$=\frac{\mu_0 b}{\pi(\kappa_0+1)}[k\frac{R^{2(k-1)}}{h^{k-1}}-\frac{R^{2(k-1)}}{h^{k-1}}-k\frac{R^{2k}}{h^{k+1}}+\frac{R^{2k}}{h^{k+1}}-\frac{R^{2(k-1)}}{h^{k-1}}]$$

$$=\frac{\mu_0 b}{\pi(\kappa_0+1)}[(k-2)\frac{R^{2(k-1)}}{h^{k-1}}-(k-1)\frac{R^{2k}}{h^{k+1}}]$$

$$=\frac{\mu_0 b}{\pi(\kappa_0+1)}A_k;A_k=[(k-2)\frac{R^{2(k-1)}}{h^{k-1}}-(k-1)\frac{R^{2k}}{h^{k+1}}]$$

$$a_k' = -\frac{\mu_0 b}{\pi(\kappa_0+1)}\frac{R^{2(k-1)}}{\bar{h}^{k-1}} + \frac{\mu_0 b}{\pi(\kappa_0+1)}(k-1)R^2 A_{k-2}; a_{k-2} = \frac{\mu_0 b}{\pi(\kappa_0+1)}A_{k-2}$$

$$= \frac{\mu_0 b}{\pi(\kappa_0+1)}A_k'; A_k' = (k-1)R^2 A_{k-2} - \frac{R^{2(k-1)}}{\bar{h}^{k-1}}$$

Thus we obtain,

$$\Phi(z) = \frac{\mu_0 b}{\pi(\kappa_0+1)}[\frac{1}{z-h} - \frac{1}{z}] - \frac{\mu b}{\pi(\kappa_0+1)}\frac{R^4}{h^3}\frac{1}{z^2} + \sum_{k=3}^{\infty}\frac{\mu b}{\pi(\kappa_0+1)}A_k z^{-k}$$

$$= \frac{\mu_0 b}{\pi(\kappa_0+1)}[\frac{1}{z-h} - \frac{1}{z} - \frac{R^4}{h^3}\frac{1}{z^2} + \sum_{k=3}^{\infty}A_k z^{-k}] \tag{18a}$$

$$\Psi(z) = \frac{-i\mu_0 b(i)}{\pi(\kappa_0+1)}\frac{1}{z-h} + \frac{i\mu_0 b(i)}{\pi(\kappa_0+1)}\frac{h}{(z-h)^2} + \frac{i\mu_0 b(i)}{\pi(\kappa_0+1)}\frac{1}{z} - \frac{2\mu_0 b}{\pi(\kappa_0+1)}\frac{R^2}{h}\frac{1}{z^2} + \sum_{k=3}^{\infty}\frac{\mu_0 b}{\pi(\kappa_0+1)}A_k' z^{-k}$$

$$= \frac{\mu_0 b}{\pi(\kappa_0+1)}[\frac{1}{z-h} + \frac{h}{(z-h)^2} - \frac{1}{z} - \frac{2R^2}{h}\frac{1}{z^2} + \sum_{k=3}^{\infty}A_k' z^{-k}] \tag{18b}$$

Again,

$$\Phi'(z) = \frac{\mu_0 b}{\pi(\kappa_0+1)}[-\frac{1}{(z-h)^2} + \frac{1}{z^2} - \frac{2R^4}{h^3}\frac{1}{z^3} - \sum_{k=3}^{\infty}kA_k z^{-(k+1)}]$$

$$\bar{\Phi}(z) = \frac{\mu_0 b}{\pi(\kappa_0+1)}[\frac{1}{\bar{z}-h} - \frac{1}{\bar{z}} - \frac{R^4}{h^3}\frac{1}{\bar{z}^2} + \sum_{k=3}^{\infty}A_k \bar{z}^{-k}]$$

For continuous distribution of edge dislocations, the potential functions are written as

$$\Phi(z) = \frac{\mu_0 b}{\pi(\kappa_0+1)}\int_R^{R+l}[\frac{1}{z-h} - \frac{1}{z} - \frac{R^4}{h^3}\frac{1}{z^2} + \sum_{k=3}^{\infty}A_k z^{-k}]b(h)dh \tag{19a}$$

$$\Phi'(z) = \frac{\mu_0 b}{\pi(\kappa_0+1)}\int_R^{R+l}[-\frac{1}{(z-h)^2} + \frac{1}{z^2} - \frac{2R^4}{h^3}\frac{1}{z^3} - \sum_{k=3}^{\infty}kA_k z^{-(k+1)}]b(h)dh \tag{19b}$$

$$\bar{\Phi}(z) = \frac{\mu_0 b}{\pi(\kappa_0+1)}\int_R^{R+l}[\frac{1}{\bar{z}-h} - \frac{1}{\bar{z}} - \frac{R^4}{h^3}\frac{1}{\bar{z}^2} + \sum_{k=3}^{\infty}A_k \bar{z}^{-k}]b(h)dh \tag{19c}$$

$$\Psi(z) = \frac{\mu_0 b}{\pi(\kappa_0+1)}\int_R^{R+l}[\frac{1}{z-h} + \frac{h}{(z-h)^2} - \frac{1}{z} - \frac{2R^2}{h}\frac{1}{z^2} + \sum_{k=3}^{\infty}A_k' z^{-k}]b(h)dh \tag{19d}$$

Substitution of Eq. (19)into Eq. (4a)provides

$$[\sigma_r^d + i\sigma_{r\theta}^d]_{\mathrm{I}} = \frac{\mu_0 b}{\pi(\kappa_0+1)}\int_R^{R+l}[2\{\frac{1}{z-h} - \frac{1}{z} - \frac{R^4}{h^3}\frac{1}{z^2} + \sum_{k=3}^{\infty}A_k z^{-k}\} + \{-\frac{\bar{z}}{(z-h)^2} + \frac{\bar{z}}{z^2} + \frac{2R^4}{h^3}\frac{\bar{z}}{z^3}$$

$$-\sum_{k=3}^{\infty} kA_k \bar{z} z^{-(k+1)} + \frac{1}{z-h} + \frac{h}{(z-h)^2} - \frac{1}{z} - \frac{2R^2}{h}\frac{1}{z^2} + \sum_{k=3}^{\infty} A'_k z^{-k}\}e^{2i\theta}]b(h)dh$$

Along the *x* axis,θ=0, $z = re^{i\theta} = r = \bar{z}$

$$[\sigma_r^d + i\sigma_{r\theta}^d]_{\mathrm{I}} = \frac{\mu_0 b}{\pi(\kappa_0+1)}\int_R^{R+l}[\{\frac{2}{r-h} - \frac{2}{r} - \frac{2R^4}{h^3}\frac{1}{r^2} + 2\sum_{k=3}^{\infty} A_k r^{-k} - \frac{r}{(r-h)^2} + \frac{1}{r} + \frac{2R^4}{h^3}\frac{1}{r^2} - \sum_{k=3}^{\infty} kA_k r^{-k} + \frac{1}{r-h} + \frac{h}{(r-h)^2}$$

$$-\frac{1}{r} - \frac{2R^2}{h}\frac{1}{r^2} + \sum_{k=3}^{\infty} A'_k r^{-k}]b(h)dh$$

$$= \frac{\mu_0 b}{\pi(\kappa_0+1)}\int_R^{R+l}[\{\frac{3}{r-h} - \frac{2}{r} - \frac{r}{(r-h)^2} + \frac{h}{(r-h)^2} - \frac{2R^2}{h}\frac{1}{r^2} + \sum_{k=3}^{\infty}(2-k)A_k r^{-k} + \sum_{k=3}^{\infty} A'_k r^{-k}]b(h)dh$$

$$= \frac{\mu_0 b}{\pi(\kappa_0+1)}\int_R^{R+l}[\{\frac{2}{r-h} - \frac{2}{r} - \frac{2R^2}{h}\frac{1}{r^2} + \sum_{k=3}^{\infty}(2-k)A_k r^{-k} + \sum_{k=3}^{\infty} A'_k r^{-k}]b(h)dh$$

So,

$$[\sigma_r^d + i\sigma_{r\theta}^d]_{\mathrm{I}} = \frac{2\mu_0 b}{\pi(\kappa_0+1)}\int_R^{R+l}[\{\frac{1}{r-h} - \frac{1}{r} - \frac{R^2}{h}\frac{1}{r^2} + \frac{1}{2}\sum_{k=3}^{\infty}(2-k)A_k r^{-k} + \frac{1}{2}\sum_{k=3}^{\infty} A'_k r^{-k}]b(h)dh \qquad (20)$$

Assume, *r=R+x ; h=R+s, dh=ds* .applying in Eq. (20) we get,

$$[\sigma_r^d + i\sigma_{r\theta}^d]_{\mathrm{I}} = \frac{2\mu_0 b}{\pi(\kappa_0+1)}\int_0^{l}[\{\frac{1}{x-s} - \frac{1}{R+x} - \frac{R^2}{R+s}\frac{1}{(R+x)^2} + \frac{1}{2}\sum_{k=3}^{\infty}(2-k)A_k (R+x)^{-k} + \frac{1}{2}\sum_{k=3}^{\infty} A'_k (R+x)^{-k}]b(s)ds \qquad (21)$$

where,

$$A_k = (k-2)\frac{R^{2(k-1)}}{(R+s)^{k-1}} - (k-1)\frac{R^{2k}}{(R+s)^{k+1}} \qquad (22a)$$

$$A'_k = (k-1)R^2 A_{k-2} - \frac{R^{2(k-1)}}{(R+s)^{k-1}} \qquad (22b)$$

If we now consider another dislocation located on the *x* axis just diametrically opposing the previous dislocation at a distance *h=-h=-(R+s).F*or this dislocation we set β=90^o and b_1=-*b*

$$e^{i\beta} = \cos\beta + i\sin\beta = \cos 90 + i\sin 90 = i$$

$$e^{-i\beta} = \cos\beta - i\sin\beta = \cos 90 - i\sin 90 = -i$$

Equation (17) reduces to

$$\Phi(z) = \frac{i\mu_0 b(i|)}{\pi(\kappa_0+1)}\frac{1}{z+h} - \frac{i\mu_0 b(i)}{\pi(\kappa_0+1)}\frac{1}{z} + a_2\frac{1}{z^2} + \sum_{k=3}^{\infty} a_k z^{-k}$$

$$= \frac{\mu b}{\pi(\kappa_0+1)}[-\frac{1}{z+h} + \frac{1}{z}] + a_2\frac{1}{z^2} + \sum_{k=3}^{\infty} a_k z^{-k}$$

$$\Psi(z) = \frac{-i\mu_0 b(-i)}{\pi(\kappa_0+1)}\frac{1}{z+h} + \frac{i\mu_0 b(i)}{\pi(\kappa_0+1)}\frac{h}{(z+h)^2} + \frac{i\mu_0 b(-i)}{\pi(\kappa_0+1)}\frac{1}{z} + a_2'\frac{R^2}{h}\frac{1}{z^2} + \sum_{k=3}^{\infty} a_k' z^{-k}$$

$$= -\frac{\mu_0 b}{\pi(\kappa_0+1)}\frac{1}{z+h} + \frac{\mu_0 b}{\pi(\kappa_0+1)}\frac{h}{(z+h)^2} + \frac{\mu_0 b}{\pi(\kappa_0+1)}\frac{1}{z} + a_2'\frac{R^2}{h}\frac{1}{z^2} + \sum_{k=3}^{\infty} a_k' z^{-k}$$

Again,

$$B_m = Pi(b_1 - ib_2)e^{-i\beta} = Pb = \frac{\mu_0 b}{\pi(\kappa_0+1)}$$

$$B_p = Pi(b_1 + ib_2)e^{i\beta} = -Pb = -\frac{\mu_0 b}{\pi(\kappa_0+1)}$$

$$a_2 = -B_p\frac{R^4}{\bar{h}^3} + \frac{B_m R^2}{\bar{h}} + B_p\frac{hR^2}{\bar{h}^2}$$

$$= \frac{\mu_0 b}{\pi(\kappa_0+1)}\frac{R^4}{(-h)^3} + \frac{\mu_0 b}{\pi(\kappa_0+1)}\frac{R^2}{h} - \frac{\mu_0 b}{\pi(\kappa_0+1)}\frac{R^2}{h}$$

$$= -\frac{\mu_0 b}{\pi(\kappa_0+1)}\frac{R^4}{h^3}\ ;$$

$$a_2' = -B_p\frac{R^2}{h} + \frac{B_m R^2}{\bar{h}}$$

$$= \frac{\mu_0 b}{\pi(\kappa_0+1)}\frac{R^2}{(-h)} + \frac{\mu_0 b}{\pi(\kappa_0+1)}\frac{R^2}{(-h)}$$

$$= -\frac{2\mu_0 b}{\pi(\kappa_0+1)}\frac{R^2}{h}\ .$$

$$a_k = (k-1)\bar{B}_p[\frac{hR^{2(k-1)}}{\bar{h}^k} - \frac{R^{2k}}{\bar{h}^{k+1}}] + B_m\frac{R^{2(k-1)}}{\bar{h}^{k-1}}; k \geq 3$$

$$= -(k-1)\frac{\mu_0 b}{\pi(\kappa_0+1)}[\frac{R^{2(k-1)}}{(-h)^{k-1}} - \frac{R^{2k}}{(-h)^{k+1}}] - \frac{\mu_0 b}{\pi(\kappa_0+1)}\frac{R^{2(k-1)}}{(-h)^{k-1}}$$

$$= -\frac{\mu_0 b}{\pi(\kappa_0+1)}[k\frac{R^{2(k-1)}}{h^{k-1}} - \frac{R^{2(k-1)}}{h^{k-1}} - k\frac{R^{2k}}{h^{k+1}} + \frac{R^{2k}}{h^{k+1}} + \frac{R^{2(k-1)}}{h^{k-1}}]$$

$$= -\frac{\mu_0 b}{\pi(\kappa_0+1)}[(k-2)\frac{R^{2(k-1)}}{(-1)^{k-1}h^{k-1}} - (k-1)\frac{R^{2k}}{(-1)^{k+1}h^{k+1}}]$$

$$= -\frac{\mu_0 b}{\pi(\kappa_0+1)}A_k; A_k = [(k-2)\frac{R^{2(k-1)}}{(-1)^{k-1}h^{k-1}} - (k-1)\frac{R^{2k}}{(-1)^{k+1}h^{k+1}}]$$

$$a'_k = \frac{\mu_0 b}{\pi(\kappa_0+1)}\frac{R^{2(k-1)}}{\bar{h}^{k-1}} - \frac{\mu_0 b}{\pi(\kappa_0+1)}(k-1)R^2 A_{k-2}; a_{k-2} = -\frac{\mu_0 b}{\pi(\kappa_0+1)}A_{k-2}$$

$$= \frac{\mu_0 b}{\pi(\kappa_0+1)}A'_k; A'_k = (k-1)(k-4)\frac{R^{2(k-2)}}{(-1)^{k-3}h^{k-3}} - (k-2)^2\frac{R^{2(k-1)}}{(-1)^{k-1}h^{k-1}}$$

Thus we obtain,

$$\Phi(z) = -\frac{\mu_0 b}{\pi(\kappa_0+1)}[\frac{1}{z+h} - \frac{1}{z}] - \frac{\mu_0 b}{\pi(\kappa_0+1)}\frac{R^4}{h^3}\frac{1}{z^2} - \sum_{k=3}^{\infty}\frac{\mu_0 b}{\pi(\kappa_0+1)}A_k z^{-k}$$

$$= -\frac{\mu_0 b}{\pi(\kappa_0+1)}[\frac{1}{z+h} - \frac{1}{z} + \frac{R^4}{h^3}\frac{1}{z^2} + \sum_{k=3}^{\infty}A_k z^{-k}] \tag{23a}$$

$$\Psi(z) = -\frac{\mu_0 b}{\pi(\kappa_0+1)}\frac{1}{z+h} + \frac{\mu_0 b}{\pi(\kappa_0+1)}\frac{h}{(z+h)^2} + \frac{\mu_0 b}{\pi(\kappa_0+1)}\frac{1}{z} - \frac{\mu_0 b}{\pi(\kappa_0+1)}\frac{2R^2}{h}\frac{1}{z^2} - \frac{\mu_0 b}{\pi(\kappa_0+1)}\sum_{k=3}^{\infty}A'_k z^{-k}$$

$$= -\frac{\mu_0 b}{\pi(\kappa_0+1)}[\frac{1}{z+h} - \frac{h}{(z+h)^2} - \frac{1}{z} + \frac{2R^2}{h}\frac{1}{z^2} + \sum_{k=3}^{\infty}A'_k z^{-k}] \tag{23b}$$

Again,

$$\Phi'(z) = -\frac{\mu_0 b}{\pi(\kappa_0+1)}[-\frac{1}{(z+h)^2} + \frac{1}{z^2} - \frac{2R^4}{h^3}\frac{1}{z^3} - \sum_{k=3}^{\infty}kA_k z^{-(k+1)}]$$

$$\bar{\Phi}(z) = -\frac{\mu_0 b}{\pi(\kappa_0+1)}[\frac{1}{\bar{z}+h} - \frac{1}{\bar{z}} + \frac{R^4}{h^3}\frac{1}{\bar{z}^2} + \sum_{k=3}^{\infty}A_k \bar{z}^{-k}]$$

For continuous distribution of edge dislocations, the potential functions are written as

$$\Phi(z) = -\frac{\mu_0 b}{\pi(\kappa_0+1)}\int_R^{R+l}[\frac{1}{z+h} - \frac{1}{z} + \frac{R^4}{h^3}\frac{1}{z^2} + \sum_{k=3}^{\infty}A_k z^{-k}]b(h)dh \tag{24a}$$

$$\Phi'(z) = -\frac{\mu_0 b}{\pi(\kappa_0+1)}\int_R^{R+l}[-\frac{1}{(z+h)^2} + \frac{1}{z^2} - \frac{2R^4}{h^3}\frac{1}{z^3} - \sum_{k=3}^{\infty}kA_k z^{-(k+1)}]b(h)dh \tag{24b}$$

$$\bar{\Phi}(z) = -\frac{\mu_0 b}{\pi(\kappa_0+1)}\int_R^{R+l}[\frac{1}{\bar{z}+h} - \frac{1}{\bar{z}} + \frac{R^4}{h^3}\frac{1}{\bar{z}^2} + \sum_{k=3}^{\infty}A_k \bar{z}^{-k}]b(h)dh \tag{24c}$$

$$\Psi(z) = -\frac{\mu_0 b}{\pi(\kappa_0+1)}\int_R^{R+l}[\frac{1}{z+h} - \frac{h}{(z+h)^2} - \frac{1}{z} + \frac{2R^2}{h}\frac{1}{z^2} + \sum_{k=3}^{\infty}A'_k z^{-k}]b(h)dh \tag{24d}$$

Substitution of Eq. (24)into Eq. (4a)provides

$$[\sigma_r^d + i\sigma_{r\theta}^d]_{\mathrm{II}} = -\frac{\mu_0 b}{\pi(\kappa_0+1)}\int_R^{R+l}[2\{\frac{1}{z+h}-\frac{1}{z}+\frac{R^4}{h^3}\frac{1}{z^2}+\sum_{k=3}^{\infty}A_k z^{-k}\}+\{-\frac{\bar{z}}{(z+h)^2}+\frac{\bar{z}}{z^2}-\frac{2R^4}{h^3}\frac{\bar{z}}{z^3}$$

$$-\sum_{k=3}^{\infty}kA_k\bar{z}z^{-(k+1)}+\frac{1}{z+h}-\frac{h}{(z+h)^2}-\frac{1}{z}+\frac{2R^2}{h}\frac{1}{z^2}+\sum_{k=3}^{\infty}A_k' z^{-k}\}e^{2i\theta}]b(h)dh$$

Along the *x* axis,θ=0, $z = re^{i\theta} = r = \bar{z}$

$$[\sigma_r^d + i\sigma_{r\theta}^d]_{\mathrm{II}} = \frac{\mu_0 b}{\pi(\kappa_0+1)}\int_R^{R+l}[\{\frac{2}{r+h}-\frac{2}{r}+\frac{2R^4}{h^3}\frac{1}{r^2}+2\sum_{k=3}^{\infty}A_k r^{-k}-\frac{r}{(r+h)^2}+\frac{1}{r}-\frac{2R^4}{h^3}\frac{1}{r^2}-\sum_{k=3}^{\infty}kA_k r^{-k}+\frac{1}{r+h}-\frac{h}{(r+h)^2}$$

$$-\frac{1}{r}+\frac{2R^2}{h}\frac{1}{r^2}+\sum_{k=3}^{\infty}A_k' r^{-k}]b(h)dh$$

$$=-\frac{\mu_0 b}{\pi(\kappa_0+1)}\int_R^{R+l}[\{\frac{3}{r+h}-\frac{2}{r}-\frac{r}{(r+h)^2}-\frac{h}{(r+h)^2}+\frac{2R^2}{h}\frac{1}{r^2}+\sum_{k=3}^{\infty}(2-k)A_k r^{-k}+\sum_{k=3}^{\infty}A_k' r^{-k}]b(h)dh$$

$$=-\frac{\mu_0 b}{\pi(\kappa_0+1)}\int_R^{R+l}[\{\frac{2}{r+h}-\frac{2}{r}+\frac{2R^2}{h}\frac{1}{r^2}+\sum_{k=3}^{\infty}(2-k)A_k r^{-k}+\sum_{k=3}^{\infty}A_k' r^{-k}]b(h)dh$$

So,

$$[\sigma_r^d + i\sigma_{r\theta}^d]_{\mathrm{II}} = -\frac{2\mu_0 b}{\pi(\kappa_0+1)}\int_R^{R+l}[\{\frac{1}{r+h}-\frac{1}{r}+\frac{R^2}{h}\frac{1}{r^2}+\frac{1}{2}\sum_{k=3}^{\infty}(2-k)A_k r^{-k}+\frac{1}{2}\sum_{k=3}^{\infty}A_k' r^{-k}]b(h)dh \qquad (25)$$

Assume, *r=R+x ; h=R+s, dh=ds* .applying in Eq. (24) we get,

$$[\sigma_r^d + i\sigma_{r\theta}^d]_{\mathrm{II}} = -\frac{2\mu_0 b}{\pi(\kappa_0+1)}\int_0^{l}[\{\frac{1}{2R+x+s}-\frac{1}{R+x}+\frac{R^2}{R+s}\frac{1}{(R+x)^2}+\frac{1}{2}\sum_{k=3}^{\infty}(2-k)A_k(R+x)^{-k}+\frac{1}{2}\sum_{k=3}^{\infty}A_k'(R+x)^{-k}]b(s)ds \qquad (26)$$

where,

$$A_k = (k-2)\frac{R^{2(k-1)}}{(-1)^{k-1}(R+s)^{k-1}}-(k-1)\frac{R^{2k}}{(-1)^{k+1}(R+s)^{k+1}} \qquad (27a)$$

$$A_k' = (k-1)(k-4)\frac{R^{2(k-2)}}{(-1)^{k-3}(R+s)^{k-3}}-(k-2)^2\frac{R^{2(k-1)}}{(-1)^{k-1}(R+s)^{k-1}} \qquad (27b)$$

Now, combining Eqs. (21) and (25) gives the resultant circumferential stress component of the disturbed stress field along the crack line of crack I as:

$$\sigma_\theta^d = \frac{2\mu_0}{\pi(k_0+1)}\int_0^{l}[\frac{1}{x-s}+f_1(r,h)-\frac{1}{2R+x+s}-f_2(r,h)]b(s)ds \qquad (28)$$

where

$$f_1(r,h) = -\frac{1}{R+x} - \frac{R^2}{R+s}\frac{1}{(R+x)^2} + \frac{1}{2}\sum_{k=3}^{\infty}(2-k)A_k(R+x)^{-k} + \frac{1}{2}\sum_{k=3}^{\infty}A_k'(R+x)^{-k} \qquad (29a)$$

$$f_1(r,h) = -\frac{1}{R+x} + \frac{R^2}{R+s}\frac{1}{(R+x)^2} + \frac{1}{2}\sum_{k=3}^{\infty}(2-k)A_k(R+x)^{-k} + \frac{1}{2}\sum_{k=3}^{\infty}A_k'(R+x)^{-k} \qquad (29b)$$

The boundary condition along the crack line of crack I given by Eq. (4.24) reduce to

$$\frac{2\mu_0}{\pi(k_0+1)}\int_0^l [\frac{1}{x-s} + f_1(r,h) - \frac{1}{2R+x+s} - f_2(r,h)]b(s)ds = -p(S_f\frac{\sigma_\theta^h}{\sigma_u}+1); R_i \le r \le R_i + l\,,\ \theta = 0^0 \qquad (30)$$

Equation (30) is the singular integral equations for the unknown density function $b(s)$, which is normalized over the interval [-1,+1] by using the substitutions

$$H = \frac{2t}{l} - 1, \qquad (31a)$$

$$T = \frac{2s}{l} - 1, \qquad (31b)$$

$$D = \frac{2R}{l}. \qquad (31c)$$

From Eqs. (29) we can get,

$$x = \frac{l}{2}(H+1); s = \frac{l}{2}(T+1); R = \frac{l}{2}D$$

$$R+x = \frac{l}{2}(D+H+1); R+s = \frac{l}{2}(D+T+1); 2R+x+s = \frac{l}{2}(2D+H++T+2)$$

$$b(s) = b(\frac{l}{2}T) = B(T); ds = \frac{l}{2}dt$$

Substituting above values in Eqs (22) we get,

$$A_k = (k-2)\frac{(\frac{l}{2})^{2(k-1)}D^{2(k-1)}}{(\frac{l}{2})^{k-1}(D+T+1)^{k-1}} - (k-1)\frac{(\frac{l}{2})^{2k}D^{2k}}{(\frac{l}{2})^{k+1}(D+T+1)^{k+1}}$$

$$= (\frac{l}{2})^{k-1}[(k-2)\frac{D^{2(k-1)}}{(D+T+1)^{k-1}} - (k-1)\frac{D^{2k}}{(D+T+1)^{k+1}}]$$

$$= (\frac{l}{2})^{k-1} B_k ; B_k = [(k-2)\frac{D^{2(k-1)}}{(D+T+1)^{k-1}} - (k-1)\frac{D^{2k}}{(D+T+1)^{k+1}}]$$

$$A'_k = (k-1)(k-4)\frac{(\frac{l}{2})^{2(k-2)} D^{2(k-2)}}{(\frac{l}{2})^{(k-3)}(D+T+1)^{k-3}} - (k-2)^2 \frac{(\frac{l}{2})^{2(k-2)} D^{2(k-1)}}{(\frac{l}{2})^{(k-1)}(D+T+1)^{k-1}}$$

$$= (k-1)(k-4)\frac{(\frac{l}{2})^{(k-1)} D^{2(k-2)}}{(D+T+1)^{k-3}} - (k-2)^2 \frac{(\frac{l}{2})^{(k-1)} D^{2(k-1)}}{(D+T+1)^{k-1}}$$

$$= (\frac{l}{2})^{k-1} B'_k ; B'_k = (k-1)(k-4)\frac{D^{2(k-2)}}{(D+T+1)^{k-3}} - (k-2)^2 \frac{D^{2(k-1)}}{(D+T+1)^{k-1}}$$

From Eqs (27) we get,

$$A_k = (k-2)\frac{(\frac{l}{2})^{2(k-1)} D^{2(k-1)}}{(-1)^{k-1}(\frac{l}{2})^{k-1}(D+T+1)^{k-1}} - (k-1)\frac{(\frac{l}{2})^{2k} D^{2k}}{(-1)^{k+1}(\frac{l}{2})^{k+1}(D+T+1)^{k+1}}$$

$$= (\frac{l}{2})^{k-1}[(k-2)\frac{D^{2(k-1)}}{(-1)^{k-1}(D+T+1)^{k-1}} - (k-1)\frac{D^{2k}}{(-1)^{k+1}(D+T+1)^{k+1}}]$$

$$= (\frac{l}{2})^{k-1} C_k ; C_k = (k-2)\frac{D^{2(k-1)}}{(-1)^{k-1}(D+T+1)^{k-1}} - (k-1)\frac{D^{2k}}{(-1)^{k+1}(D+T+1)^{k+1}}$$

$$A'_k = (k-1)(k-4)\frac{(\frac{l}{2})^{2(k-2)} D^{2(k-2)}}{(-1)^{k-3}(\frac{l}{2})^{k-3}(D+T+1)^{k-3}} - (k-2)^2 \frac{(\frac{l}{2})^{2(k-1)} D^{2(k-1)}}{(-1)^{k-1}(\frac{l}{2})^{k-1}(D+T+1)^{k-1}}$$

$$= (\frac{l}{2})^{k-1}[(k-1)(k-4)\frac{D^{2(k-2)}}{(-1)^{k-3}(D+T+1)^{k-3}} - (k-2)^2 \frac{D^{2(k-1)}}{(-1)^{k-1}(D+T+1)^{k-1}}]$$

$$= (\frac{l}{2})^{k-1} C'_k ; C'_k = (k-1)(k-4)\frac{D^{2(k-2)}}{(-1)^{k-3}(D+T+1)^{k-3}} - (k-2)^2 \frac{D^{2(k-1)}}{(-1)^{k-1}(D+T+1)^{k-1}}$$

Applying these values in equation (28) we get,

$$\sigma_\theta^d = \frac{2\mu_0}{\pi(k_0+1)} \int_{-1}^{1} [\{\frac{1}{(H-T)} - \frac{1}{(D+H+1)} - \frac{D^2}{(D+T+1)(D+H+1)^2} + \frac{1}{2}\sum_{k=3}^{\infty}(2-k)B_k(D+H+1)^{-k} +$$

$$\frac{1}{2}\sum_{k=3}^{\infty}(2-k)B'_k(D+H+1)^{-k}\} + \{-\frac{1}{(2D+H+T+2)} + \frac{1}{(D+H+1)} - \frac{D^2}{(D+T+1)(D+H+1)^2} -$$

$$\frac{1}{2}\sum_{k=3}^{\infty}(2-k)C_k(D+H+1)^{-k}-\frac{1}{2}\sum_{k=3}^{\infty}(2-k)C'_k(D+H+1)^{-k}\}]B(T)dT$$

$$\sigma_\theta^d=\frac{2\mu_0}{\pi(\kappa_0+1)}\int_{-1}^{1}[\frac{1}{H-T}+G_1(H,T)+G_2(H,T)+G'_1(H,T)+G'_2(H,T)+G'_3(H,T)]B(T)dT$$

where

$$G_1(H,T)=-\frac{1}{D+H+1}-\frac{D^2}{(D+T+1)(D+H+1)^2},$$

$$G_2(H,T)=\frac{1}{2}\sum_{k=3}^{\infty}(2-k)B_k(D+H+1)^{-k}+\frac{1}{2}\sum_{k=3}^{\infty}B'_k(D+H+1)^{-k},$$

$$G'_1(H,T)=-\frac{1}{2D+H+T+2}$$

$$G'_1(H,T)=\frac{1}{D+H+1}-\frac{D^2}{(D+T+1)(D+H+1)^2}$$

$$G'_2(H,T)=-\frac{1}{2}\sum_{k=3}^{\infty}(2-k)C_k(D+H+1)^{-k}-\frac{1}{2}\sum_{k=3}^{\infty}C'_k(D+H+1)^{-k}$$

Finally, we obtain

$$\frac{2\mu_0}{\pi(\kappa_0+1)}\int_{-1}^{1}[\frac{1}{H-T}+G_1(H,T)+G_2(H,T)+G'_1(H,T)+G'_2(H,T)+G'_3(H,T)]B(T)dT$$

$$=-p(S_f\frac{\sigma_\theta^h}{\sigma_u}+1);-1\le H\le 1$$

(32)

The density function $B(T)$ can be expressed as the product of a fundamental function $w(T)$ which characterizes the bounded-singular behavior of $B(T)$ and a bounded continuous function $\varphi(T)$ in the closed interval $-1 \le T \le +1$. Thus we can formulate

$$B(T)=w(T)\varphi(T).$$ (33)

In the present case, the fundamental function can be given by

$$w(T)=\sqrt{\frac{(1+T)}{(1-T)}}.$$ (34)

Using the Gauss-Jacobi integral formula corresponding to the weight function in Eq. (34) in the manner developed by Erdogan et al. [57] Eq. (32) can be converted to a system of algebraic equations to determine the unknowns $\varphi(T_j)$ as follows

$$\frac{2\mu_0}{(\kappa_0+1)}\sum_{j=1}^{N}(1+T_j)\left[\frac{1}{H_i-T_j}+G_1(H_i,T_j)+G_2(H_i,T_j)+G_1'(H_i,T_j)+G_2'(H_i,T_j)+G_3'(H_i,T_j)\right]\phi(T_j)$$
$$=-\frac{2N+1}{2}\left[\sigma_\theta^h(H_i)+p\right];\ i=1,2,3,...,N;-1\le H\le 1 \tag{36}$$

The integration and collocation points are given by

$$T_j=\cos\left(\frac{2j-1}{2N+1}\pi\right);\ j=1,2,3,...,N, \tag{37a}$$

$$H_i=\cos\left(\frac{2\pi i}{2N+1}\right);\ i=1,2,3,...,N. \tag{37b}$$

It can be readily shown that the stress intensity factor can be derived as[58]

$$K_I=\sqrt{2\pi l}\,\frac{2\mu_0}{(\kappa_0+1)}\varphi(+1), \tag{38}$$

where $\varphi(+1)$ is computed by Krenk's interpolation formula [59] given by

$$\varphi(+1)=\frac{2}{2N+1}\sum_{j=1}^{N}\frac{\sin\left(\frac{2j-1}{2N+1}N\pi\right)}{\tan\left(\frac{2j-1}{2N+1}\frac{\pi}{2}\right)}\varphi(T_j). \tag{39}$$

The solution of Eq. (36) provides the unknowns $\varphi(T_j)$ which are used in Eq. (39) to determine the value of $\varphi(+1)$ and then the stress intensity factor can be computed from Eq. (38).